University of Alberta

Receiver Processing and Limited-Feedback User Scheduling for Multiuser MIMO and MIMO-OFDM Downlink

by

Mohsen Eslami

A thesis submitted to the Faculty of Graduate Studies and Research
in partial fulfillment of the requirements for the degree of

Doctor of Philosophy

Department of Department of Electrical and Computer Engineering

Fall 2009
Edmonton, Alberta

Examining Committee

Witold A. Krzymień, Electrical and Computer Engineering

Robert Heath, Electrical and Computer Engineering,
University of Texas - Austin

Ioanis Nikolaidis, Computing Science

Yindi Jing, Electrical and Computer Engineering

Chintha Tellambura, Electrical and Computer Engineering

بابدان مقصد عالی نتوانیم رسید

هم اگر پیش نهد لطف شما گامی چند

To that lofty desire, we cannot attain

Unless your favour advanceth some paces

Hafez's Divan, Ghazal 182.

Abstract

Multiple-input multiple-output orthogonal frequency division multiplexing (MIMO-OFDM) has been proposed for many emerging standards and seems to be a promising solution for future high data rate wireless communications. In the first part of this thesis, a novel sub-optimum detection method called unified successive interference cancellation (U-SIC) for spatially multiplexed multicarrier code division multiplexing (SM-MC-CDM) transmission is proposed. It is shown that compared to the spatially multiplexed OFDM (SM-OFDM), the frequency domain spreading in SM-MC-CDM systems results in an additional diversity gain. Analytical results for the performance and capacity of zero-forcing (ZF) U-SIC are provided. The results demonstrate significant performance improvement over other existing methods of comparable complexity. Performance of turbo-coded SM-MC-CDM transmission is also investigated.

In the next part of the thesis, multiuser MIMO downlink is considered. Efficient transmission schemes based on zero-forcing (ZF) linear receiver processing, eigenmode transmission and partial channel state information are proposed. The proposed schemes utilize a handshaking procedure between the BS and the users to select (schedule) a subset of users and determine the precoding matrix at the base station (BS). The advantage of the proposed limited feedback schemes lies in their relatively low complexity scheduling algorithms and high sum rate throughput, even for a small pool of users.

Next, net throughput is used as a benchmark to compare several MIMO-OFDM downlink transmission schemes with complete CSIT and also with limited feedback. Considering limited feedback per-chunk (a chunk consists of a number of adjacent subcarriers in frequency and consecutive OFDM symbols in time) user scheduling for MIMO-OFDM downlink, it is shown that there exists a chunk size which maximizes the average net throughput. It is shown that the net throughput maximizing chunk size depends on the number of users in the system and the communication channel's characteristics. Finally, future directions for possible research are given.

Acknowledgements

I would like to express my profound appreciation and sincere gratitude to my advisor, Dr. Witold A. Krzymień, for his guidance, patience and support throughout this work. I am very grateful for his insights and advice. I would also like to thank Dr. Xiaodai Dong for her support and guidance during the first two years of my Ph.D. program.

I would like to thank my advisory committee and candidacy examination committee, Dr. Chintha Tellambura, Dr. Ivan Fair, Dr. Masoud Ardakani, and Dr. Janelle Harms for their constructive feedback on my work, especially at the early stages of my Ph.D. program. I also would like to thank Dr. Robert Heath, Dr. Ioanis Nikolaidis and Dr. Yindi Jing for serving on my Ph.D. defense committee and for their valuable feedback on my thesis.

This doctoral work was funded by TRLabs, the Rohit Sharma Professorship, and National Science and Engineering Research Council (NSERC) of Canada, which I would like to acknowledge.

This thesis would have not been possible without the support of Dr. Amir Masoud Rabiei, who has probably been my closest friend over the duration of my doctoral studies. I am also indebted to Reza Nikjah, Alireza Ghaderipoor, Dr. Boon Chin, Saeed Fouladifard, Dr. Shreeram Sigdel, Kevin Jacobson, Robert Elliott, and Dr. Sasan Haghani for their friendship and many insightful discussions. I would also like to thank Dr. Iman Izadi, Alireza Farhangfar, Moslem Noori, Mahdi Ramezani, Arash Talebi and Raman Yazdani who have assisted me. I am grateful to all my friends, fellow students and colleagues at the 5th floor of Electrical and Computer Engineering Research Facility (ECERF) at University of Alberta for making my graduate years enjoyable.

Finally I would like to thank my family members. My parents, Moossa and Soraya, whose endless love, kindness and sacrifice enabled all my life achievements. Their inspiring compassion, sincerity, support and encouragement is nothing that I

can describe or thank in words. I would also like to thank my dear brother Majid, my lovely sisters Maryam and Narges for their cheerfulness and emotional support. Last but not least, I would like to thank the love of my life, Effatsadat, for her sacrifice, patience and endless support. The greatest gift that I was blessed with during my Ph.D. years is my son, Amir Mehdi. I also thank him for bringing sweetness to my life and for his patience with my studies.

Table of Contents

List of Tables

List of Figures

Abbreviations

3GPP	3rd generation partnership project
AWGN	Additive white Gaussian noise
BC	Broadcast channel
BS	Base station
CDMA	Code division multiple access
CSI	Channel state information
CSIT	Channel state information at transmitter
DAB	Digital audio broadcasting
DVB	Digital video broadcasting
DPC	Dirty paper coding
FDM	Frequency division multiplexing
ICI	Inter-carrier interference
i.i.d.	Independent and identically distributed
ISI	Inter-symbol interference
ISRD	Iterative subcarrier reconstruction detection
LRA	Lattice reduction aided
LTE	Long term evolution
MC-CDM	Multicarrier code division multiplexing
MC-DS-CDMA	Multicarrier direct sequence code division multiple access
MIMO	Multiple-input multiple-output
MIMO BC	Multiple-input multiple-output broadcast channel
MIMO MAC	Multiple-input multiple-output multiple access channel
MMSE	Minimum mean square error
MU-MIMO	Multiuser multiple-input multiple-output
OFDM	Orthogonal frequency division multiplexing
Rx	Receiver
SDMA	Space division multiple access
SIC	Successive interference cancellation
SINR	Signal to interference plus noise ratio
SM-MC-CDM	Spatially multiplexed multicarrier code division multiplexing
SM-OFDM	Spatially multiplexed orthogonal frequency division multiplexing
Tx	Transmitter
U-SIC	Unified successive interference cancellation
V-BLAST	Vertical Bell Labs layered space-time architecture
WiMAX	Worldwide inter-operability for microwave access

WLAN	Wireless local area network
ZF	Zero forcing
ZMCSCG	Zero mean circular symmetric complex Gaussian

List of Notations

$\mathbf{A}$	Matrix $\mathbf{A}$ (boldface capital letter)
$\mathbf{a}$	Vector $\mathbf{a}$ (boldface lowercase letter)
$\mathrm{E}[\cdot]$	Expected value
$\min(a, b)$	Minimum value of a and b
$\mathrm{vec}\{\cdot\}$	Vectorization operation
$\otimes$	Kronecker matrix product
$(\cdot)^T$	Matrix transpose
$(\cdot)^H$	Conjugate transpose of a matrix
$(\cdot)^\dagger$	Moor-Penrose psudoinverse of a matrix
$\Re\{\cdot\}$	Real part of a matrix
$\Im\{\cdot\}$	Imaginary part of a matrix
$E\{\cdot\}$	Expectation operation
$\mathbf{A}(k, :)$	The k^{th} row of the matrix $\mathbf{A}$
$\|\mathbf{A}\|$	Frobenius norm of the matrix $\mathbf{A}$
$\det\{\cdot\}$	Determinant of a matrix
$\mathrm{trace}\{\cdot\}$	Trace of a matrix

Chapter 1

Introduction

1.1 Motivation

Wireless links have the key advantage of enabling communication between mobile users. However, currently deployed wireless systems can only achieve data rates far lower than wire and fiber links. Multiple-input multiple-output (MIMO) transmission and orthogonal frequency division multiplexing (OFDM) are two promising techniques that can potentially enable reliable wireless communication at much higher data rates. MIMO and OFDM are currently the underlying technology for many emerging wireless standards such as IEEE 802.11n, WiMAX, and 3GPP Long Term Evolution (LTE). In addition, OFDM has already been adopted in several wireless standards such as IEEE 802.11a and 802.11g wireless local area network (WLAN) standards, digital video broadcasting (DVB) and digital audio broadcasting (DAB).

When OFDM is considered, spreading the data over a number of subcarriers, which is known as multicarrier code divison multiplexing (MC-CDM) or spread spectrum OFDM, increases the reliability of the communication link as it helps avoiding the loss of data over subcarriers which are in a deep fade. While MC-CDM or spread spectrum OFDM has been well studied in the literature, not much work has been done on issues related to combining MIMO and MC-CDM. In the first part of this thesis we investigate the effectiveness of frequency domain spreading in a MIMO-OFDM system and the way it interacts with channel coding.

It is now well known that in a multiuser MIMO wireless system, to explore full capacity of the system in terms of its sum rate, which is defined as the sum of the achievable rates of individual users, not only capacity achieving point-to-point techniques are required, but also serving multiple users with best channel conditions

is a must. Over the downlink, from the base station to the users, finding the best subset of users (scheduling) requires information of user channel conditions at the base station (BS), which for systems with large number of users is very challenging. Scheduling, resource allocation and transmitter/receiver processing for multiuser MIMO/MIMO-OFDM based on limited feedback bring about some interesting and challenging problems. In the second part of this work, our goal is to investigate some of these interesting problems and come up with low complexity high throughput algorithms.

1.2 Multiple-Input Multiple-Output Wireless Communications

The use of multiple receive antennas for diversity goes back to early radio pioneers. Winters and Salz at Bell Labs published several papers on beamforming application of multiple-antennas in 1980s and early 1990s [1, 2]. Paulraj, Tarokh, Raleigh, Cioffi, Foschini, Gans and Telatar were among the key the contributors to the field of multiple-antenna wireless communications in 1990s [3, 4, 5, 6]. In 1998, Bell Labs was the first to demonstrate a laboratory prototype of spatial multiplexing (SM) MIMO, and showed its great spectral efficiency advantage over single-input single-output (SISO) systems [7]. The capacity of certain MIMO channels with memory was derived in 1974 by Brandenburg and Wyner [8]. In the theoretical work by Telatar [9] in 1999, it was shown that in a rich scattering environment the capacity of a MIMO link increases linearly with the minimum of the number of receive and transmit antennas.

MIMO technology can be considered a breakthrough in wireless communication system design. In addition to the time and frequency dimensions that are exploited in conventional SISO wireless systems, MIMO systems exploit the space dimension as well. The benefits of MIMO technology can be listed as array gain, spatial diversity gain, spatial multiplexing gain and interference reduction. Space-time codes and Bell Labs Layered Space-Time (BLAST) architecture are two popular realizations of spatial diversity and spatial multiplexing, respectively.

1.3 Orthogonal Frequency Division Multiplexing Systems

High data rates over frequency selective fading channels lead to inter-symbol interference (ISI). One way of overcoming ISI is dividing the channel into a number of non-overlapping parallel subchannels of which each is frequency flat. The non-overlapping subchannel structure of this solution to the ISI problem, results in insufficient utilization of the the spectrum. In mid-1960' the idea of frequency division multiplexing (FDM) with overlapping subchannel signal spectra was proposed and led to increased spectral efficiency. The subchannels must be arranged such that the sidebands of the individual subcarriers overlap without causing inter-carrier interference (ICI). This is achieved when signals on different subcarriers are orthogonal and that is the principal idea behind orthogonal frequency division multiplexing (OFDM) [10, 11]. By dividing the transmission channel into a number of narrowband subchannels and transmitting a low rate data on each of these subchannels the frequency selective channel is transformed into a set of parallel flat fading channels and a one-tap equalizer on each subchannel is enough to compensate for the channel's dispersive effect on the composite signal's phase and magnitude. For practical applications, the modulation and demodulation in an OFDM system are implemented with the discrete Fourier transform using a fast Fourier transform algorithm making the transceiver design simple [12]. For a comprehensive study on OFDM the interested reader is referred to [13, 14].

1.4 Multicarrier Spread Spectrum Systems

Since 1993, various combinations of multi-carrier modulation with the spread spectrum technique have been introduced. Two main variants of multicarrier spread spectrum exist, namely MC-CDM (or OFDM-CDM) and MC-DS-CDM.

MC-CDM is based on serial concatenation of direct sequence spreading with multicarrier modulation [15, 16, 17, 18, 19, 20]. In MC-CDM each data symbol is spread over several subcarriers in frequency domain to take advantage of the multipath diversity of the frequency-selective mobile radio channel, which leads to more reliable communications and also to higher spectral efficiency in cellular systems. In a multiuser environment, MC-CDMA may be used for the purpose of multiple access where each spreading code is assigned to one of the users [18, 21]. For

the choice of spreading code, there exists a number of options from which orthogonal codes are most commonly used. The reason is that orthogonal codes, such as Walsh-Hadamard codes, guarantee the absence of inter-code interference in flat fading channels and minimize interference in frequency-selective fading channels.

MC-DS-CDMA is another way of combining multicarrier schemes with spread spectrum techniques and is usually considered for the uplink of multiuser systems [22, 23]. In this scheme the data is spread in time on each subcarrier. Joint frequency and time spreading have also been considered [24]. The interested reader is referred to [23] for further details on the subject.

1.5 Multiuser Multiple-Input Multiple-Output Techniques

Consider many mobile users interested in communicating through a common hub with each other as well as with other users connected to the backbone telecommunication network. As opposed to radio or TV broadcast cases where the same message is broadcast to all users, in the network considered here, each user receives and transmits its own message and there exist means of two-way communication between the common point and each user terminal. Cellular systems are an example of multiuser systems in which the base station is the common hub through which all user terminals in a given cell try to communicate.

The issues of such a network when the base station and user terminals are each equipped with a single antenna have been around for some time now and are well studied in the literature. However, recently there has been a great interest in multiuser MIMO (MU-MIMO) systems and extending the point-to-point MIMO benefits to MU-MIMO. In MU-MIMO systems and on the uplink, multiple users transmit simultaneously over the same bandwidth to a common hub receiver (a scheme referred to as multiple access channel (MAC)) or on the downlink a common hub transmits to multiple users (a scheme referred to as the broadcast channel (BC)). The hub uses multiple antennas whereas the users may use either single or multiple antennas. An important task in MU-MIMO is user scheduling to maximize system sum-capacity, while preserving required fairness of service.

In MU-MIMO, capacity becomes a K-dimensional region defining the set of all rate vectors $(R_1, \ldots, R_K)$ simultaneously achievable by all K users. A widely-known scheme of MU-MIMO is space-division multiple access (SDMA), which is a channel

access method based on creating parallel spatial pipes through spatial multiplexing and/or diversity achieving techniques, that enable superior performance. One example of MAC and BC is a cellular system where the base station may have $M > 1$ antennas and each of the K mobiles may have $N \geq 1$ antennas.

It has been shown that the sum-capacity of the MU-MIMO downlink can be achieved by dirty paper coding (DPC) [25], which is a transmitter multiuser encoding strategy based on interference presubtraction. DPC requires finding the optimum set of precoding matrices and the optimal power allocation strategy for all user terminals as well as non-causal channel coding of each terminal's stream(s), which is practically impossible in real-time systems. Therefore, suboptimum transmission strategies such as different forms of generalized beamforming have been considered in the literature. In MU-MIMO beamforming, linear or non-linear transmitter precoding algorithms together with user scheduling are designed to maximize the system's sum rate or some other related objective function (e.g., sum rate under fairness constraint). Unfortunately, most beamforming algorithms considered assume availability of perfect channel state information at the transmitter, which presents a big challenge to their practical implementation. To overcome this challenge, suboptimal MU-MIMO downlink transmission based on partial channel state information (CSI) has been studied in the literature ([26, 27] and references therein contain an overview of the subject).

1.6 Summary of Contributions

The scope of this dissertation encompasses novel physical layer SM-MC-CDM detection schemes and MIMO/MIMO-OFDM downlink limited feedback user scheduling and resource allocation schemes. The main contributions presented in this dissertation are as follows.

- **MIMO-MC-CDM detection**

  A novel sub-optimum detection method for spatially multiplexed multicarrier code division multiplexing (SM-MC-CDM) communications is proposed. To take advantage of diversity and multiplexing while mitigating the interference, a low complexity efficient detector employing unified successive interference cancellation (SIC) is designed and its performance is compared with that of a number of sub-optimum detectors using simulations over spa-

tially uncorrelated and correlated frequency selective fading MIMO channels. Further performance improvement is achieved by adopting an iterative subcarrier reconstruction-detection algorithm in conjunction with the unified SIC. The results demonstrate significant performance improvement over other existing methods of comparable complexity. Numerical results obtained with different numbers of antennas and subcarriers are presented to show the achievable frequency domain diversity gain offered by the new detection algorithm. Performance of turbo-coded SM-MC-CDM transmission is also investigated [28, 29, 30].

- **Performance evaluation of zero-forcing unified successive interference cancelling detector for MIMO-MC-CDM**

  The unified successive interference canceler (U-SIC) is an efficient detector for SM-MC-CDM systems. An analytical approach to the performance of zero-forcing (ZF) U-SIC for SM-MC-CDM communications is presented. For a system with equal number of transmit and receive antennas, an approximation for the probability density function of post detection SNR is used to derive a closed-form analytical upper-bound and approximations for the probability of error and the ergodic capacity. It is shown that SM-MC-CDM with ZF U-SIC is able to achieve higher diversity order than that achieved by ZF and minimum mean squared error (MMSE) V-BLAST detectors used on each subcarrier of a MIMO-OFDM system with the same number of subcarriers. The diversity order obtained increases with the number of subcarriers. It is also shown that the ergodic capacity of the system decreases with increasing number of subcarriers [31].

- **Low complexity scheduling and resource allocation schemes for MIMO/MIMO-OFDM downlink with limited channel state information feedback**

  The downlink of a multiuser system is considered, in which the base station (BS) and the user terminals are both equipped with multiple antennas. Efficient transmission schemes based on ZF linear receiver processing, eigenmode transmission and partial channel state information are proposed. The proposed schemes utilize a handshaking procedure between the BS and the users to select (schedule) a subset of users and determine the precoding matrix at

the BS. The advantage of the proposed limited feedback schemes lies in their relatively low-complexity scheduling algorithms and high sum rate throughput, even for a small pool of users. For large user pools and when the number of antennas at each user terminal is at least equal to the number of antennas at the BS, we show that the proposed scheme is asymptotically optimum in the sense that it achieves the same sum rate as the optimum scheme as the number of users approaches infinity [32, 33, 34, 35].

- **Net throughput maximization of limited feedback MIMO-OFDM downlink with per chunk user scheduling**
  Limited feedback MIMO-OFDM downlink with per chunk user scheduling is considered. By grouping adjacent subcarriers into chunks, the amount of required feedback is reduced. Based on net throughput criterion, it is shown that there exist an optimum chunk size which maximizes the net throughput. To even further reduce the feedback requirement, an opportunistic feedback scheme is proposed and a close approximation for its net throughput is obtained. The net throughput of the proposed scheme is compared with various limited feedback MIMO-OFDM downlink strategies. The results show that by increasing the number of users in the system, the net throughput of most existing MIMO-OFDM downlink schemes reduces to zero for a moderate to small size user pools, whereas the proposed scheme's net throughput slightly increases, before decreasing to zero at a significantly lower rate with respect to the number of users in the system and when that number is relatively large (> 1000) [36, 37].

1.7 Dissertation Outline

Chapter 2 begins with a brief overview of the SM-MC-CDM system. Then, the receiver structure and different detection schemes for SM-MC-CDM are discussed. Next, the proposed detection algorithm is introduced and its complexity is discussed. SM-MC-CDM with channel coding is also considered, where turbo decoding is incorporated with the proposed detection scheme. Finally some numerical results are presented.

Chapter 3 deals with the performance evaluation of ZF U-SIC detector proposed for SM-MC-CDM. First an approximation for the distribution of post-processing SNR is derived, which is then used to derive performance bounds for the aforemen-

tioned detector. Finally, some numerical results are presented to verify the analysis.

Chapters 4 and 5 are devoted to limited feedback multiuser MIMO. In Chapter 4, the system model for multiuser MIMO downlink is described. Two well known transmission schemes based on limited feedback are briefly outlined before a new transmission techniques based on limited feedback for MU-MIMO downlink is presented. Next, an asymptotic analysis of the proposed transmission scheme for the case when the number of users approaches infinity is presented. Numerical results are presented at the end of the chapter. In chapter 5, first the MIMO-OFDM downlink system model is presented and the term net throughput is defined. Next, limited feedback MIMO-OFDM downlink with per chunk user scheduling is outlined and its average sum rate is analyzed. An opportunistic feedback scheme for per chunk user scheduling is proposed later in the chapter, which reduces the amount of feedback. Numerical results and summary are given at the end of the chapter. Finally, Chapter 6 summarizes the key points in this thesis and proposes some directions for future work.

Chapter 2

An Efficient Low Complexity Detector for Spatially Multiplexed MC-CDM

In this chapter we consider spatially multiplexed multicarrier code division multiplexing (SM-MC-CDM) communication systems, where the data symbols are spread over a number of subcarriers using orthogonal spreading codes. As a result, SM-MC-CDM is expected to be able to exploit more frequency/multipath diversity compared to MIMO-OFDM communications. However, over the multipath frequency selective fading channel, due to the loss of orthogonality between the codewords at the receiver, crosstalk not only occurs between different transmit antennas, but also between different subcarriers. Consequently, the detection process is more involved than in MIMO-OFDM.

A number of MIMO-OFDM detectors have been modified for SM-MC-CDM communication [21, 38, 39, 40]. In [38] linear MMSE and successive interference cancellation (SIC) MMSE detectors have been studied for spatially multiplexed MC-CDMA systems where SIC is performed on individual subcarriers (without ordering). In [39] a new CDM transform is obtained which minimizes the error probability of V-BLAST detector and is applied to MC-CDM and MIMO-MC-CDM systems. It has been shown that the new CDM transform improves the system performance. However, the new transform matrix depends on the channel noise variance and an exhaustive search is required to determine its elements. In [40], lattice reduction aided (LRA) detection has been proposed for SM-MC-CDM. However, as it will be discussed later in this work, LRA detection is not suitable for systems with a larger number of subcarriers. In [41], per-subcarrier parallel interference cancel-

lation (PIC) has been combined with iterative subcarrier reconstruction-detection (ISRD) [42] and it has been shown that ISRD improves the performance when combined with per-subcarrier PIC.

In this chapter we present a new detection method for point-to-point SM-MC-CDM communications, which achieves high performance with a reasonably low complexity. In [43] it has been shown that in MIMO Rayleigh fading channels there is always a fundamental trade-off between spatial multiplexing and diversity gains. Our goal in this chapter is to explore the additional diversity gain offered by the frequency domain spreading while not losing any degrees of freedom (any spatial multiplexing gain), through efficient detector design. The main contributions of this work are: 1) Proposing a low complexity detection algorithm for SM-MC-CDM. Our numerical results show that for medium to high SNRs the proposed detector achieves significantly better performance compared to SM-OFDM with V-BLAST detection over each subcarrier. The diversity order achieved with the proposed detector is higher than that of maximum likelihood detector (MLD) over each subcarrier. 2) The effect of using frequency domain spreading in a coded SM-OFDM link is investigated by considering turbo coded SM-MC-CDM. The results show that the frequency domain spreading improves the system performance, especially for systems that use short turbo codes.

To reduce or cancel inter-substream interference, we consider linear MIMO processing on each subcarrier. The output signal from linear processors is de-spread before detection. We show that the post-processing SNR of each substream is the same on all subcarriers after de-spreading. Therefore, our proposed detector de-spreads and detects substreams successively in descending order of their post-processing SNR. Once the data of each substream are detected, its corresponding re-modulated signal component is spread and subtracted from the received signal. This is similar to V-BLAST detection, however, frequency domain spreading improves the reliability of the detected data of each substream. We refer to this detection process, in which ordered SIC is used on all subcarriers (with the same ordering) as unified SIC. Further performance improvement is achieved through ISRD, which is applied after linear MIMO processing for detection of each substream. In contrast to the scheme proposed by [41], which uses PIC to reduce inter-substream interference on all individual subcarriers followed by ISRD to detect all individual substreams, we propose linear MIMO processing with ordered SIC according to each

substream's post-processing SNR followed by ISRD to detect data of each substream (all substreams are not detected in one step). Numerical results show the proposed detector outperforms ZF V-BLAST and MMSE V-BLAST detectors used on individual subcarriers of MIMO-OFDM. Finally, complexity of the proposed detector and performance of the coded system are evaluated using computer simulations.

The chapter is organized as follows. Section 2.1 describes the system model. In Section 2.2 the receiver structure and different detection schemes for SM-MC-CDM are discussed. The proposed detection algorithm is introduced in Section 2.3, followed by the numerical results in Section 2.4. Finally Section 2.5 concludes this work.

2.1 System Model

2.1.1 Transmitter model

The transmitter structure for SM-MC-CDM is shown in Fig. 2.1. Consider $M \times L$ data symbols to be transmitted. After being de-multiplexed into M groups, where M denotes the number of Tx antennas, the L data symbols on the m^{th} antenna, $\mathbf{d}^{(m)} = [d_1^{(m)} \dots d_L^{(m)}]^T$, are code division multiplexed. Here, we assume there are L subcarriers available for transmission. Orthogonal Walsh codes are used for spreading and each symbol is multiplied with a length L spreading code before the L spread symbols are summed up to form the frequency domain length L vector $\mathbf{x}^{(m)} = \left[X_1^{(m)} \dots X_L^{(m)}\right]^T$, where

$$\mathbf{x}^{(m)} = \mathbf{C}_L \mathbf{d}^{(m)} \tag{2.1}$$

The matrix $\mathbf{C}_L$,

$$\mathbf{C}_L = \frac{1}{\sqrt{L}} \begin{bmatrix} \mathbf{C}_{\frac{L}{2}} & \mathbf{C}_{\frac{L}{2}} \\ \mathbf{C}_{\frac{L}{2}} & -\mathbf{C}_{\frac{L}{2}} \end{bmatrix}, \tag{2.2}$$

is the normalized Walsh-Hadamard transformation matrix [44] where $L = 2^n$, $n \geq 1$ and $\mathbf{C}_1 = 1$. Consequently on each subcarrier we have a MIMO channel with the following input vector

$$\mathbf{x}_l = \left[X_l^{(1)} X_l^{(2)} \dots X_l^{(M)}\right]^T, \quad 1 \leq l \leq L. \tag{2.3}$$

The OFDM modulator on each Tx antenna consists of an IFFT block, parallel to serial converter followed by a cyclic prefix insertion unit and a digital to analog

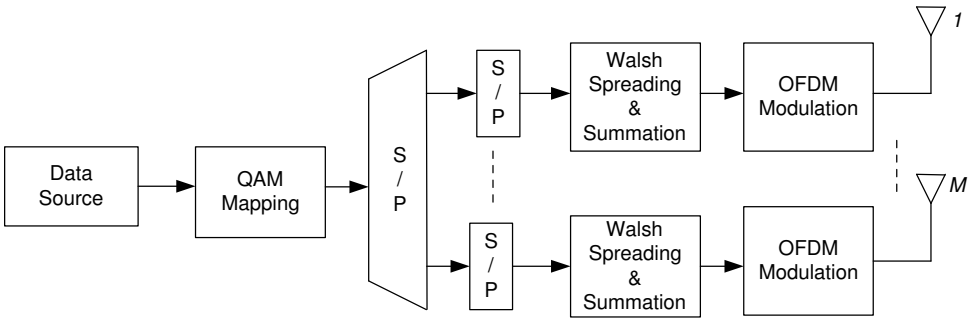

Figure 2.1: SM-MC-CDM transmitter structure.

converter (DAC). The length of the cyclic prefix is assumed to be greater than the largest maximum excess delay over all spatial channels. Perfect synchronization is assumed at the receiver.

2.1.2 Channel model

Here we consider the frequency selective MIMO channel model used in [45, 46], accounting for antenna and path correlations, as well as the i.i.d. Rayleigh model. In the model with correlations, at each sampling time a path tap is represented by an $N \times M$ matrix where N is the number of receive (Rx) antennas ($N \geq M$). Consider $\{\mathbf{Q}_p\}_{p=0,\ldots,P-1}$, to be the time domain representation of the multipath MIMO channel where the number of resolvable paths, P, is determined by the maximum delay spread of the channel. Antenna and path correlations are taken into account using the Kronecker product of correlation matrices. Consider the following relation for stacking of all $\mathbf{Q}_p$ matrix columns,

$$\mathbf{q} = \left[\text{vec}\{\mathbf{Q}_0\}^T \ldots \text{vec}\{\mathbf{Q}_{P-1}\}^T\right]^T. \tag{2.4}$$

The correlation matrix $\mathbf{R}$ is then given by

$$\mathbf{R} = E\left\{\mathbf{q}\mathbf{q}^H\right\} \tag{2.5}$$

and is expressed in the form of $\mathbf{R} = \mathbf{R}_p \otimes \mathbf{R}_t^T \otimes \mathbf{R}_r$. Matrices $\mathbf{R}_t$ and $\mathbf{R}_r$ represent transmitter and receiver antenna correlations respectively, while $\mathbf{R}_p$ defines path correlations. The assumptions for the validity of this (Kronecker) correlation model have been given in [47] and later the validity of this model has been investigated in [48, 49, 50]. Using the matrix $\mathbf{R}$, the multipath MIMO channel can be expressed as

$$\mathbf{q} = \mathbf{R}^{\frac{1}{2}}\mathbf{q}_w \tag{2.6}$$

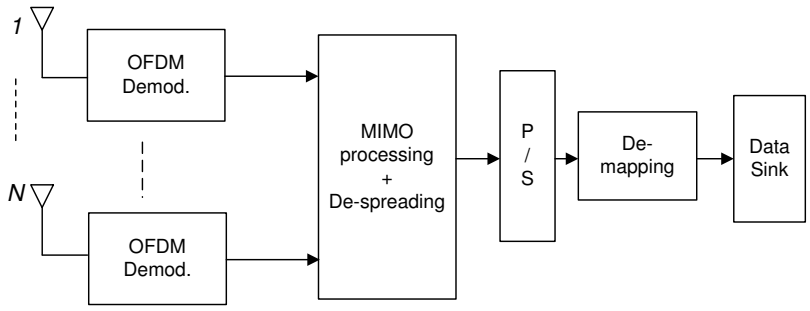

Figure 2.2: SM-MC-CDM receiver structure.

where $\mathbf{q}_w$ is an $MNP \times 1$ white zero-mean circularly symmetric complex Gaussian (ZMCSCG) channel vector with variance of 0.5 per dimension. The space frequency channel at the l^{th} tone is obtained as

$$\mathbf{H}_l = \sum_{p=0}^{P-1} \mathbf{Q}_p e^{-j\frac{2\pi}{L}(l-1)p}, \quad 1 \leq l \leq L. \tag{2.7}$$

The channel is assumed to be perfectly known at the receiver, but not at the transmitter.

2.2 Receiver Structure

Fig. 2.2 depicts the receiver structure for the SM-MC-CDM system. The OFDM demodulator removes the cyclic prefix and performs FFT on the received time domain samples. The resulting frequency domain samples from all receiver antennas are fed to the MIMO detector. After MIMO detection and de-spreading, the block of $M \times L$ symbols is parallel-to-serial converted before de-mapping.

The received signal arriving at the array of N antennas and on the l^{th} subcarrier, $\mathbf{y}_l = [Y_l^{(1)} Y_l^{(2)} \dots Y_l^{(N)}]^T$, is given by

$$\mathbf{y}_l = \mathbf{H}_l \mathbf{x}_l + \mathbf{w}_l, \quad 1 \leq l \leq L \tag{2.8}$$

where $\mathbf{w}_l$ is the zero mean complex AWGN noise vector with $E\{\mathbf{w}_l \mathbf{w}_l^H\} = \sigma_w^2 \mathbf{I}_N$. The total transmit power is normalized to one, i.e., trace $\left[E\{\mathbf{x}\mathbf{x}^H\}\right] = 1$. The SM-MC-CDM detection schemes are presented in the next subsection.

2.2.1 Detection and de-spreading

The received data block on all subcarriers and antennas, $\boldsymbol{y} = [\mathbf{y}^{(1)^T} \dots \mathbf{y}^{(N)^T}]^T$, is related to the input data symbols, $\boldsymbol{d} = [\mathbf{d}^{(1)^T} \dots \mathbf{d}^{(M)^T}]^T$, as follows

$$\boldsymbol{y} = \boldsymbol{\mathcal{H}}\boldsymbol{d} + \boldsymbol{w} \tag{2.9}$$

where

$$\boldsymbol{\mathcal{H}} = \begin{bmatrix} \mathbf{D}_{11}\mathbf{C}_L & \dots & \mathbf{D}_{1M}\mathbf{C}_L \\ \vdots & \ddots & \vdots \\ \mathbf{D}_{N1}\mathbf{C}_L & \dots & \mathbf{D}_{NM}\mathbf{C}_L \end{bmatrix}. \tag{2.10}$$

The $\mathbf{D}_{ij}$ matrices are $L \times L$ diagonal matrices containing the L frequency domain samples of the communication channel between the i^{th} Tx antenna and the j^{th} Rx antenna, i.e., $\mathbf{D}_{ij}$ has $\{H_{ij}^{(1)}, H_{ij}^{(2)}, \dots, H_{ij}^{(L)}\}$ on its main diagonal and zeros elsewhere. Vector $\boldsymbol{w}$ contains $L \times N$ noise samples. From (2.9) we can derive the maximum likelihood detection (MLD) criterion for the SM-MC-CDM system as

$$\hat{\boldsymbol{d}} = \arg\min_{\boldsymbol{d}} \|\boldsymbol{y} - \boldsymbol{\mathcal{H}}\boldsymbol{d}\|^2. \tag{2.11}$$

Note that MLD requires an exhaustive search through all possible δ^{ML} transmitted vectors where δ is the constellation size associated with the specific modulation scheme employed. In other words, the Rx complexity is exponential in the number of Tx antennas times the number of subcarriers. Therefore, real time realization of the MLD for a typical number of subcarriers and antennas is not feasible. Furthermore, considering the large matrix dimensions that need to be handled, tree-based sphere detection schemes [51], which are simplified versions of MLD while achieving performance close to MLD, have higher and SNR dependent complexity compared to linear detectors [52, 53], which have lower and SNR independent complexity [54]. Even lattice reduction aided (LRA) detector [55], which achieves the same diversity as MLD [56] and has been applied to SM-MC-CDM with small number of subcarriers[57, 40], is not suitable for SM-MC-CDM with moderate to large number of subcarriers. This is due to its relatively high complexity [58, 59] and a power penalty in performance, which increases with the dimension of the lattice. In [60] it has been shown that when using Lenstra, Lenstra and Lovász (LLL) [61] algorithm for lattice reduction (LLL is the most widely used scheme for lattice reduction) followed by a linear ZF detector, there exist an SNR penalty (compared to MLD) which is upper bounded by a factor that increases linearly with the dimension of the lattice (dimension of $\boldsymbol{\mathcal{H}}$). Therefore, overall, linear detectors are a more suitable solution for SM-MC-CDM detection and will be considered in this work.

The most commonly known types of linear MIMO detectors are ZF and MMSE detectors for which the corresponding detection matrices are defined as follows [3]

$$\begin{aligned} \mathbf{G}_l &= (\mathbf{H}_l^H \mathbf{H}_l)^{-1} \mathbf{H}_l^H, \\ \mathbf{G}_l &= \left(\mathbf{H}_l^H \mathbf{H}_l + M\sigma_{w_l}^2 \mathbf{I}_M\right)^{-1} \mathbf{H}_l^H. \end{aligned} \tag{2.12}$$

On the other hand V-BLAST is a type of non-linear detector. In V-BLAST detection, the data substreams are detected in a specific order that is determined by the substreams post-detection signal to interference plus noise ratio (SINR). After detecting each substream using linear MMSE or ZF detectors, the channel signature on the detected symbol multiplied by the detected symbol is subtracted out from the received signal vector, which results in a modified received vector with less interference. The substreams are detected in a descending order of post-detection SINR to minimize the probability of error and error propagation in detection.

2.3 The Proposed Detection Scheme

Fig. 2.3 shows the proposed detector structure. We assume ordered successive detection of substreams. To find the detection ordering, the SINR value for each substream is required. In this section we will first evaluate the SINR of each substream and based on the obtained result design an SIC type of detector. To determine the order of the substream detection, the SINRs on all subcarriers have to be evaluated. For the purpose of spatial layer separation MMSE detector is considered on each subcarrier, and the final results are modified later for the case of ZF detector. The m^{th} MIMO detector output over all subcarriers equals

$$\begin{aligned} \mathbf{z}^{(m)} &= \acute{\mathbf{x}}^{(m)} + \acute{\mathbf{w}}^{(m)} \\ &= \begin{bmatrix} \boldsymbol{\psi}_1(m,:)\mathbf{x}_1 \\ \vdots \\ \boldsymbol{\psi}_L(m,:)\mathbf{x}_L \end{bmatrix} + \begin{bmatrix} \mathbf{G}_1(m,:)\mathbf{w}_1 \\ \vdots \\ \mathbf{G}_L(m,:)\mathbf{w}_L \end{bmatrix} \end{aligned} \tag{2.13}$$

where

$$\boldsymbol{\psi}_i = \mathbf{G}_i\mathbf{H}_i, \quad 1 \leq i \leq L. \tag{2.14}$$

For the case of ZF detection, the matrix $\boldsymbol{\psi}_i$ equals the identity matrix. The L detector outputs corresponding to the spread signal of the m^{th} Tx antenna, $\mathbf{z}^{(m)}$, are de-spread during the next detection stage which results in

$$\begin{aligned} \mathbf{r}^{(m)} &= \mathbf{C}_L^{-1}\mathbf{z}^{(m)} \\ &= \mathbf{C}_L\acute{\mathbf{x}}^{(m)} + \mathbf{C}_L\acute{\mathbf{w}}^{(m)} \end{aligned} \tag{2.15}$$

where due to the orthogonality property of the Walsh-Hadamard spreading matrix

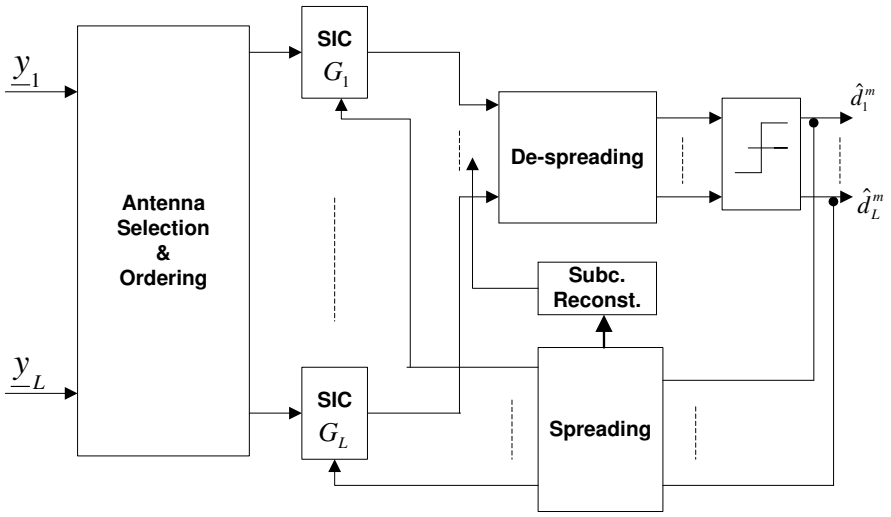

Figure 2.3: The block diagram of the proposed detector for SM-MC-CDM communications.

(2.2) $\mathbf{C}_L^{-1} = \mathbf{C}_L$. The l^{th} term of the vector $\mathbf{r}^{(m)}$ equals

$$\begin{aligned} r_l^{(m)} &= \sum_{i=1}^{L} |\mathbf{C}_{l,i}|^2 \boldsymbol{\psi}_i(m,m) d_l^{(m)} + \sum_{\substack{j=1 \\ j\neq l}}^{L} \sum_{i=1}^{L} \mathbf{C}_{l,i}\mathbf{C}_{i,j} \boldsymbol{\psi}_i(m,m) d_j^{(m)} \\ &+ \sum_{i=1}^{L} \sum_{n=1}^{L} \mathbf{C}_{l,i}\mathbf{C}_{i,n} \sum_{\substack{k=1 \\ k\neq m}}^{M} \boldsymbol{\psi}_i(m,k) d_n^{(k)} + \mathbf{C}(l,:)\acute{\mathbf{w}}^{(m)} \\ &= \frac{1}{L} \sum_{i=1}^{L} \boldsymbol{\psi}_i(m,m) d_l^{(m)} + \hat{w}_1^{(m)} + \hat{w}_2^{(m)} + \hat{w}_3^{(m)} \end{aligned} \tag{2.16}$$

where $\mathbf{C}_{l,i}$ denotes the element of the matrix $\mathbf{C}_L$ at the lth row and ith column. In (2.16), the first term corresponds to the desired symbol, the second term corresponds to inter-subcarrier interference from the same Tx antenna and the third term corresponds to the interference from other Tx antennas. The last term represents the channel noise and is a zero-mean Gaussian random variable with variance

$$\sigma^2_{\hat{w}_3^{(m)}} = \frac{\sigma_w^2}{L} \sum_{i=1}^{L} \mathbf{G}_i(m,:)\mathbf{G}_i^H(m,:). \tag{2.17}$$

For large ML products, according to the central limit theorem [62], the terms $\hat{w}_1$ and $\hat{w}_2$ can be approximated as samples of Gaussian random variables with zero mean and variances equal to

$$\sigma^2_{\hat{w}_1^{(m)}} = \frac{1}{L^2}\left(L\sum_{i=1}^{L}|\boldsymbol{\psi}_i(m,m)|^2 - |\sum_{i=1}^{L}\boldsymbol{\psi}_i(m,m)|^2\right),$$
$$\sigma^2_{\hat{w}_2^{(m)}} = \frac{1}{L}\left(\sum_{\substack{k=1\\k\neq m}}^{M}\sum_{i=1}^{L}|\boldsymbol{\psi}_i(m,k)|^2\right), \tag{2.18}$$

respectively. The derivations of variances in (2.17) and (2.18) are given in the Appendix A. Using (2.16), the SINR per symbol on each subcarrier is obtained as

$$\Gamma_l^{(m)} = \frac{\frac{1}{L^2}|\sum_{i=1}^{L}\boldsymbol{\psi}_i(m,m)|^2}{\sigma^2_{\hat{w}_1^{(m)}} + \sigma^2_{\hat{w}_2^{(m)}} + \sigma^2_{\hat{w}_3^{(m)}}}, \quad 1 \leq l \leq L \tag{2.19}$$

where $\Gamma_l^{(m)}$ denotes the SINR. Equation (2.19) reveals that $\Gamma_l^{(m)}$ is independent of the subcarrier index l and only depends on the choice of the Tx antenna index, m. Therefore our detection strategy begins with finding the first Tx antenna, m_1, such that

$$m_1 = \arg\max_m \Gamma_l^{(m)}. \tag{2.20}$$

This is similar to the V-BLAST detector, for which it has been shown that the optimum detection strategy for successive interference cancellation type of receiver is to choose the signal with the highest post detection SNR at each detection stage [63]. After finding m_1 according to (2.20), its corresponding L data substreams are detected, spread and canceled from the received signal (2.8). For the next substream to be detected, the $\mathbf{H}_l$ matrices are updated by replacing their m_1^{th} column with the all zero column vector and re-evaluating the $\mathbf{G}_l$ matrices. The same procedure is followed to find the data of the subsequent substreams, i.e. $\{m_2, \ldots, m_M\}$. In the numerical results section, we show the performance superiority of MMSE unified SIC for SM-MC-CDM over MMSE V-BLAST for spatially multiplexed MIMO-OFDM, i.e., a MIMO-OFDM system where MMSE V-BLAST is adopted on each subcarrier, independently.

2.3.1 Increasing the detection reliability by iterative subcarrier reconstruction-detection

In this section we consider detecting the data on each spatial layer using iterative subcarrier reconstruction-detection (ISRD) [42, 41]. The ISRD algorithm increases

the reliability of detection which itself further improves the overall system performance. The ISRD algorithm requires subcarrier detection ordering before subcarrier reconstruction. From equation (2.19) it is evident that the SINRs of all subcarriers are equal at the first reconstruction stage, however, any subcarrier chosen in the first stage will effect the SINR of the remaining subcarriers at the next ISRD stage. To find the subcarrier reconstruction ordering, let's assume that the detector is at the i^{th} stage of ISRD ($2 \leq i \leq L$) where we have reconstructed $i-1$ subcarriers and need to obtain the SINR on the remaining $L-i+1$ subcarriers. Consider the following vector at the i^{th} stage of ISRD,

$$\mathbf{z}^{(m_1),i} = \left[\mathbf{z}^{(m_1),i-1}\right]^{-l_i} + \left[\mathbf{C}\hat{\mathbf{d}}^{(m_1),i-1}\right]^{+l_i} \tag{2.21}$$

where $[\,.\,]^{-k}$ is an operator that sets the k^{th} element of its vector argument to zero and leaves the other elements unchanged. Also $[\,.\,]^{+k}$ is an operator that sets all elements of its vector argument to zero except the k^{th} element. In (2.21), l_i denotes the subcarrier index which is going to be reconstructed at the i^{th} stage of the ISRD. The initial values for the vectors in the above recursive equation are

$$\mathbf{z}^{(m_1),0} = \mathbf{z}^{(m_1)}, \quad \hat{\mathbf{d}}^{(m_1),0} = \mathcal{Q}\left(\mathbf{r}^{(m_1)}\right) \tag{2.22}$$

where $\mathcal{Q}(\cdot)$ denotes the quantization operation. The vector $\hat{\mathbf{d}}$ is updated according to

$$\hat{\mathbf{d}}^{(m_1),i} = \mathcal{Q}\left(\mathbf{C}\mathbf{z}^{(m_1),i-1}\right), \quad 2 \leq i \leq L. \tag{2.23}$$

Assuming the l^{th} element of $\mathbf{z}^{(m_1),i}$ is to be reconstructed, ($l_i = l$), we have

$$\begin{aligned} r_l^{(m_1),i} &= \mathbf{C}(l,:)\mathbf{z}^{(m_1),i} \\ &= \sum_{i_1 \in \mu_i} \mathbf{C}_{l,i_1} \left[\mathbf{C}\hat{\mathbf{d}}^{(m_1),i}\right]^{+i_1} + \sum_{i_2 \in \mu_i^c} \mathbf{C}_{l,i_2} \boldsymbol{\psi}_{i_2}(m_1,:)\mathbf{x}_{i_2} \\ &+ \sum_{i_3 \in \mu_i^c} \mathbf{C}_{l,i_3} \mathbf{G}_{i_3}(m_1,:)\mathbf{w}_{i_3} \end{aligned} \tag{2.24}$$

where the set $\mu_i = \{l_1, l_2, \ldots, l_i\}$ and μ_i^c is the complement set of μ_i such that $\mu_i \cup \mu_i^c = \{1, \ldots, L\}$. As an initial value, the set μ_i is empty, i.e., $\mu_0 = \{\}$. After

some manipulation, the following expression is obtained

$$
\begin{aligned}
r_l^{(m_1),i} &= \underbrace{\frac{1}{L}\left(i + \sum_{i_2 \in \mu_i^c} \boldsymbol{\psi}_{i_2}(m_1, m_1)\right)}_{\zeta} d_l^{(m_1)} \\
&+ \underbrace{\sum_{\substack{t=1 \\ t \neq l}}^{L} d_t^{(m_1)} \left(\sum_{i_1 \in \mu_i} \mathbf{C}_{l,i_1}\mathbf{C}_{i_1,t} + \sum_{i_2 \in \mu_i^c} \boldsymbol{\psi}_{i_2}(m_1, m_1)\mathbf{C}_{l,i_2}\mathbf{C}_{i_2,t}\right)}_{\tilde{w}^1_{m_1,i}} \\
&+ \underbrace{\sum_{i_2 \in \mu_i^c} \mathbf{C}_{l,i_2} \sum_{\substack{i_2'=1 \\ i_2' \neq m}}^{M} \boldsymbol{\psi}_{i_2}(m_1, i_2') \sum_{q=1}^{L} \mathbf{C}_{i_2,q} d_q^{i_2'}}_{\tilde{w}^2_{m_1,i}} \\
&+ \underbrace{\sum_{i_3 \in \mu^c} \mathbf{C}_{l,i_3}\mathbf{G}_{i_3}(m_1, :)\mathbf{w}_{i_3}}_{\tilde{w}^3_{m_1,i}} + \tilde{w}_e \\
&= \zeta d_l^{(m_1)} + \tilde{w}^1_{m_1,i} + \tilde{w}^2_{m_1,i} + \tilde{w}^3_{m_1,i} + \tilde{w}_e.
\end{aligned}
\tag{2.25}
$$

In (2.25) the first term corresponds to the transmitted symbol of the first substream on the l^{th} subcarrier, $\tilde{w}^1_{m_1,i}$ denotes the inter-subcarrier interference, $\tilde{w}^2_{m_1,i}$ denotes the interference from other substreams and $\tilde{w}^3_{m_1,i}$ denotes the channel noise. The subscript i denotes the i^{th} stage of the ISRD algorithm. The last term denotes the effect of errors in previous detection-reconstruction stages. Here we assume there has been no errors in the previous stages and set $\tilde{w}_e = 0$. This is an optimistic assumption, however, it makes the analysis tractable. Using the above expression the SINR of the l^{th} subcarrier ($l \in \mu_i^c$) is obtained as

$$
\Gamma_l^{(m_1),i} = \frac{\frac{1}{L^2}\left|i + \sum_{i_2 \in \mu_i^c} \boldsymbol{\psi}_{i_2}(m_1, m_1)\right|^2}{\sigma^2_{\tilde{w}^1_{m_1,i}} + \sigma^2_{\tilde{w}^2_{m_1,i}} + \sigma^2_{\tilde{w}^3_{m_1,i}}} \tag{2.26}
$$

where the variances in the denominator of (2.26) can be derived similarly to the derivation of variances (2.17) and (2.18) (given in Appendix A), and are as follows

$$
\begin{aligned}
&\sigma^2_{\tilde{w}^1_{m_1,i}} = \\
&\sum_{\substack{t=1 \\ t \neq l}}^{L} \left|\left(\sum_{i_1 \in \mu_i} \mathbf{C}_{l,i_1}\mathbf{C}_{i_1,t} + \sum_{i_2 \in \mu_i^c} \boldsymbol{\psi}_{i_2}(m_1, m_1)\mathbf{C}_{l,i_2}\mathbf{C}_{i_2,t}\right)\right|^2,
\end{aligned}
\tag{2.27}
$$

$$\sigma^2_{\tilde{w}^2_{m_1,i}} = \sum_{\substack{q=1 \\ q\neq m_1}}^{M} \sum_{i_2\in\mu_i^c} \sum_{i_2'\in\mu_i^c} \mathbf{C}_{l,i_2}\mathbf{C}_{l,i_2'}\boldsymbol{\psi}_{i_2}(m_1,q)\boldsymbol{\psi}^H_{i_2'}(m_1,q), \tag{2.28}$$

$$\sigma^2_{\tilde{w}^3_{m_1,i}} = \frac{\sigma_w^2}{L} \sum_{i_3\in\mu_i^c} \|\mathbf{G}_{i_3}(m_1,:)\|^2. \tag{2.29}$$

The denominator of (2.26) can be approximated to equal to $\sigma^2_{\tilde{w}^3_{m_1,i}}$. This approximation is valid since for low SNRs the channel noise is the dominant term compared to the interference, for high SNRs the interference terms approach zero in limit and simulation results have shown for moderate SNR region, $\tilde{w}^3_{m_1,i}$ is still the dominant term. Therefore, only $\sigma^2_{\tilde{w}^3_{m_1,i}}$ will be considered in the denominator of (2.26). In addition, by using the following approximation in the numerator of (2.26),

$$\left| i + \sum_{i_2\in\mu_i^c} \boldsymbol{\psi}_{i_2}(m_1,m_1) \right| \approx L, \tag{2.30}$$

the SINR expression given in (2.26) is simplified to

$$\Gamma_l^{(m_1),i} \approx \frac{L}{\sigma_w^2 \sum_{i_3\in\mu_i^c} \|\mathbf{G}_{i_3}(m_1,:)\|^2}. \tag{2.31}$$

Simulation results have also shown that the approximation in the numerator of (2.26) has a negligible effect on the system performance. When using ZF detectors, the matrices $\boldsymbol{\psi}_i$ equal the identity matrix, which when substituted in equations (2.27-2.28) yields $\sigma^2_{\tilde{w}^1_{m_1,i}} = 0$ and $\sigma^2_{\tilde{w}^2_{m_1,i}} = 0$. Therefore, (2.31) turns into equality when ZF detectors are adopted. The set μ_i^c contains the indices of the $L-i$ subcarriers, which have not been reconstructed yet. The i^{th} subcarrier to be reconstructed is chosen from the set μ_{i-1}^c such that the SINR of the remaining subcarriers, as given in (2.31), is maximized. This choice of subcarrier selection results in lower probability of error for the symbols on the consecutive subcarriers compared to the case where the symbols are being detected jointly after de-spreading. In other words, the i^{th} subcarrier should be selected from the set μ_{i-1}^c so that

$$\sum_{i_3\in\mu_i^c} \|\mathbf{G}_{i_3}(m_1,:)\|^2. \tag{2.32}$$

is minimized. This minimization requires reconstructing the subcarrier with the maximum value of $\|\mathbf{G}_{i_3}(m_1,:)\|^2$ at each stage as it is removed from the set μ_{i+1}^c in the next stage. After reconstructing all subcarriers and detecting the data of

the ${m_1}^{th}$ antenna, they are de-spread and subtracted out from the received signal vector on all subcarriers. For detecting the remaining $M-1$ data substreams the same procedure is followed were at the k^{th} stage, the matrices $\mathbf{H}_i,\ 1 \leq i \leq L$ are updated by substituting their ${m_{k-1}}^{th}$ column with all zero vector and re-evaluating the $\mathbf{G}_i$s. The complete detection algorithm in the form of a recursive procedure can be described as follows.

- Initialization ($k = 1$):
  - Using (2.20), find m_1, the first antenna for which data are to be detected.
  - Use ISRD algorithm to detect the data of the first antenna.
- Recursive procedure (while $k < M$):
  - To detect the data of the k^{th} antenna (m_k), spread the detected data of antenna m_{k-1} and subtract out the channel signature on the detected data multiplied by the detected data itself from the received signal on all subcarriers (unified SIC).
  - Update the channel matrices, $\mathbf{H}_l$s, by exchanging their ${m_{k-1}}^{th}$ column by an all zero column vector, followed by evaluating each subcarrier's corresponding MIMO detector, i.e., $\mathbf{G}_l$, and then $\boldsymbol{\psi}_l$ for $1 \leq l \leq L$.
  - Use ISRD algorithm to detect the data of the ${m_k}^{th}$ antenna.
  - Find m_{k+1} using (2.20).
- The ISRD algorithm:
  1. Start with the initial values given in (2.22).
  2. At the i^{th} stage ($1 \leq i \leq L$), find n_i, which is the index of the subcarrier with the highest value of $\|\mathbf{G}_{i_3}(m_k, :)\|^2$ for $i_3 \in \mu_{i-1}^c$.
  3. Evaluate $\mathbf{z}^{(m_k),i}$ followed by $\hat{\mathbf{d}}^{(m_k),i}$ using (2.21) and (2.23), respectively.
  4. Update the sets μ_i and μ_i^c and repeat steps 2 and 3 while $i \leq L$.
  5. The final output detected vector of the k^{th} Tx antenna is $\hat{\mathbf{d}}^{m_k,L}$.
- Detect the data of the Mth antenna using ISRD, following the steps described above.

2.3.2 Detector complexity

In [64] and [65] the complexity of V-BLAST for an $M \times M$ single carrier MIMO system in terms of the average number of arithmetic operations is given as $\mathcal{O}(M^4)$. As discussed in Section 2.2.1, for SM-MC-CDM system the complexity of the optimum ML detector is $\mathcal{O}(\delta^{LM})$. Our proposed detection scheme consists of two major steps, which are unified SIC and ISRD and its complexity comes mainly from these two steps. The complexity of the unified SIC is approximately equal to the complexity of L parallel V-BLAST detectors. However, in practice due to the fact that in unified SIC, the SINRs of all L subcarriers are evaluated using (2.19) and not independently over each subcarrier, the unified SIC has a slightly lower complexity than $\mathcal{O}(LM^4)$. The complexity of ISRD comes mainly from two matrix multiplications, which both involve multiplication of the matrix $\mathbf{C}_L$ by a vector. Since the matrix $\mathbf{C}_L$ has only ± 1 elements, the complexity of multiplying $\mathbf{C}_L$ by a vector is approximately determined by L addition operations (multiplication of elements with -1 is simply a change of sign). Since the two multiplication steps in ISRD process are repeated L times, the complexity of ISRD for each substream is $\mathcal{O}(2L^2)$. Then the overall complexity of the proposed scheme is approximately $\mathcal{O}(LM^4 + 2ML^2)$. This order of complexity is significantly lower than the complexity of ML detector for the constellation size, number of subcarriers and number of antennas adopted in this study.

Table 2.1 compares the complexity of different types of detectors for SM-MC-CDM in terms of the average number of arithmetic operations (real additions and

Table 2.1: Complexity comparison of different detection schemes for SM-OFDM and SM-MC-CDM over i.i.d. Rayleigh fading channel.

Detection Scheme	Average number of arithmetic operations[1]
SM-OFDM with ZF on each subcarrier	$298 \times 4 = 1192$
SM-OFDM with MMSE on each subcarrier	$812 \times 4 = 3248$
SM-OFDM with ZF-SIC per subcarrier	$748 \times 4 = 3136$
SM-OFDM with MMSE-SIC per subcarrier	$1284 \times 4 = 5136$
SM-MC-CDM with ZF-LRA (complex LLL)	$\approx 11 \times 10^4$
Proposed scheme (MMSE unified SIC + ISRD)	$\approx 4 \times 1284 + 2 \times 4^2 = 5168$
SM-MC-CDM with MLD	$\approx 4 \times 10^9$

[1]Both systems considered have $L = 4$ subcarriers, $M = N = 4$ antennas and use QPSK modulation. Except for the last two schemes, the values in this column have been taken from [54, 59].

multiplications) for a system with $M = N = 4$ antennas and $L = 4$ subcarriers with QPSK modulation. Note that for SM-MC-CDM with ZF-LRA and also MLD, the system model given in (2.9) with size 16×16 channel matrix ($\boldsymbol{\mathcal{H}}$) has been considered. In addition to complexity memory requirement of each detector could also be considered, which is beyond the scope of this thesis.

2.3.3 Coded SM-MC-CDM

Channel coding can be implemented in an SM-MC-CDM system either by cascading a channel encoder with an SM-MC-CDM transmitter or by incorporating channel coding into SM-MC-CDM transmission. From these two possibilities, we consider the latter one where spatial layers (substreams) are independently encoded. This combination is particularly of interest to us, since (as it is shown in Section V) by incorporating channel coding into our proposed SM-MC-CDM detector, a better performance compared to other alternatives is achieved. We assume a length JML coded block when using J-QAM modulation, such that one coded block can be transmitted during one SM-MC-CDM symbol time. Figures 2.4 and 2.5 show the proposed coded SM-MC-CDM transmitter and receiver block diagrams, respectively. As a case example we consider QPSK modulation and rate 1/2 punctured turbo code. For this example, we assume a size $M \times L$ information data vector $\mathbf{u}$ to be transmitted. Vector $\mathbf{u}$ is parallelized into M substreams. Each substream is encoded and the resulting encoded bits, $\mathbf{v}^{(m)}$, along with the information bits, $\mathbf{u}^{(m)}$, interleaved and mapped to QPSK constellation. At the receiver side, we have incorporated the turbo decoding with the unified SIC algorithm. In Fig. 2.4 the

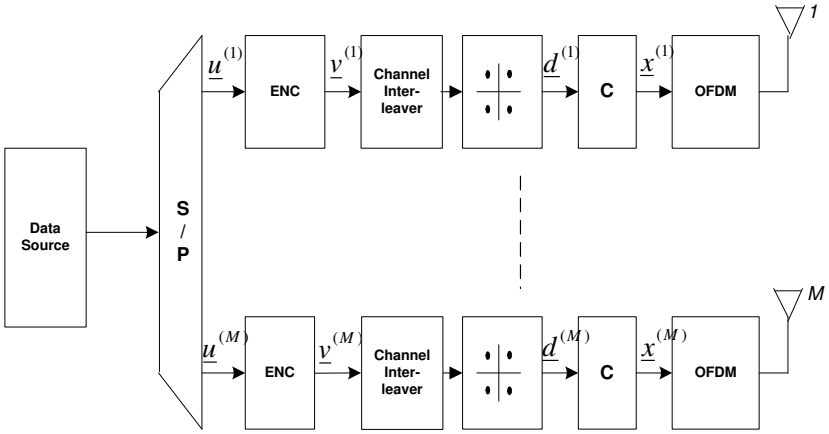

Figure 2.4: Block diagram of proposed coded SM-MC-CDM transmitter.

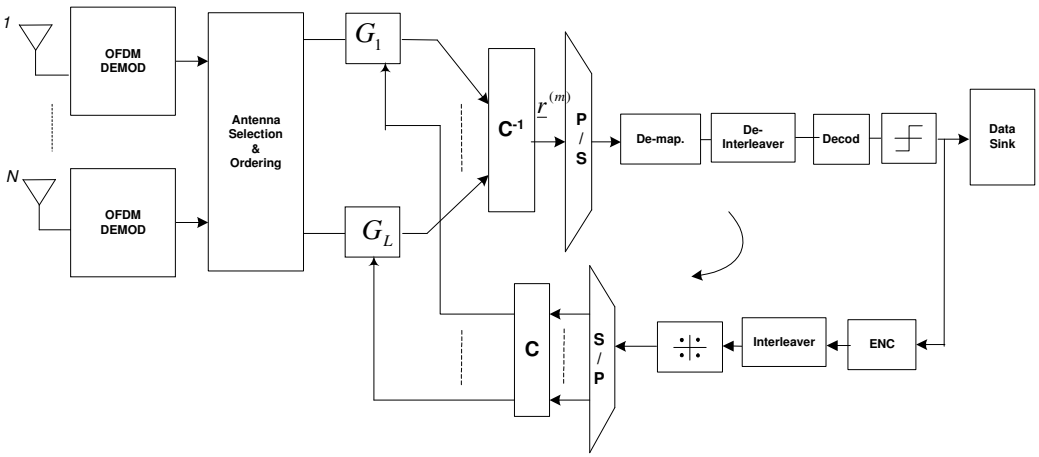

Figure 2.5: Block diagram of the proposed coded SM-MC-CDM receiver.

vectors $\mathbf{u}^{(m)}$ and $\mathbf{v}^{(m)}$ denote uncoded and coded bit vectors of the m^{th} substream, respectively. To obtain the log-likelihood ratio (LLR) for each information bit at the output of the turbo decoder considered in this work, the received vector at the output of the channel de-interleaver consists of systematic and parity bit pairs in the following form

$$\mathbf{r}^{(m)} = \left[\hat{u}_1^{(m)} \;\; \hat{v}_1^{(m)} \;\ldots\; \hat{u}_l^{(m)} \;\; \hat{v}_l^{(m)} \ldots \hat{u}_L^{(m)} \;\; \hat{v}_L^{(m)}\right]^T, \tag{2.33}$$

for the mth substream. The LLR for the lth received information bit of the mth substream is

$$\mathcal{L}(\hat{u}_l^{(m)}) = \log\left(\frac{P(u_l^{(m)} = +1|\mathbf{r}^{(m)})}{P(u_l^{(m)} = -1|\mathbf{r}^{(m)})}\right). \tag{2.34}$$

To calculate the LLR value using the trellis diagram, (2.34) is modified to the following expression [66]

$$\mathcal{L}(\hat{u}_l^{(m)}) = \log\left(\frac{\sum\limits_{(s,s',u_l^{(m=+1)})} \alpha_{l-1}^{(m)} \cdot \gamma_l^{(m)}(s,s') \cdot \beta_l^{(m)}}{\sum\limits_{(s,s',u_l^{(m=-1)})} \alpha_{l-1}^{(m)} \cdot \gamma_l^{(m)}(s,s') \cdot \beta_l^{(m)}}\right). \tag{2.35}$$

s and s' denote the encoder states where the bit $u_l^{(m)}$ is associated with the transition from state s to s'. The metrics $\alpha_{l-1}^{(m)}$ and $\beta_l^{(m)}$ are obtained using forward and backward recursive calculations (BCJR algorithm) [66]. The state transition metric, $\gamma_l^{(m)}(s,s')$, depends on the received channel values and the a priori probability of the information bit, $u_l^{(m)}$. Equation (2.35) can be further simplified to

$$\mathcal{L}(\hat{u}_l^{(m)}) = L_c r_l^{(m)} + \mathcal{L}_a(u_l^{(m)}) + \mathcal{L}_e(u_l^{(m)}) \tag{2.36}$$

where the channel reliability factor, L_c, is given by

$$L_c = 4a^{(m)}\xi^{(m)}. \tag{2.37}$$

In (2.37) we have

$$\xi^{(m)} = \frac{E\{|d_l^{(m)}|^2\}}{\sigma^2_{\hat{w}_1^{(m)}} + \sigma^2_{\hat{w}_2^{(m)}} + \sigma^2_{\hat{w}_3^{(m)}}}, \;\; a^{(m)} = \frac{1}{L}\sum_{i=1}^{L}\psi_i(m,m). \tag{2.38}$$

The interference and noise variances in the denominator of the expression given for $\xi^{(m)}$ have been given in (2.17) and (2.18). $\psi(m,m)$s are the mth diagonal elements of the matrices defined in (2.14). The a priori probability ratio for bit $\hat{u}_l^{(m)}$ is

$$\mathcal{L}_a(u_l^{(m)}) = \frac{Pr(u_l^{(m=+1)})}{Pr(u_l^{(m=-1)})}. \tag{2.39}$$

The last term in (2.36) denotes the extrinsic information value and equals

$$\mathcal{L}_e(u_l^{(m)}) = \log\left(\frac{\sum\limits_{(s,s',u_l^{(m=+1)})} \tilde{\gamma}_{l_e}^{(m)}(s,s') + \tilde{\alpha}_{l-1}(s') + \tilde{\beta}_l(s)}{\sum\limits_{(s,s',u_l^{(m=-1)})} \tilde{\gamma}_{l_e}^{(m)}(s,s') + \tilde{\alpha}_{l-1}(s') + \tilde{\beta}_l(s)}\right) \tag{2.40}$$

where the tilde above symbols denotes the logarithm of the respective values. $\tilde{\gamma}_{l_e}^{(m)}$ is obtained using the received parity bit, $\hat{v}_l^m$, and the parity bit associated with the state transition from s to s', and is given by

$$\tilde{\gamma}_{l_e}^{(m)} = \log\left(\frac{1}{2}L_c\hat{v}_l^{(m)}v_l^{(m)}\right). \tag{2.41}$$

After a number of iterations, the log-MAP decoder provides soft estimates of the decoded information bits. The final detection stage is making a hard decision on the decoded soft output values. In our study we have considered RSC(7,5) code [67] with 5 iterations of turbo decoding.

2.4 Numerical Results

In this section, the numerical results for different numbers of antennas, subcarriers and different detection schemes are presented. We consider equal numbers of Tx and Rx antennas in our study, i.e. $M = N$. Throughout this section the uncorrelated channel model refers to the channel where $\mathbf{H}_l$'s are white ZMCSCG with the variance of 0.5 per dimension. For the case of the correlated channel model, the channel

parameters are taken from [45]. $\mathbf{R}_t$ and $\mathbf{R}_r$ are Teoplitz matrices with entries $\mathbf{R}_t(i,j) = \rho^{|i-j|},\ i,j \leq M = N$, and $\mathbf{R}_r(i,j) = \rho^{|i-j|},\ i,j \leq M = N$. ρ denotes spatial correlation factor and we assume $\rho = 0.7$. The path correlation matrix, $\mathbf{R}_p$, is defined as

$$\mathbf{R}_p(m,n) = \sqrt{\gamma_m}\sqrt{\gamma_n}\lambda^{|m-n|} \tag{2.42}$$

in which we assume the path correlation factor, λ, to be equal to 0.8. The parameters $\{\gamma_m\}_{m=1}^{P}$ are such that $\gamma_m/\gamma_{m+1} = 3$ dB for $m = 1, \ldots, P-1$ and $\sum_{m=1}^{P}\gamma_m = 1$. The matrix $\mathbf{R}_p$ has $\{\gamma_1, \ldots, \gamma_P\}$ on its main diagonal. The parameter P denotes the total number of paths and we assume $P = 6$ in our study. Quasi-static fading channel is considered where the channel tap gains change independently according to the Rayleigh distribution from one OFDM block to the next. The bit error rate (BER) of the overall system is obtained with respect to E_b/N_0 where E_b is the data bit energy and N_0 is the noise one sided power spectral density. The channel is assumed to be known at the receiver.

2.4.1 Performance of different types of detectors for SM-MC-CDM

Fig. 2.6 shows the BER performance of different detectors for SM-MC-CDM communication system over the uncorrelated 4×4 MIMO channel with $L = 16$ subcarriers. ZF V-BLAST detection of the received signal over each subcarrier has a relatively poor performance due to the noise enhancement property of ZF detection and the fact that a decision has to be made on the data before de-spreading. The proposed ZF detector achieves about 8 dB gain in E_b/N_0 over the ZF V-BLAST detector at the BER of 10^{-3}. Comparing the performance of the proposed ZF detector to the unified SIC detector, BER reduction due to the application of ISRD is evident. At the 10^{-3} BER, the proposed ZF detector achieves about 4 dB gain in E_b/N_0 compared to the unified SIC.

It is also evident from Fig. 2.6 that the proposed MMSE detector has a significant performance advantage over SM-OFDM with per-subcarrier MMSE detection. Here, in addition to a great coding gain, an additional diversity gain has also been achieved. In fact, comparing the proposed detector's performance with the BER of a system with diversity order of 4, it is evident that full diversity of $N = 4$ is achieved. This result is important, because for spatially multiplexed OFDM systems without frequency domain spreading and with linear ZF or MMSE processors on each subcarrier the maximum diversity order that can be achieved is $N - M + 1$ [3].

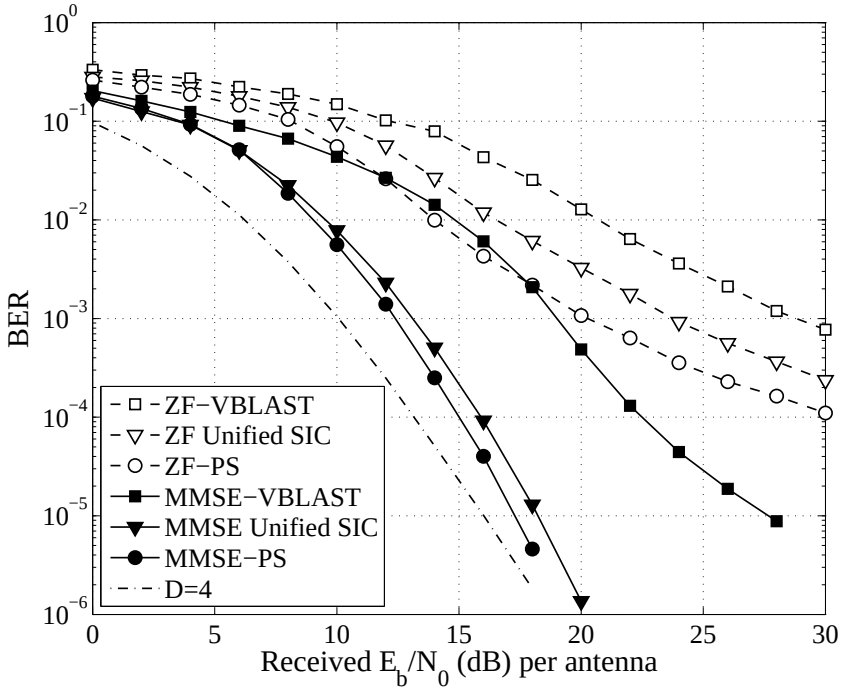

Figure 2.6: Performance of different detectors over a 4×4 uncorrelated MIMO channel with $L = 16$ subcarriers and QPSK mapping. "PS" denotes "Proposed Scheme". The plot labeled D=4 is the BER curve of a QPSK system with diversity order of 4.

Fig. 2.7 depicts the performance of different detectors over the MIMO channel with antenna and path correlations. Once again the proposed detector achieves a better performance than the V-BLAST detectors. However, due to correlation there is a penalty in performance compared to the uncorrelated case. Comparing the performance of the ZF linear detector with the proposed ZF detector, the proposed detector has about 6.5 dB gain at the BER of 10^{-2}. The SNR advantage of the proposed MMSE detector over other aforementioned detectors with MMSE criterion is also significant. At SNR of 25 dB the proposed detector achieves around two orders of magnitude performance improvement over the MMSE V-BLAST. Although the diversity order of the proposed detector has been reduced due to the channel correlations, still diversity order of almost 4 has been achieved.

2.4.2 Performance of the proposed detector with different numbers of antennas and subcarriers

Fig. 2.8 compares the BER of an SM-MC-CDM system with $M = N = 4$ antennas and with different numbers of subcarriers when using the proposed detector on the

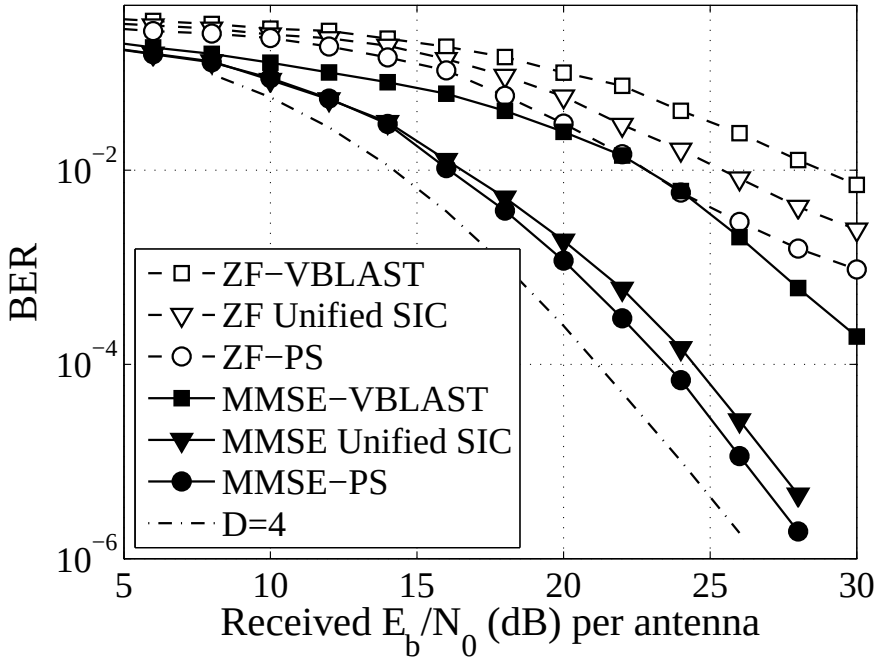

Figure 2.7: Performance of different detectors over a 4×4 correlated MIMO channel with $L = 16$ subcarriers, $\rho = 0.7$, $\lambda = 0.8$ (2.42) and QPSK modulation. The plot labeled D=4 represents the BER of a QPSK system with diversity order of 4 shifted 8 dB to the right for easy comparison.

uncorrelated fading channel. From the figure it can be seen that by increasing the number of subcarriers, thanks to the diversity and coding gains extracted by the proposed detector, the performance has improved. At the BER of 10^{-4} increasing the number of subcarriers from $L = 2$ to $L = 8$ results in 2 dB gain in E_b/N_0. Additional 1 dB gain is achieved by increasing the number of subcarriers to $L = 32$. The increase in the number of subcarriers from $L = 32$ to $L = 256$ results in a small performance improvement only at high SNRs.

In Fig. 2.9 the BER performance of SM-MC-CDM systems with different numbers of antennas and subcarriers is compared. The results are obtained with the proposed detector over the uncorrelated channel. $M = N = 2$ and $M = N = 4$ have been considered. In both cases, the increase in the number of subcarriers results in better BER performance. In single carrier MIMO link with equal number of Tx and Rx antennas, the performance of the V-BLAST detector improves with increasing number of antennas thanks to additional diversity offered by the increase in the number of Rx antennas. Fig. 2.9 shows that with the proposed detector and

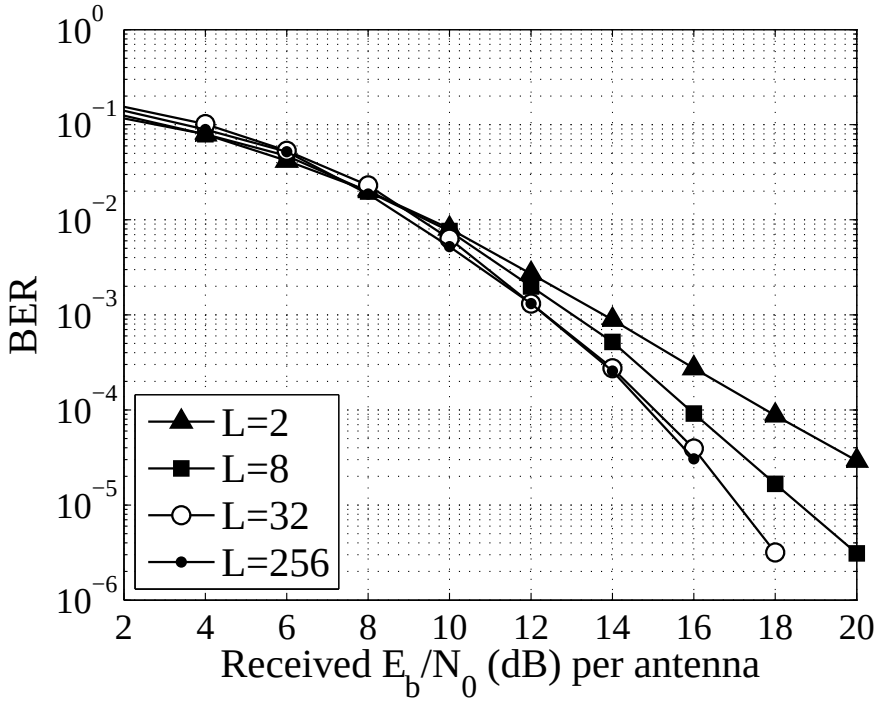

Figure 2.8: Performance of the proposed detector in SM-MC-CDM system with different numbers of subcarriers over uncorrelated 4×4 MIMO channel.

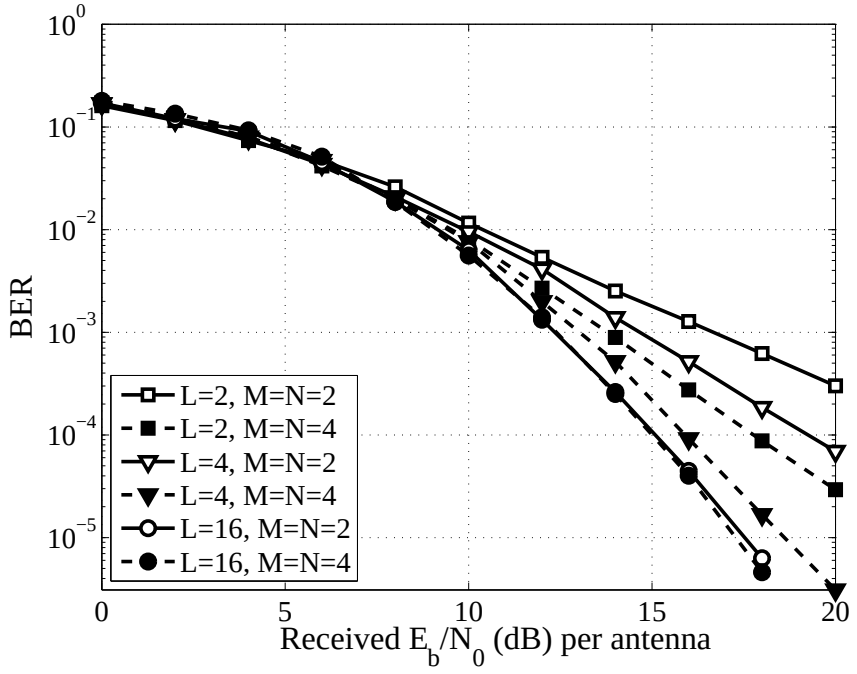

Figure 2.9: Performance of the proposed detector in an SM-MC-CDM system with different numbers of antennas and subcarriers over uncorrelated MIMO channel.

due to frequency domain spreading, the 2×2 MIMO transmission is able to achieve almost the same performance as the 4×4 MIMO transmission, both having $L = 16$ subcarriers. Intuitively, for larger L it is expected that the performance of both systems would be identical up to an increasing SNR value dependent on the number of subcarriers, L.

2.4.3 Performance of the proposed coded SM-MC-CDM system

Fig. 2.10 compares the performance of the proposed turbo coded SM-MC-CDM system shown in Figs. 2.4 and 2.5 for two values of L over uncorrelated and correlated channels. Turbo coding of each substream combined with unified SIC has been able to reduce the system BER significantly. With $L = 64$ subcarriers and for the uncorrelated and correlated channels at the BER of 10^{-5}, the proposed coded scheme has been able to achieve 8.6 dB and 10.3 dB gain over the uncoded unified SIC detector, respectively. As expected, increasing L results in additional frequency

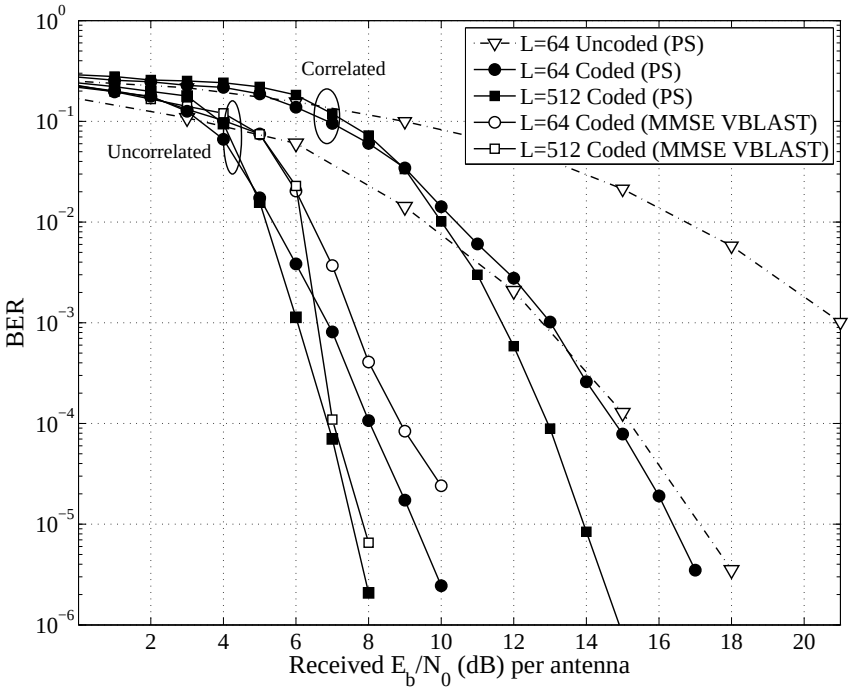

Figure 2.10: Performance of turbo coded SM-MC-CDM with $L = 64$ and $L = 512$ subcarriers over the uncorrelated and correlated 4×4 MIMO channels. PS denotes the proposed scheme. The scheme denoted as Coded (MMSE V-BLAST) refers to concatenation of turbo encoding with SM-OFDM at Tx, and per subcarrier MMSE V-BLAST with turbo decoding at Rx.

domain diversity and also increases the turbo code interleaver size, and as a result the system performance improves. For the case of the correlated channel with $L = 512$, the effect of a larger interleaver size increases the SNR gain to 2.4 dB at the BER of 10^{-5} over the system with $L = 64$ subcarriers. At BER of 10^{-5}, the system having $L = 512$ subcarriers achieves 1.7 dB gain in E_b/N_0 over the system with $L = 64$ subcarriers, both operating on a 4×4 uncorrelated MIMO channel. BER of the proposed turbo encoded SM-MC-CDM system is also compared to the performance of a turbo encoded SM-OFDM system, which uses MMSE V-BLAST detectors on each subcarrier. The figure shows that the proposed scheme achieves a lower BER compared to the SM-OFDM system. The performance advantage of the proposed scheme is more significant for a smaller number of subcarriers and shorter channel codes.

2.5 Summary

This chapter has proposed a reduced complexity sub-optimal detection method for a spatially multiplexed multicarrier code division multiplexing link. The proposed detector's performance has been compared to the performance of a number of reduced complexity detectors described in the literature. It has been shown that the proposed detector for SM-MC-CDM, which uses a linear processor on each subcarrier, is able to achieve diversity order of MLD applied independently on individual subcarriers of SM-OFDM. Performance of the coded SM-MC-CDM system evaluated numerically shows that frequency domain spreading used in SM-MC-CDM is effective in improving the system performance, and the performance gain due to spreading is more significant for short (weaker) channel codes.

Chapter 3

Performance of Spatially Multiplexed MC-CDM with Zero-Forcing Unified Successive Interference Cancellation Detection

3.1 Introduction

A unified successive interference cancellation detector for SM-MC-CDM was proposed in Chapter 2. In this chapter we examine its performance more thoroughly using analytical performance evaluation methods. The performance of single carrier V-BLAST has been studied in a number of papers [68, 69]. To the best of our knowledge, the exact analytical solution for the performance of V-BLAST system for arbitrary number of Tx and receive (Rx) antennas has not been found yet. The difficulty in the analysis of V-BLAST comes mainly from two sources. One is the effect of error propagation from each detected layer to the subsequent ones. When considering the optimum ordering of spatial layers adopted by V-BLAST, the correlation which exists between the post-detection SNR of different layers is the second factor, which makes the analysis difficult. Nevertheless, for some specific numbers of antennas good approximate analytical solutions have been found.

In [68], closed form analytical expressions have been derived for ZF V-BLAST detector which take into account the effect of error propagation for an arbitrary number of Tx and Rx antennas. However, [68] has not considered the effect of ordering. [70, 71] have considered the effect of ordering and SNR correlation on the

system performance for the case of $2 \times N$, where N is the number of Rx antennas. Still, the effect of error propagation has not been considered in those analyses. In [72], the performance of $2 \times N$ ordered ZF and MMSE SIC has been evaluated, once again without considering error propagation. In [69], by using an asymptotic approach the authors have shown that for the general case of M Tx and N Rx antennas the diversity order of both ZF and MMSE V-BLAST equals $N - M + 1$.

In this chapter, we approximate the probability density function (PDF) of inverse post-detection SNR for ZF U-SIC, assuming perfect CSI at the receiver and equal number of transmit and receive antennas. It is shown that a very close approximation for the PDF of the inverse of post-detection SNR is the inverse-gamma distribution [73]. As a result, the distribution of post-detection SNR is approximated by gamma distribution. The unknown parameters of the inverse-gamma distribution are obtained using maximum likelihood (ML) estimation [74]. The approximation is then used to obtain the PDF of post detection SNR. It is shown that these parameters depend on the number of subcarriers used in the SM-MC-CDM system.

Using the PDF of post-detection SNR, an analytical upper-bound is derived for the probability of error, which is used to obtain the diversity order. It is shown that SM-MC-CDM with ZF U-SIC is able to reach a diversity order slightly greater than $N - M + 1$, which is the maximum diversity order achieved using V-BLAST detectors over each subcarrier of spatially multiplexed MIMO-OFDM. The diversity order of SM-MC-CDM increases with increasing number of subcarriers. However, as we will explain later, the ergodic capacity of the system decreases with increasing number of subcarriers.

3.2 Post-Processing SNR for ZF Unified-SIC

3.2.1 Preliminaries

In this subsection some preliminaries are provided which later will be used to approximate the PDF of post detection SNR. Using (2.19) for the post processing SNR

of ZF U-SIC we have

$$\begin{aligned}\gamma^{(m)} &= \frac{LE_s}{M\sigma_n^2 \sum_{l=1}^{L} \mathbf{G}_l(m,:)\mathbf{G}_l(m,:)^H} \\ &= \frac{\frac{E_s}{M\sigma_n^2}}{\frac{1}{L}\sum_{l=1}^{L}\left[\mathbf{G}_l\mathbf{G}_l^H\right]_{mm}} \\ &= \frac{\frac{E_s}{M\sigma_n^2}}{\frac{1}{L}\sum_{l=1}^{L}\left[(\mathbf{H}_l^H\mathbf{H}_l)^{-1}\right]_{mm}}\end{aligned} \tag{3.1}$$

where $[\mathbf{U}]_{mm}$ denotes the mth diagonal term of the matrix $\mathbf{U}$.

The QR decomposition of each of the $\mathbf{H}_l$ matrices results in

$$\mathbf{H}_l = \mathbf{Q}_l\mathbf{R}_l, \quad N \geq M \tag{3.2}$$

where

$\mathbf{R}_l$ is an $M \times M$ upper triangular matrix with real diagonal elements and $\mathbf{Q}_l$ is an $N \times M$ matrix with orthonormal columns.

The following theorems will be used in the next subsection to derive the PDF of post-processing SNR. The first theorem can be found in [75].

Theorem 1: Let $\mathbf{H}$ be an $N \times M$ standard complex Gaussian matrix (i.i.d. complex zero-mean Gaussian entries with identical variances of $\frac{1}{M}$) and $N \geq M$. Denote its QR decomposition by $\mathbf{H} = \mathbf{QR}$. The entries of $\mathbf{R}$ are independent and its diagonal entries, r_{ii} for $i \in 1, \ldots, M$, are such that $2Mr_{ii}^2$ is a chi-squared random variables with $2(N-i+1)$ degrees of freedom, while the off-diagonal entries, r_{ij} for $i < j$, are independent zero-mean complex Gaussian with variance $\frac{1}{M}$.

The next theorem can be found in [76].

Theorem 2 (Generalized Central Limit Theorem): Consider $S_N = a_1 + a_2 + \cdots + a_N$ as the summation of N independent random variables, each with a PDF that follows a power-law tail (decaying with $1/t^{\alpha}$, where $1 < \alpha < 3$), and therefore its variance is infinite. S_N will tend to Lévy skew alpha-stable or in brief stable Lévy distribution as the number of terms, N, grows.

There is no general analytical solution for the PDF of stable Lévy distribution [76], however, it has an analytical characteristic function given in terms of its parameters.

3.2.2 PDF of the post-processing SNR

Lemma 1: For each $\left[(\mathbf{H}_l^H\mathbf{H}_l)^{-1}\right]_{mm}$ there exists a column permutation π_m of $\mathbf{H}_l$

such that

$$(r_{MM}^{(l,\pi_m)})^{-2} = \left[(\mathbf{H}_l^H \mathbf{H}_l)^{-1}\right]_{mm} \tag{3.3}$$

where $r_{MM}^{(l,\pi_m)}$ is the Mth diagonal term of the $\mathbf{R}_l^{(\pi_m)}$. The matrix $\mathbf{R}_l^{(\pi_m)}$ is obtained by QR decomposition of $\mathbf{H}_l^{(\pi_m)}$, which itself is obtained by exchanging the mth and Mth columns of $\mathbf{H}_l$. See Appendix B for the proof.

The exact distribution of $\gamma^{(m_1)}$, which involves order statistics is complicated to derive. This is due to the fact that as stated in [71] the $\gamma^{(m)}$s are correlated, which makes it very difficult to obtain the distribution of $\gamma^{(m_1)}$, where $m_1 = \arg\max_m \gamma^{(m)}$. In [71] it has been shown that due to this correlation, selecting the largest $\gamma^{(m)}$ value would not result in increased diversity order. It is also shown in [71] that for $M = 2$ Tx and any number of Rx antennas ordering will result in approximately 3 dB SNR gain compared to the case with no ordering. In the following analysis we do not consider ordering. However, by comparing the final BER bound with simulation results it is shown that there is about 4.8 dB signal to noise ratio (SNR) gap between the derived upper bound and simulation results, which is partially due to ordering. Using Lemma 1, the post-processing SNR value, $\gamma^{(1)}$, of the first substream processed (since in our analysis we do not account for ordering, this is not necessarily the substream with the largest post-processing SNR) according to (3.1) is:

$$\begin{aligned} \gamma^{(1)} &= \frac{\zeta}{\frac{1}{L}\sum_{l=1}^{L}(r_{MM}^{(l)})^{-2}} \\ &= \frac{\zeta}{\kappa} \end{aligned} \tag{3.4}$$

where $\zeta = \frac{E_s}{M\sigma_n^2}$ and $\kappa = \frac{1}{L}\sum_{l=1}^{L}(r_{MM}^{(l)})^{-2}$. In (3.4), the permutation index of $r_{MM}^{(l)}$ has been discarded, since for any permutation, π_m, $r_{MM}^{(l)}$ has the same distribution. In the following, an approximation for the PDF of κ is introduced. By modifying Theorem 1, and assuming the elements of the standard complex Gaussian matrix mentioned in Theorem 1 have unit variances, twice the square of the mth diagonal element of $\mathbf{R}_l$, $2(r_{mm}^{(l)})^2$, will have a chi-squared PDF with $2(N - m + 1)$ degrees of freedom. Focusing on the Mth element which corresponds to the first detected layer, and assuming $N = M$, it can be shown that $(r_{MM}^{(l)})^2$ has an exponential PDF with mean equal to 1, i.e., $f_{(r_{MM}^{(l)})^2}(t) = e^{-t}, \quad t \geq 0$. Since the exponential PDF is a special case of gamma PDF [62], $(r_{MM}^{(l)})^{-2}$ has inverse-gamma distribution [73]

given by

$$f_{(r_{MM}^{(l)})^{-2}}(t) = \frac{e^{-1/t}}{t^2}, \quad t \geq 0. \tag{3.5}$$

The general form of the inverse-gamma PDF is given by [73]

$$f_{(r_{MM}^{(l)})^{-2}}(t) = \frac{\beta^\alpha}{\Gamma(\alpha)t^{\alpha+1}} e^{-\beta/t}, \quad t \geq 0. \tag{3.6}$$

All the moments of this random variable are infinite, and the PDF of the sum of inverse-gamma random variables can not be found in a closed form. Since the mean and variance of the elements of the sum do not exist, the central limit theorem can not be applied here. However, according to Theorem 2 (the generalized central limit theorem) the sum converges to a stable Lévy distribution [76]. Since evaluating the parameters of the stable Lévy distribution using the characteristic function is very difficult and none of the moments exists for the sum, we consider an approximation for the PDF of the sum. Nevertheless, Theorem 2 ensures that the sum has a PDF.

Our simulation results show that the inverse gamma PDF given by (3.6) with optimized parameters α and β is a good approximation for the PDF of κ, the inverse of the normalized post-processing SNR. In the following, we explain that with the optimized parameters α and β, the approximate PDF will have the same tail behavior as the stable Lévy distribution.

The PDF of κ obtained using simulations for $L = 16$ is shown in Fig. 3.1 along with the approximate inverse-gamma PDF. As seen in Fig. 3.1, the approximate PDF agrees very well with the sample data, especially in the tail region. The cumulative distribution function (CDF) is also in good agreement with simulation results as shown in Fig. 3.2. Estimates of α and β for different values of L are obtained using ML estimation [74, 77] with a sample space of size 10^6 and are given in Table 1. The mean square error (MSE) between the approximate pdf and the one obtained from simulations at hundred equally-spaced points from zero to one hundred is found to be less than 0.01 for the results provided in Table 3.1.

Table 3.1: Parameters for the PDF of κ for different values of L

L	α	β
4	1.18	1.93
8	1.21	2.23
16	1.30	2.85
64	1.40	3.76

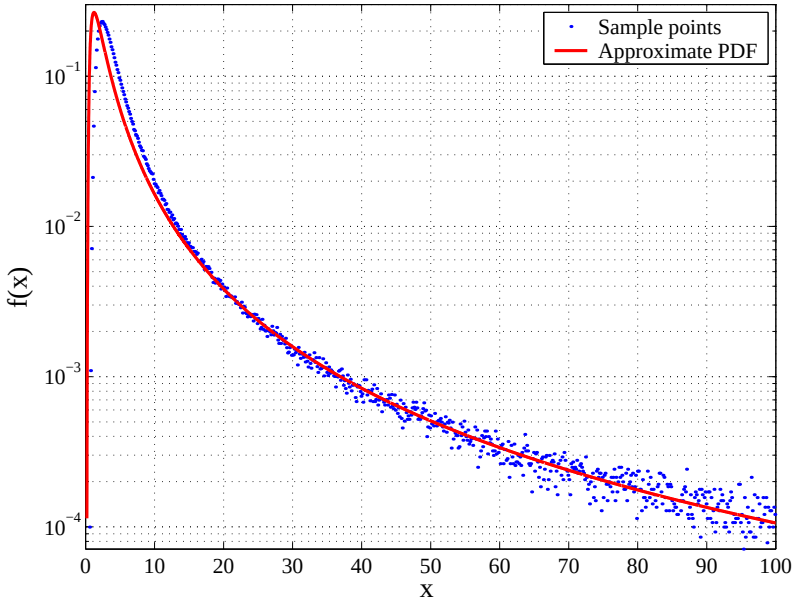

Figure 3.1: Comparison of the PDF of κ obtained using simulations with the approximate PDF (solid line) for $L = 16$. The dots show the sample points of the PDF obtained from simulations.

After finding the parameters of the PDF of κ, determining the corresponding PDF of $\frac{1}{\kappa}$, which has gamma distribution

$$f_{\frac{1}{\kappa}}(t) \approx \frac{\beta^{\alpha}}{\Gamma(\alpha)} t^{\alpha-1} e^{-\beta t} \quad t \geq 0, \tag{3.7}$$

is straightforward. An approximation for the distribution of $\gamma^{(1)}$ is then obtained as

$$f_{\gamma^{(1)}}(r) \approx \frac{(\frac{\beta}{\zeta})^{\alpha} r^{\alpha-1}}{\Gamma(\alpha)} e^{-\frac{\beta}{\zeta} r}, \quad r \geq 0. \tag{3.8}$$

3.3 Performance Evaluation

3.3.1 Upper bound on the probability of error

Similarly to single carrier V-BLAST detectors, the error probability of ZF U-SIC is dominated by the detection error of the first layer. As a result the error probability of the first layer could be considered an upper bound for the error probability of the SM-MC-CDM with ZF U-SIC (the system error probability is obtained by averaging over the error probability of all spatial layers). The probability of a bit error for QPSK signaling is then upper bounded by

$$P_e \leq \int_0^{\infty} \mathcal{Q}\left(\sqrt{t}\right) f_{\gamma^{(1)}}(t) dt, \quad \mathcal{Q}(x) = \frac{1}{\sqrt{(2\pi)}} \int_x^{\infty} e^{-\frac{r^2}{2}} dr. \tag{3.9}$$

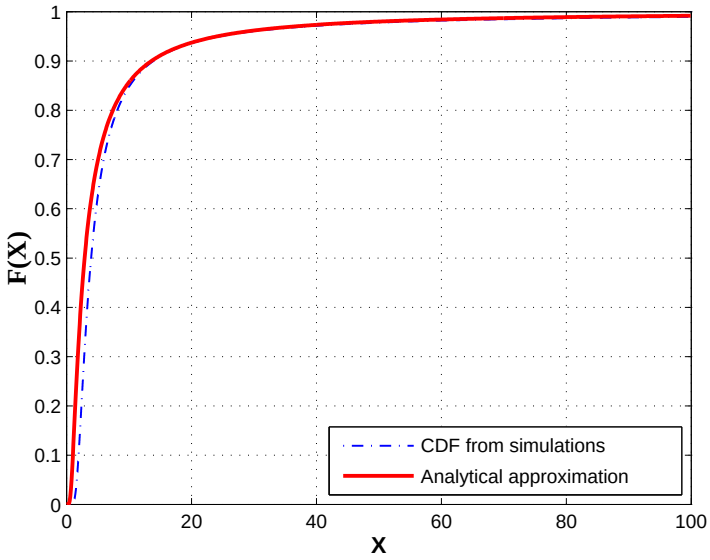

Figure 3.2: CDF of κ from simulations compared to the approximate CDF for $L = 16$.

Using Craig's formula [78] for the $\mathcal{Q}(\cdot)$ function:

$$\mathcal{Q}(x) = \frac{1}{\pi}\int_0^{\pi/2} e^{-\frac{x^2}{2\sin^2\theta}}d\theta, \tag{3.10}$$

the following expression is obtained

$$P_e \leq \frac{(\frac{\beta}{\zeta})^\alpha}{\pi\Gamma(\alpha)}\int_0^{\pi/2}\int_0^{\infty} t^{\alpha-1}e^{-(\frac{\beta}{\zeta}+\frac{1}{2\sin^2(\theta)})t}dtd\theta \tag{3.11}$$

which using the identity [79]

$$\int_0^{\infty} t^{\alpha-1}e^{-ut}dt = \frac{\Gamma(\alpha)}{u^\alpha} \tag{3.12}$$

and substituting u by $\frac{\beta}{\zeta} + \frac{1}{2\sin^2(\theta)}$ can be further simplified to [80],

$$\begin{aligned} P_e &\leq \frac{1}{\pi}\int_0^{\pi/2}\left(\frac{\sin^2(\theta)}{\sin^2(\theta)+\frac{\zeta}{2\beta}}\right)^\alpha d\theta \\ &= \frac{\sqrt{\frac{c}{\pi}}}{2(1+c)^{\alpha+\frac{1}{2}}}\frac{\Gamma(\alpha+1/2)}{\Gamma(\alpha+1)}F(1,\alpha+\frac{1}{2};\alpha+1;\frac{1}{1+c}). \end{aligned} \tag{3.13}$$

$F(\cdot,\cdot;\cdot,\cdot)$ is the Gaussian hypergeometric function [79] and $c = \frac{\zeta}{2\beta}$.

The diversity order is defined as [69]

$$\rho = -\lim_{\zeta\to\infty}\frac{\log(P_e)}{\log(\zeta)}. \tag{3.14}$$

To obtain the diversity order of SM-MC-CDM, the Gaussian hypergeometric function is replaced by its series representation [79]

$$F(1,\alpha+\frac{1}{2};\alpha+1;\frac{1}{1+c}) = \sum_{n=0}^{\infty} \frac{(\alpha+\frac{1}{2})_n}{n!(\alpha+1)_n(1+c)^n} \tag{3.15}$$

where $(a)_n = (a)(a+1)\dots(a+n-1)$ is the rising factorial. As ζ approaches infinity, the first term in the series becomes the dominant term and

$$\begin{aligned}
\rho &= -\lim_{\zeta\to\infty} \frac{\log(P_e)}{\log(\zeta)} \\
&= -\lim_{\zeta\to\infty} \frac{\log\left(\frac{\sqrt{\frac{\zeta}{2\pi\beta}}}{2(1+\frac{\zeta}{2\beta})^{\alpha+\frac{1}{2}}} \frac{\Gamma(\alpha+1/2)}{\Gamma(\alpha+1)} \left(1+\sum_{n=1}^{\infty} \frac{(\alpha+\frac{1}{2})_n}{n!(\alpha+1)_n(1+\frac{\zeta}{2\beta})^n}\right)\right)}{\log(\zeta)} \\
&= -\lim_{\zeta\to\infty} \frac{\log\left((1+\frac{\zeta}{2\beta})^{-\alpha-\frac{1}{2}}(\frac{\zeta}{2\pi\beta})^{\frac{1}{2}}\right) + \log\left(\frac{\Gamma(\alpha+\frac{1}{2})}{2\Gamma(\alpha+1)}\right)}{\log(\zeta)} \\
&= \alpha.
\end{aligned} \tag{3.16}$$

Once again referring to Table I, it shows that α is slightly greater than one for $L > 1$ and increases with increasing number of subcarriers. This means that the diversity order of SM-MC-CDM with ZF U-SIC slightly increases as the number of subcarriers, L, increases.

3.3.2 Analysis of ergodic capacity

The instantaneous capacity of ZF V-BLAST without channel state information at the transmitter is given by [81]

$$C = M \min_{\nu=1,\dots,M} \left\{\log_2\left(1+\gamma^{(\nu)}\right)\right\} \tag{3.17}$$

where $\gamma^{(\nu)}$ is the SNR of the νth layer. Similarly, for the case of ZF U-SIC the capacity is determined by the spatial layer with the minimum SNR. Here, we assume the first detected layer has the minimum SNR among the M layers, which leads to the following approximation for the capacity of the SM-MC-CDM

$$\begin{aligned}
C_{ZF-SIC} &= \frac{1}{L}\sum_{l=1}^{L} M \min_{\nu=1,\dots,M} \left\{\log_2\left(1+\gamma_l^{(\nu)}\right)\right\} \\
&\approx M\log_2\left(1+\gamma^{(1)}\right)
\end{aligned} \tag{3.18}$$

As it has been shown in Section 3.2, the post-processing SNR of the mth layer for all L de-spreader outputs is the same and therefore, the subscript l is discarded.

The accuracy of the approximation in (3.18) is verified in Section 3.4. Furthermore, the ergodic capacity is obtained as

$$\begin{aligned}\bar{C} &\approx E_{\gamma^{(1)}}\{C_{ZF-SIC}\} \\ &\approx \int_0^\infty M \log_2(1+t) f_{\gamma^{(1)}}(t) dt \\ &= \int_0^\infty M \log_2(1+t) \frac{(\frac{\beta}{\zeta})^\alpha}{\Gamma(\alpha)} t^{\alpha-1} e^{-\frac{\beta}{\zeta}t} dt\end{aligned} \tag{3.19}$$

The integral in (3.19) has a closed form solution [82] given by

$$\bar{C} \approx \frac{M(\frac{\beta}{\zeta})^\alpha}{\ln(2)\Gamma(\alpha)} \mathrm{G}_{2,3}^{3,1}\left(\frac{\beta}{\zeta}\middle| \begin{matrix} -\alpha,\, 1-\alpha \\ 0,\, -\alpha,\, -\alpha \end{matrix}\right) \tag{3.20}$$

where $\mathrm{G}_{p,q}^{m,n}\left(z\middle| \begin{matrix} a_p \\ b_q \end{matrix}\right)$ is the Meijer's G-function [79]. Approximate ergodic capacity of ZF V-BLAST can be obtained from (3.20) for $\alpha = 1$ and $\beta = 1$. In the next section the analytical performance bound and the capacity approximation are compared with numerical results.

3.4 Numerical Results

For all the results presented in this section, a 4×4 MIMO-OFDM system is considered. Fig. 3.3 shows the BER advantage of ZF U-SIC over per subcarrier ZF V-BLAST with $L = 16$ subcarriers. At BER of 10^{-4} there is about 8.5 dB gain in SNR for ZF U-SIC over ZF V-BLAST. Fig. 3.4 shows the BER performance of ZF U-SIC detector for $L = 4$ and $L = 64$ subcarriers. Comparing the analytical bound with the simulation results, it is evident that for high SNRs the upper bound has an almost constant gap of 4.8 dB with the BER curve obtained using simulations. This SNR gap is the result of using BER of all spatial layers instead of only considering the first layer as well as the optimum ordering of spatial layers in the simulations, neither of which have been taken into account when deriving the BER upper bound.

In Fig. 3.5, the approximate ergodic capacity of the SM-MC-CDM system with U-SIC is shown for $L = 4$, 16 and $L = 64$ subcarriers, and compared to the semi-analytical results. To obtain the semi-analytical results, random channel matrices were generated and the SNR values were obtained using (3.1). Then the instantaneous capacity for each channel realization was obtained using the exact formula in (3.18) and averaged over a large number of channel realizations. The approximation (3.20) in the previous section follows the semi-analytical results very closely.

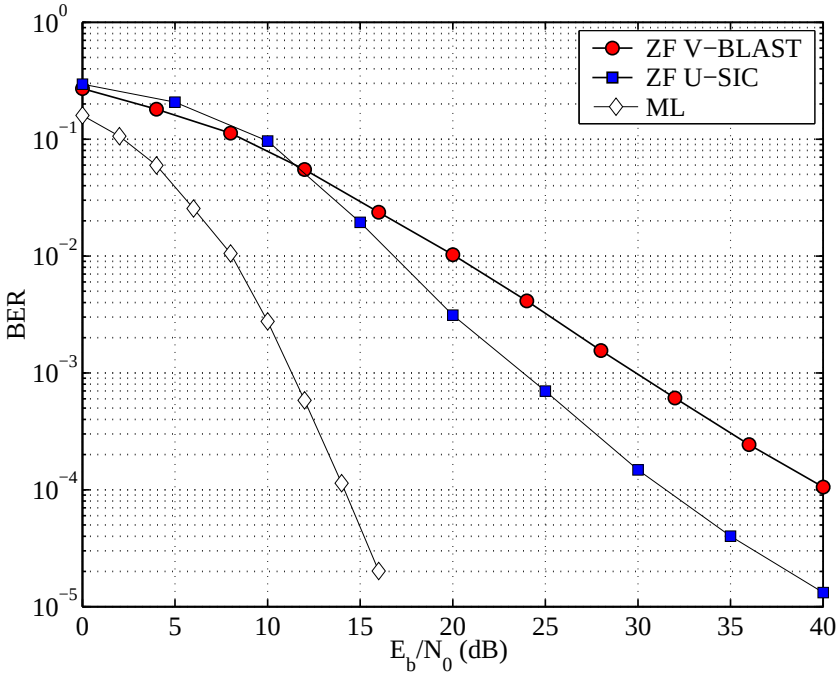

Figure 3.3: Performance comparison of ZF U-SIC and ZF V-BLAST receivers for SM-MC-CDM and MIMO-OFDM, respectively. The two systems have the same parameters, i.e. $L = 16$ subcarriers, $M = 4$ Tx and $N = 4$ Rx antennas. Performance of the maximum likelihood (ML) detector over each subcarrier has been plotted as a benchmark.

Especially for $L = 16$, the gap between the analytical approximation and the semi-analytical results is very small. From the figure, it can be seen that by increasing the number of subcarriers the ergodic capacity decreases. In addition, for $L = 4$ subcarriers the approximate ergodic capacity falls below the semi-analytical results, while as the number of subcarriers, L, increases the approximate curves get closer to the semi-analytical results and ultimately move above the semi-analytical curves, e.g. for $L = 64$.

To find an explanation for this behaviour of the approximate capacity, recall Section 3.2 in which to obtain (3.20) two approximations have been used: 1) Assumption of the first spatial layer as the layer with the minimum post-processing SNR among the M layers; 2) The use of the approximate pdf (3.8) for the post-processing SNR. It is very difficult to quantify the contribution of each of these approximations to the difference between the semi-analytical and approximate capacity results. Nevertheless, from (3.17) it can be inferred that for the L values for which the semi-analytical curves fall below the approximate curves, the effect

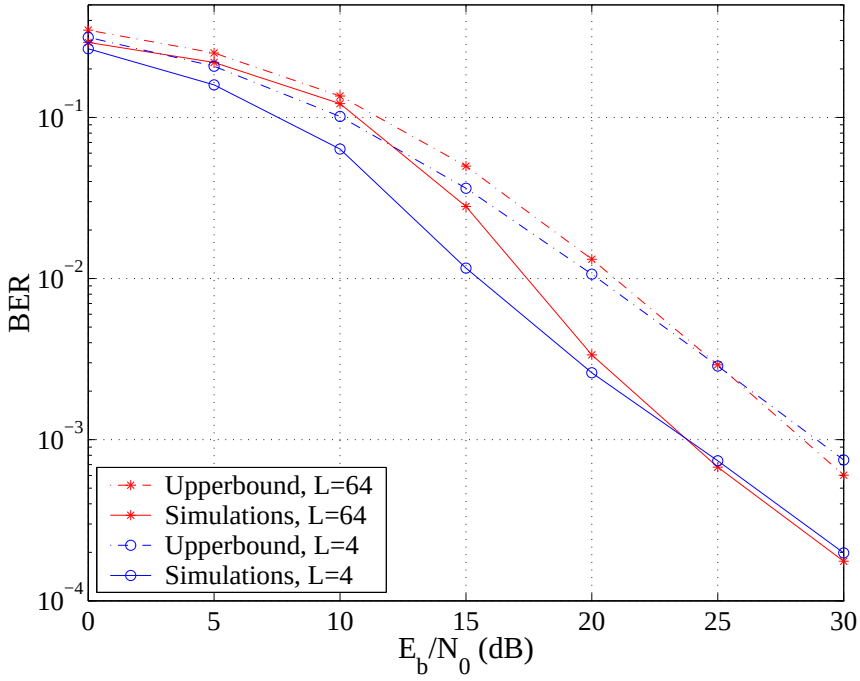

Figure 3.4: The BER performance of SM-MC-CDM with U-SIC compared with the upper bound of (3.13).

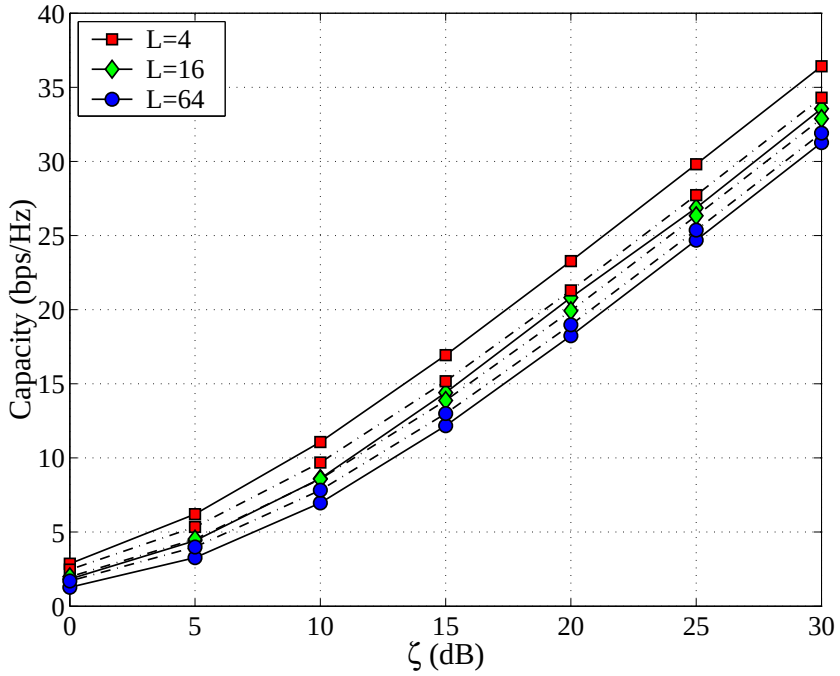

Figure 3.5: The ergodic capacity of SM-MC-CDM with U-SIC compared with the approximation of (3.20) for $L = 4$, 16 and $L = 64$ subcarriers. The dash-dotted lines are the approximate curves. $\zeta = \frac{E_s}{M\sigma_n^2}$.

of the first approximation is more dominant, while for small values of L where the semi-analytical curve is above the approximate curve, the pdf approximation tends to be the dominant factor in causing the capacity gap.

Figures 3.4 and 3.5 show that increasing the number of subcarriers leads to a somewhat lower BER (at high SNRs), whereas the ergodic capacity decreases slightly. Inspection of the PDF curves shown in Fig. 3.6 helps to clarify the two effects. In Fig. 3.6, the approximate PDFs of $\gamma^{(1)}$ for $L = 4$ and $L = 64$ have been plotted at $\zeta = 30$ dB. According to (3.9), the upper bound for BER is obtained by evaluating the ensemble average of $\mathcal{Q}(\sqrt{x})$ over x. The function $\mathcal{Q}(x)$ decreases exponentially with square of its argument, x, i.e. its value becomes dramatically smaller for large values of x. Hence, the average BER is primarily determined by $\gamma^{(1)}$'s PDF for small values of x. Fig. 3.6 shows that the system with $L = 64$ subcarriers has a smaller PDF for small values of x, which explains its lower BER. On the other hand, according to (3.19) the ergodic capacity is obtained by evaluating the ensemble average of $\log_2(1+x)$ over x. The $\log_2(\cdot)$ function increases logarithmically with its argument, therefore, the system with a larger PDF at large values of x will have a higher capacity, which as seen on Fig. 3.6, is the SM-MC-CDM system with a smaller number of subcarriers ($L = 4$).

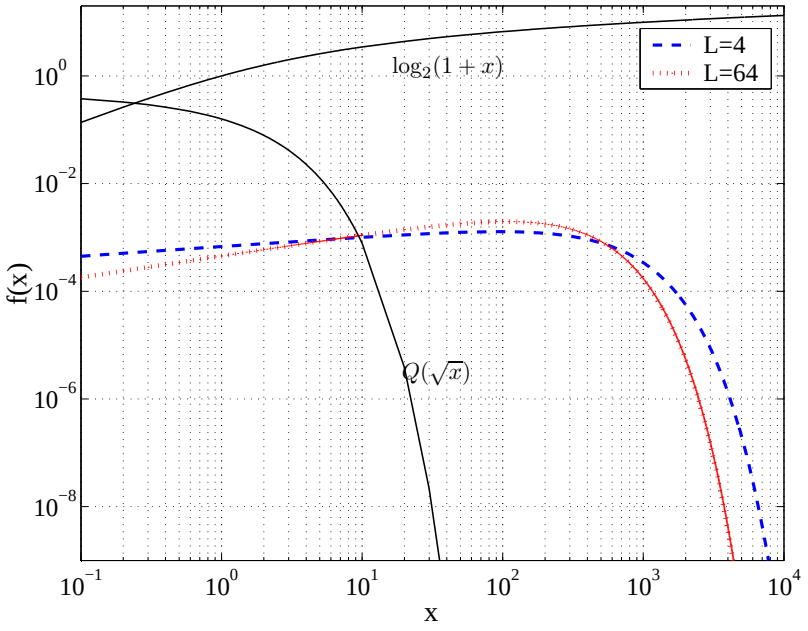

Figure 3.6: PDF of $\gamma^{(1)}$ for $L = 4$ and $L = 64$ subcarriers at $\zeta = 30$ dB.

To conclude this section, we note that the increase in the number of subcarriers will lead to a better performance at high SNRs (high values ofζ) due to the gradual increase in the diversity order. However, the diversity order does not have a significant effect on the system performance at the medium range of SNR. On the other hand, the effect of increasing L is significant for decreasing the ergodic capacity for all practical values of SNR. Therefore, in order to take advantage of ZF U-SIC and when there are a large number of subcarriers available for transmission, it is recommended to divide the subcarriers into a number of sub-bands, each consisting of a smaller number of subcarriers.

3.5 Summary

In this chapter we have presented an analytical approach to the performance evaluation of ZF unified successive interference cancellation (U-SIC) detector for spatially multiplexed MC-CDM communications. A very close approximation for the PDF of the reciprocal of post detection SNR has been found to be the inverse-gamma distribution. The approximation was then used to obtain the PDF of post detection SNR. A closed form analytical bound and an approximation have been derived for the probability of error and the ergodic capacity, respectively. It was shown that in an SM-MC-CDM system with equal number of Tx and Rx antennas, ZF U-SIC is able to achieve diversity order $\rho = \alpha > 1$, which is slightly greater than the diversity order achieved by ZF and MMSE V-BLAST detectors in single carrier systems. The diversity order increases with the number of subcarriers, while the ergodic capacity decreases with increasing number of subcarriers.

Chapter 4

Efficient Transmission Schemes for Multiuser MIMO Downlink with Linear Receivers and Partial Channel State Information

4.1 Introduction

In recent years, the interest in multiuser multiple-input multiple-output (MU-MIMO) systems and transmission strategies that in multiuser environment would enable capacity gains similar to those in point-to-point spatial multiplexing MIMO has increased [83, 84, 85].

In a multiuser downlink with the base station (BS) equipped with multiple antennas, multiple users can be served simultaneously. In fact, it has been shown that to obtain the MU-MIMO downlink sum capacity, transmitting to several users simultaneously must be considered [25]. Since the number of users in the system is usually greater than the maximum number that can be served simultaneously through spatial multiplexing, user selection is required. User selection (or scheduling) favours users that experience better propagation conditions while being sufficiently separated in space. Such user scheduling leads to multiuser diversity gain [86, 87], which increases with increasing number of users awaiting transmission.

It has been shown that the capacity of the MU-MIMO downlink can be achieved by dirty paper coding (DPC) [25], which is a transmitter multiuser encoding strategy employing interference presubtraction. DPC requires nonlinear search for optimal

precoding matrices as well as non-causal channel coding for the users, which is practically impossible in real-time systems. Therefore, suboptimum transmission strategies such as different forms of beamforming have been considered in the literature. In MU-MIMO beamforming, linear or non-linear transmitter precoding algorithms together with user scheduling are designed to maximize the system's sum rate or some other related objective function (e.g. sum rate under fairness constraint). Unfortunately, most beamforming algorithms considered assume availability of perfect channel state information at the transmitter, which presents a big challenge to their practical implementation ([26, 27] and references therein contain an overview of the subject).

To overcome this challenge, suboptimal MU-MIMO downlink transmission using partial channel state information at the transmitter (CSIT) has been studied in the literature. Some of the proposed approaches can be applied to systems with only single antenna user terminals [88, 89, 90, 91, 92, 93], while some accommodate multiple antenna user terminals [94, 95, 96, 97, 98, 99, 100]. When multiple antenna user terminals are considered, often it is assumed that all user terminals have the same number of antennas. This might not be the case in practice. However, schemes which rely on this assumption may use antenna selection to satisfy it. Most of the existing MU-MIMO downlink schemes using partial CSIT fall under three main categories:

1. *Transmission schemes based on availability of quantized channel state information at the BS (limited feedback)*
   The quantized CSI is used to utilize a variant of beamforming at the BS. See [101] and references therein for further details.

2. *User scheduling and precoder selection from a codebook of vectors/matrices known a priori to both the BS and the users*
   The scheme proposed in [94] called transmit beam matching (TBM) is one example. It extends the per-user unitary rate control (PU^{2}RC)[102, 103] approach to multiple antenna users. PU^{2}RC is Samsung Electronic's proposal to the 3rd Generation Partnership Project (3GPP). The proposed approach is characterized by the relatively low complexity structure of PU^{2}RC and it uses pseudo-inversion of the channel matrix in order to minimize inter-stream interference at each user's terminal. However, when users have fewer antennas

than the base station, the pseudo-inverse operation can not completely eliminate inter-stream interference, which leads to some performance degradation. A similar approach called random precoding has been introduced in [96].

3. *Eigenmode transmission with partial CSIT*
   One example is [97], which employs singular value decomposition (SVD) of user channel matrices and data transmission on the eigenmode with the largest gain. Another example is [104], in which the authors propose a combination of zero-forcing beamforming (ZF-BF) with eigenmode transmission.

All schemes mentioned above use precoding at the BS. In addition to precoding at the BS, multiple antenna users can use their antennas to process their received signal vector using relatively low complexity linear schemes such as zero-forcing (ZF) or minimum mean squared error (MMSE) processing and send back some sort of channel quality indicator (CQI), e.g., SINR or achievable rate, to the BS. One example is [98], in which a MIMO downlink scheme with opportunistic feedback is proposed. In this scheme users use ZF linear processors and send back the quality indicator for each spatial channel to the base station according to an opportunistic feedback protocol. The main contribution of [98] lies in their feedback protocol and not the transmission scheme itself.

In this chapter, we present a transmission scheme for MU-MIMO downlink using eigenmode transmission and ZF linear processing, which only requires partial (or incomplete) CSIT and falls under the third category mentioned above. With the number of Rx antennas of each user terminal (assuming all have the same number of antennas) being less or greater than the number of transmit antennas, two transmission strategies are proposed. For systems where the number of Rx antennas is greater than or equal to the number of Tx antennas, one user is selected to receive data through eigenmode transmission and its right eigenvector matrix is used for precoding, while other selected users use ZF linear processing. When the number of Rx antennas of each user terminal is less than the number of Tx antennas at the base station, partial CSIT at the base station is used to design a precoding matrix such that the number of interfering streams at the selected user terminals (after Rx pre-processing) is reduced to the number of Rx antennas, and ZF receiver processing can be efficiently applied. Analytical expressions and approximations are derived for the sum rate of the proposed scheme and also for time division multiplexing

(TDM) with eigenmode transmission.

4.2 System Model

Consider a Gaussian MIMO broadcast channel where the base station is equipped with M antennas and there are K homogeneous users each equipped with N antennas. A quasi-static Rayleigh fading model is considered for the channel where the channel gains do not change within a frame and change independently from frame to frame following complex Gaussian distribution. The kth user receives the following signal vector

$$\mathbf{y}_k = \mathbf{H}_k\mathbf{x} + \mathbf{n}_k, \tag{4.1}$$

where $\mathbf{H}_k \in \mathbb{C}^{N\times M}$ is the downlink channel gain matrix between the base station and the kth user and $\mathbf{n}_k \in \mathbb{C}^{N\times 1}$ is the noise vector. Both $\mathbf{H}_k$ and $\mathbf{n}_k$ are assumed to have independently and identically distributed (i.i.d.) zero mean unit variance complex Gaussian elements, $\mathcal{CN}(0,1)$. The vector $\mathbf{x}$ is the transmitted signal vector such that trace $\left\{\mathbf{E}[\mathbf{x}\mathbf{x}^H]\right\} = P_T$. Hence, the average signal to noise ratio (SNR) equals P_T, which also defines the average power constraint of the base station. The data symbol vector $\mathbf{s}$ is a size $M\times 1$ vector. When precoding is used, the precoding matrix is denoted by $\mathbf{\Psi}$ where $\mathbf{x} = \mathbf{\Psi}\mathbf{s}$, and in case of spatial multiplexing $\mathbf{\Psi} = \mathbf{I}_{M\times M}$. Let the total rate delivered by the base station to the users during one time slot be R. Then the expected throughput of the system is obtained by taking ensemble average of R over $\mathbf{H}_k$s, i.e., $R_{Ave} = \mathrm{E}_{\mathbf{H}_1,\ldots,\mathbf{H_K}}\{R\}$. Throughout the chapter, the terms system throughput and sum rate are used interchangeably.

4.3 Eigenmode Transmission

Consider singular value decomposition (SVD) of the kth user's channel gain matrix,

$$\mathbf{H}_k = \mathbf{U}_k\mathbf{\Sigma}_k\mathbf{V}_k^H \tag{4.2}$$

where $\mathbf{U}_k = [\ \mathbf{u}_1^{(k)} \ \ldots \ \mathbf{u}_N^{(k)}\ ]$ and $\mathbf{V}_k = [\ \mathbf{v}_1^{(k)} \ \ldots \ \mathbf{v}_M^{(k)}\ ]$ are $N\times N$ left singular vector and $M\times M$ right singular vector unitary matrices, respectively. The matrix $\mathbf{\Sigma}_k$ is an $N\times M$ diagonal matrix with nonnegative numbers (singular values) on its diagonal. Consider data transmission to only one user at any given time. When the transmitter has the knowledge of $\mathbf{H}_k$, it precodes the transmitted signal by $\mathbf{V}_k$, while the kth receiver uses $\mathbf{U}_k^H$ as its receive processing matrix. Therefore, the channel is

diagonalized into parallel interference-free channels, also called eigenchannels [105], where the gain of each channel equals its corresponding singular value. In this case, the rate delivered to user k (in bits/s/Hz) is obtained as

$$R_k = \sum_{m=1}^{M} \log_2 \left(1 + \rho_m \lambda_m^{(k)}\right) \tag{4.3}$$

where $\lambda_m^{(k)} = \sigma_m^{(k)^2}$ is the mth eigenvalue of $\mathbf{H}_k^H \mathbf{H}_k$ while $\sigma_m^{(k)}$ is the mth singular value of $\mathbf{H}_k$. ρ_m denotes the power given to the mth data stream and $\sum_{m=1}^{M} \rho_m = P_T$. The optimum power distribution over the spatial channels is obtained through water-filling [105]. For the case of equal power allocation we have $\rho_m = P_T/M$. This transmission scheme has been considered within the context of time-division multiplexing (TDM) where the users send back their achievable rate, R_k, to the base station and the base station selects the user with the largest rate for transmission in each time slot. Compared to multiuser MIMO schemes in which multiple users are served simultaneously, this scheme is very suboptimal as it does not take full advantage of multiuser diversity, which implies that some of the eigenmodes of the selected user's channel matrix might be very weak. Moreover, it is shown that the maximum achievable sum rate of TDM with eigenmode transmission is only a small fraction of of the sum capacity of MIMO broadcast channels [106]. In fact, DPC can achieve a linear increase of sum rate, which becomes $\min(M, K)$ times that of TDM [106].

4.4 Zero-Forcing Receiver Processing and Scheduling Based on Partial Side Information

In case $N \geq M$, with spatial multiplexing at the base station when an independent data stream is transmitted from each Tx antenna and ZF receiver processing is used at each user terminal, the scheduled users can detect their data without inter-stream interference [107]. The assumption of $N \geq M$ for large M values does not reflect any existing MU-MIMO downlink design, especially for nomadic user terminals. Nevertheless, for small values of M ($M \leq 4$) according to current wireless standards which consider multiple antenna user terminals, e.g., Worldwide Interoperability for Microwave Access (WiMAX), this is a valid assumption.

ZF receiver processing at the kth user is applied by multiplying the received

signal by

$$\mathbf{G}_k = (\mathbf{H}_k^H \mathbf{H}_k)^{-1} \mathbf{H}_k^H. \tag{4.4}$$

The post-processing SNR of the mth data stream at user k is then given as [108]

$$\gamma_m^{(k)} = \frac{\rho}{\left[(\mathbf{H}_k^H \mathbf{H}_k)^{-1}\right]_{mm}} \tag{4.5}$$

where $\rho = \frac{P_T}{M}$ and $[\mathbf{A}]_{mm}$ denotes the mth diagonal term of the matrix $\mathbf{A}$. Once the base station is informed of the post processing SNR of a specific data stream by all users, it will assign that data stream to the user with the highest post-processing SNR. Therefore, the sum rate (in bits/s/Hz) will be given by

$$R_{ZF} = \sum_{m=1}^{M} \log_2 \left(1 + \gamma_m^{(\hat{k}_m)}\right) \tag{4.6}$$

where $\hat{k}_m = \arg\max_k \gamma_m^{(k)}$. While this scheme is asymptotically optimal [107], i.e.,

$$\lim_{K \to \infty} \frac{\mathrm{E}\{R_{ZF}\}}{\mathrm{E}\{R_{DPC}\}} = 1 \tag{4.7}$$

where R_{DPC} is the sum rate of the DPC scheme, for small pool of users it achieves a relatively poor sum rate.

4.5 The Proposed Transmission Scheme: Eigenmode Transmission with Zero-Forcing Receiver Processing

In the next subsections our proposed transmission scheme is presented for two scenarios. In the first scenario, the user terminals have at least equal number of antennas to that of the base station ($M \leq N$) and in the second scenario the base station has more antennas than the user terminals ($M > N$).

4.5.1 Case $N \geq M$: Precoding with right singular vector matrix

The proposed scheme is presented in an algorithmic form as follows,

1. All the users perform SVD of their own channel and report back a single rate value evaluated according to $r_{k,M_s} = \sum_{i=1}^{M_s} \log_2(1 + \rho\lambda_i^{(k)})$ where $\rho = P_T/M$. The parameter M_s is evaluated beforehand for a given set of system parameters and will be discussed in the next subsection. $\lambda_i^{(k)}$s are the ordered eigenvalues of the matrix $\mathbf{W}_k = \mathbf{H}_k^H \mathbf{H}_k$, which is a complex Wishart matrix (when entries of $\mathbf{H}_k$ are i.i.d. complex zero mean Gaussian) [109]. The eigenvalues are assumed to be ordered with $\lambda_1^{(k)}$ being the largest eigenvalue.

2. The base station scheduler selects the user with the largest r_k (user k_s) and asks that user to send its $\mathbf{V}_{k_s}$ matrix to the base station. The matrix $\mathbf{V}_{k_s}$ is obtained through the SVD of the selected users' channel matrix. The matrix $\mathbf{V}_{k_s}$ is then used as the precoding matrix, $\mathbf{\Psi} = \mathbf{V}_{k_s}$. User k_s will receive its data through the first M_s , $(M_s < M)$ data streams (encompassing data symbols $s_1, s_2, \ldots, s_{M_s}$), using $\mathbf{U}_{k_s}^H$ as its receiver processing matrix (eigenmode transmission).

3. Each user except user k_s will estimate its equivalent channel, which at this stage is $\tilde{\mathbf{H}}_u = \mathbf{H}_u \mathbf{V}_{k_s}$ for the uth user. Then all users (except user k_s) will apply ZF linear processing using the estimated equivalent channel and send back the post-processing SNR of data streams M_s+1 to M to the base station.

4. For each of the remaining $M - M_s$ data streams, the base station selects the user with the highest post-processing SNR.

Finding the optimum number of eigenmodes (M_s)

Since the precoding matrix, $\mathbf{\Psi}$, in this case is a unitary matrix, the statistics of the equivalent channel $\tilde{\mathbf{H}}_k = \mathbf{H}_k \mathbf{\Psi}$ do not change. Assuming the first M_s data symbols have been assigned to user k_s and the remaining $M - M_s$ to users with ZF receivers, which have the highest post-processing SNR, the average sum rate is obtained by taking the ensemble average of the rate contribution from eigenmode transmission on the first M_s eigenmodes, $R_{eig}(M_s)$, and the rate contribution from the remaining $M - M_s$ data streams using linear ZF receiver processing, $R_{ZF}(M - M_s)$ over a large number of channel realizations:

$$\begin{aligned} R_{Ave} &= E\{R_{eig}(M_s)\} + E\{R_{ZF}(M - M_s)\} \\ &= E\left\{\sum_{l=1}^{M_s} \log_2(1 + \rho\lambda_l^{(k_s)})\right\} + E\left\{\sum_{m=M_s+1}^{M} \log_2(1 + \rho\xi_{m,v^*})\right\} \end{aligned} \tag{4.8}$$

where $\xi_{m,v^*} = \frac{1}{[(\tilde{\mathbf{H}}_{v_m^*}^H \tilde{\mathbf{H}}_{v_m^*})^{-1}]_{mm}}$ and $[\cdot]_{mm}$ denotes the mth diagonal term of its matrix argument. The user v_m^* is the user which has the largest post-processing SNR for the mth data stream among $K - 1$ users (user k_s has been subtracted out from the set $\{1, \ldots, K\}$), i.e.,

$$v_m^* = \arg \max_{k, k \neq k_s} \xi_{m,k}, \quad M_s < m \leq M. \tag{4.9}$$

The probability density function (pdf) of ξ_{m,v_m^*} for a square system $M = N$ is obtained using order statistics and is given by [108]

$$f_{\xi_{m,v_m^*}}(x) = (K-1)(1-e^{-x})^{K-2}e^{-x}, \quad M_s < m \leq M, \;\; x \geq 0 \tag{4.10}$$

which is independent of data stream's index, m. For a non square system ($N > M$), the exponential functions in (4.10) are replaced with chi-square distribution functions with $2(N-M+1)$ degrees of freedom [108]. Using (4.10), the expected throughput contribution from ZF Rx processing is obtained as

$$E\{R_{ZF}(M-M_s)\} = (M-M_s)\int_0^\infty \log_2(1+\rho x) f_{\xi_{m,v_m^*}}(x)dx \tag{4.11}$$

which for the case of $M = N$ is further simplified to [108]

$$E\{R_{ZF}(M-M_s)\} = \frac{(M-M_s)(K-1)}{\ln(2)} \sum_{q=0}^{K-2} \frac{1}{q+1}\binom{K-2}{q}(-1)^q \exp\left(\frac{q+1}{\rho}\right) \mathrm{E}_1\left(\frac{q+1}{\rho}\right) \tag{4.12}$$

where $\mathrm{E}_1(.)$ is the exponential integral function [110]. To obtain the expected throughput of the eigenmode transmission, the pdf of ordered eigenvalues of $\mathbf{W}_k$ is required. The joint pdf of the ordered eigenvalues is given by [111]

$$p_\lambda(\lambda_1, \ldots, \lambda_M) = K_c e^{-\sum_{i=1}^M \lambda_i} \prod_{i=1}^M \lambda_i^{N-M} \prod_{1 \leq i < j \leq M} (\lambda_i - \lambda_j)^2 \tag{4.13}$$

where $K_c^{-1} = \prod_{i=1}^M \Gamma(M-i+1)\Gamma(N-i+1)$ is the product of $2M$ Gamma functions. For $M_s > 1$, closed form analytical expression for the average throughput contribution from eigenmode transmission, $\mathrm{E}\{R_{eig}\}$, is very complicated to evaluate. However, a close approximation for $\mathrm{E}\{R_{eig}\}$ can be obtained using the following proposition.

Proposition 1 *For a Gaussian MIMO broadcast channel with M transmit antennas and K users each equipped with $N \geq M$ receive antennas, a close approximation to the average sum rate of eigenmode transmission on the first $M_s (\leq M)$ eigenmodes is*

$$\mathrm{E}\{R_{eig}\} \approx \frac{\sigma_{r_{k,M_s}}}{0.1975}\left[0.5264^{\frac{0.135}{K}} - (1-0.5264^{\frac{1}{K}})^{0.135}\right] + \mu_{r_{k,M_s}} \tag{4.14}$$

where

$$\begin{aligned} \sigma^2_{r_{k,M_s}} &= \sum_{i=1}^{M_s}\sum_{j=1}^{M_s}\left(\mathrm{E}\{R^{(k)}_{\lambda_i}R^{(k)}_{\lambda_j}\} - \mathrm{E}\{R^{(k)}_{\lambda_i}\}\,\mathrm{E}\{R^{(k)}_{\lambda_j}\}\right) \\ \mu_{r_{k,M_s}} &= \sum_{l=1}^{M_s}\int_0^\infty \log_2(1+\rho x) p_\lambda(\lambda_l^{(k)})(x)dx \end{aligned} \tag{4.15}$$

and $R_{\lambda_i}^{(k)} = \log_2(1+\rho\lambda_i^{(k)})$ is the achievable rate on the ith eigenmode.

Proof 1 *See Appendix C.*

Based on the system parameters, M, N, ρ and K and by using (4.11) and (4.14) an optimum M_s value can be found such that it maximizes the average sum rate. In what follows, a case example is considered.

Case $M = 3$, $N = 3$

We consider four possibilities for this case,

- The proposed scheme with $M_s = 1$.

  The average sum rate for this scheme is obtained as

  $$\begin{aligned} R_{Ave} &= \mathrm{E}\{R_{eig}(1)\} + \mathrm{E}\{R_{ZF}(2)\} \\ R_{Ave} &= \int_0^\infty K\log_2(1+\rho x)[F_\lambda(\lambda_1)]^{K-1}p_\lambda(\lambda_1)dx + 2\int_0^\infty \log_2(1+\rho x) f_{\xi_{m,v_m^*}}(x)dx \end{aligned} \tag{4.16}$$

  with the pdf and CDF of λ_1 given at the bottom of this page.

- The proposed scheme with $M_s = 2$.

  In this case the average sum rate is obtained as

  $$\begin{aligned} R_{Ave} &= \mathrm{E}\{R_{eig}(2)\} + \mathrm{E}\{R_{ZF}(1)\} \\ R_{Ave} &\approx \sigma_{r_{k,2}}\Phi^{-1}(0.5264^{\frac{1}{K}}) + \mu_{r_{k,2}} + \int_0^\infty \log_2(1+\rho x) f_{\xi_{m,v_m^*}}(x)dx \end{aligned} \tag{4.18}$$

  where $\sigma_{r_{k,2}}$ and $\mu_{r_{k,2}}$ are obtained using equation (4.15), and marginal and joint eigenvalue distributions are given at the bottom of this page.

$$\begin{aligned} p_\lambda(\lambda_1) &= 0.25e^{-\lambda_1}\Big[(12-24\lambda_1+24\lambda_1^2-8\lambda_1^3+\lambda_1^4) - 2(12-12\lambda_1+6\lambda_1^2+2\lambda_1^3+\lambda_1^4)e^{-\lambda_1} \\ &\quad + 12e^{-2\lambda_1}\Big],\ \lambda_1 \geq 0 \\ F_\lambda(\lambda_1) &= 1 - 0.25e^{-\lambda_1}\left[(12+12\lambda_1^2-4\lambda_1^3+\lambda_1^4) - (12+12\lambda_1^2+4\lambda_1^3+\lambda_1^4)e^{-\lambda_1} + 4e^{-2\lambda_1}\right] \\ p_\lambda(\lambda_2) &= e^{-3\lambda_2}\left[-6+0.5e^{\lambda_2}(12-12\lambda_2+6\lambda_2^2+2\lambda_2^3+\lambda_2^4)\right],\ \lambda_2 \geq 0 \\ p_\lambda(\lambda_3) &= 3e^{-3\lambda_3},\quad \lambda_3 \geq 0 \\ p_\lambda(\lambda_1,\lambda_2) &= 0.25[24-12\lambda_1+2\lambda_1^2-12\lambda_2+8\lambda_1\lambda_2-2\lambda_1^2\lambda_2+2\lambda_2^2-2\lambda_1\lambda_2^2+\lambda_1^2\lambda_2^2 \\ &\quad - 2e^{-\lambda_2}(12-6\lambda_1+\lambda_1^2+6\lambda_2-2\lambda_1\lambda_2+\lambda_2^2)](\lambda_1-\lambda_2)^2e^{-(\lambda_1+\lambda_2)} \end{aligned} \tag{4.17}$$

- Selecting user k which achieves the largest rate and only serving that user in each time slot (TDM with eigenvalue distribution). The average sum rate in this case is approximated by (4.14) with $M_s = M = 3$ and using [112] where more simplified expressions (for case $M = M_s$) have been given for $\sigma_{r_{k,3}}$ and $\mu_{r_{k,3}}$.

- ZF receiver processing scheme based on partial side information.

  The average sum rate for this scheme is obtained as

$$R_{Ave} = 3 \int_0^\infty \log_2(1+\rho x) f_{\xi_{m,v_m^*}}(x) dx \tag{4.19}$$

The average sum rates of the four cases considered above will be compared in Section 4.6.

General case of M and N

To find the optimum M_s, one has to find the smallest eigenvalue, λ_t, for which $\mathrm{E}\{R_{eig}(t)\} > \mathrm{E}\{R_{ZF}(M-t)\}$. Then the optimum value for M_s is $M_s = t$. To obtain $R_{eig}(t)$, the marginal pdf, CDF, and joint pdfs of $\lambda_l^{(k)},\ 1 \le l \le t$ are required, which can be obtained using (4.13). $\mathrm{E}\{R_{eig}(t)\}$ is then approximated using (4.14).

Scaling Law of Sum Rate of the Proposed Scheme

In this subsection, the asymptotic behaviour of the average sum rate of the proposed scheme described in V.A is investigated for systems with a large number of users. First we start with the following lemma:

Lemma 2 *For fixed M, N, and ρ we have,*

$$\lim_{K\to\infty} \frac{\mathrm{E}\{R_{eig}(M_s)\}}{M_s \ln[\ln(K)]} \le 1 \tag{4.20}$$

where $\ln(\cdot)$ is the natural logarithm.

Proof 2 *An upper bound for r_{k,M_s} is*

$$\begin{aligned} r_{k,M_s} &= \sum_{l=1}^{M_s} \log_2(1+\rho\lambda_l^{(k)}) \\ &\le M_s \log_2(1+\rho\lambda_1^{(k)}) \\ &\le M_s \log_2(1+\rho\sum_{m=1}^{M}\lambda_m^{(k)}) \\ &= M_s \log_2(1+\rho\,\mathrm{trace}(\mathbf{W}_k)) \end{aligned} \tag{4.21}$$

Using the definition of the trace of a matrix,

$$\begin{aligned}\operatorname{trace}(\mathbf{W}_k) &= \operatorname{trace}(\mathbf{H}_k^H \mathbf{H}_k) \\ &= \sum_{n=1}^{N} \sum_{m=1}^{M} |h_{n,m}^{(k)}|^2\end{aligned} \tag{4.22}$$

which is a chi-squared random variable with $2MN$ *degrees of freedom. Since* $R_{eig}(M_s) = \arg\max_{1 \le k \le K} r_{k,M_s}$*, according to [113, 107] we have*

$$\lim_{K \to \infty} \frac{\log_2 \left(1 + \rho \operatorname{trace}(\mathbf{W}_k)\right)}{\ln \left[\ln (K)\right]} = 1 \tag{4.23}$$

and that completes the proof.

As the sum capacity (obtained by DPC) for M_s data streams asymptotically increases with $M_s \ln \left[\ln (M_s K)\right]$ [114], $R_{eig}(M_s)$ is not asymptotically optimum. However, the following theorem shows the proposed scheme with $M_s = 1$ is asymptotically optimal.

Theorem 3 *The proposed scheme is asymptotically optimal*

$$\lim_{K \to \infty} \frac{R_{Ave}}{\mathrm{E}\{R_{DPC}\}} = 1. \tag{4.24}$$

Proof 3 *When* K *is very large, referring to Lemma 1,*

$$R_{Ave} = \mathrm{E}\{R_{eig(1)}\} + (M-1)\,\mathrm{E}\{R_{ZF}(M-1)\}. \tag{4.25}$$

According to [115]

$$\begin{aligned}\mathrm{E}\{R_{DPC}\} &\le M\,\mathrm{E}\{\log_2(1 + \rho \lambda_{1,max})\} \\ &= M\,\mathrm{E}\{R_{eig}(1)\}\end{aligned} \tag{4.26}$$

where $\lambda_{1,max} = \max_{k=1,\ldots,K} \lambda_1^{(k)}$*. Also [107]:*

$$\lim_{K \to \infty} \frac{\mathrm{E}\{R_{ZF}(M-1)\}}{\mathrm{E}\{R_{DPC}\}} = \frac{1}{M}. \tag{4.27}$$

Considering (4.26) and (4.27),

$$\begin{aligned}\lim_{K \to \infty} \frac{R_{Ave}}{\mathrm{E}\{R_{DPC}\}} &\ge \frac{1}{M} + \frac{M-1}{M} \\ &= 1.\end{aligned} \tag{4.28}$$

and since DPC has the optimum scaling sum rate, the ratio in the above equation can not be greater than one.

Lemma 2 and Theorem 3 make one expect that as the number of users increases the optimum M_s value will decrease to one. In Table 4.1, the optimum M_s values for $M = 4$ to $M = 7$ antennas have been given for systems with equal numbers of Tx and Rx antennas along with the percentage sum rate increase achieved by using the proposed scheme over the transmission schemes based on ZF receiver processing and TDM, when there are $K = 30$ users available in the system and at $\rho = 10$ dB SNR. The gain of the proposed scheme over ZF receiver processing and TDM with eigenmode transmission schemes (TDM in brief) have been normalized to the sum rate of these schemes, respectively (i.e., $\frac{R_{Ave} - \mathrm{E}\{R_{ZF}(M)\}}{\mathrm{E}\{R_{ZF}(M)\}} \times 100$ for the case of ZF Rx processing). As seen in Table I, the proposed scheme provides a significant sum rate increase over ZF receiver processing and TDM for different numbers of antennas. For example for the case of $M = 6$ Tx and $N = 6$ Rx antennas, the proposed scheme exceeds the sum rate of that achieved by ZF receiver processing scheme by about 29 %.

Table 4.1: Optimum M_s values and the percentage increase of the proposed scheme's sum rate over ZF and TDM schemes for different numbers of antennas.

$M(= N)$	4	5	6	7
Optimum M_s	2	3	4	4
Percentage increase over ZF (%)	20.60	24.68	29.07	33.86
Percentage increase over TDM (%)	20.60	19.69	17.89	17.59

4.5.2 Case $N < M$: Null space precoding based on singular vector selection

In this section, the general algorithm proposed for this case is presented before a novel scheme for the specific case of $M = 3$ Tx and $N = 2$ Rx antennas, is provided.

Assume the precoding matrix to consist of M vectors each selected from the right singular vector matrix of a selected user (there is a possibility that one user contributes more than one vector) given in general form by

$$\mathbf{\Psi} = \left[\begin{array}{ccc} \mathbf{v}_{p_1}^{(k_1)} & \dots & \mathbf{v}_{p_M}^{(k_M)} \end{array} \right], \tag{4.29}$$

where $k_i \in \{1, \dots, K\}$ and $p_i \in \{1, \dots, M\}$. The signal vector at the kth user, $k \in \{k_1, \dots, k_M\}$, after eigenmode Rx pre-processing (multiplying the received signal vector by $\mathbf{U}^{(k)^H}$) is

$$\mathbf{z}_k = \underbrace{\mathbf{\Sigma}_k \mathbf{V}_k^H \mathbf{\Psi}}_{\mathbf{\Delta}_k} \mathbf{x} + \tilde{\mathbf{n}}_k. \tag{4.30}$$

Considering the fact that the last $M-N$ columns of $\mathbf{\Sigma}_k$ are all zero columns, and also for $i \neq j$, $\mathbf{v}_k^{(i)^H}\mathbf{v}_k^{(j)} = 0$, it can be shown that when Ψ contains contains $M-N$ rightmost vectors of $\mathbf{V}_k$, then the nonzero terms of $\mathbf{\Delta}_k$ form the following submatrix

$$\tilde{\mathbf{\Delta}}_k = \tilde{\mathbf{\Sigma}}_k \tilde{\mathbf{V}}_k^H \tilde{\mathbf{\Psi}} \tag{4.31}$$

where $\tilde{\mathbf{\Delta}}_k$ is an $N \times N$ matrix, $\tilde{\mathbf{\Sigma}}_k$ is an $N \times N$ square diagonal matrix with N singular values on its diagonal, $\tilde{\mathbf{V}}_k$ contains only the first N columns of $\mathbf{V}_k$, and $\tilde{\Psi}$ contains N vectors that belong to $\mathbf{V}_{k_i}$s where $k_i \in \{k_1, \ldots, k_M\}$ and $k_i \neq k$. In this case, (4.30) can be rewritten as

$$\tilde{\mathbf{z}} = \tilde{\mathbf{\Delta}}_k \tilde{\mathbf{x}} + \tilde{\mathbf{n}}_k \tag{4.32}$$

where $\tilde{\mathbf{x}}$ is a size N vector and is obtained by eliminating $M-N$ terms from $\mathbf{x}$. Then user k uses $\mathbf{G}_k = \tilde{\mathbf{\Delta}}_k^{-1}$ as its receiver processing matrix to detect N out of the total M transmitted data streams.

For the kth receiver to be able to detect its data using ZF receiver processing, the number of interfering data streams (after Rx pre-processing) must be not greater than N. In another words, the matrix $\mathbf{\Delta}_k$ must have $M-N$ zero columns. This further implies that the precoding matrix needs to contain $M-N$ basis vectors of the null space (space spanned by the right most $M-N$ vectors of $\mathbf{V}_k$) of each selected users channel matrix. Therefore, $\lfloor \frac{M}{M-N} \rfloor$ users can be served simultaneously ($\lfloor \cdot \rfloor$ denotes floor of its argument). Therefore, to be able to take greater advantage of multiuser diversity, N should be as close as possible to M with the best case being $N = M-1$. When $N < M/2$ this scheme would be identical to TDM.

Since the post processing SNR of each data stream in this case depends on the precoding matrix and each selected user's $\mathbf{\Sigma}$ and $\mathbf{V}$ matrices, finding users with channel conditions that maximize the sum rate based on partial CSIT turns out to be not straightforward. Nevertheless, a heuristic approach would be to adopt a two stage user selection, where in the first stage a set of users is selected based on a CQI, e.g., largest singular value. In the next stage, the selected users send back their full CSI to the BS and the BS broadcasts their CSI to all users. Then, knowing the CSI of the selected users, each user (outside of the set of selected users) substitutes itself sequentially for each of the selected users and evaluates the resulting sum rate for each substitution. If a user finds that by substituting itself for one of the selected users, the sum rate increases, it will inform the BS of it. The BS will update the

user set according to the suggestion of the user which has reported the maximum increase in the sum rate. Our results show that the sum rate obtained by adopting this scheme and user selection based on the largest eigenvalue achieves a higher sum rate compared to TDM, while the gap between the sum rate of this scheme and the optimum DPC increases as the number antennas increases. In the following section we present an efficient transmission scheme for the special case of $M = 3$ and $N = 2$.

Case $M = 3$, $N = 2$

Considering the general idea discussed for null space precoding based on eigenvector selection, in this case we consider two possibilities for the precoding matrix. One possibility is to construct $\mathbf{\Psi}$ using three vectors each taken from right singular vector matrix of a distinct user's channel matrix. Therefore, three users can be served and each user's data sees only one interfering data stream. However, in order to find the best set of users which maximizes the sum rate, the base station either requires full channel state information of all users which results in a considerably increased complexity compared to partial CSIT schemes, or an approach similar to the one discussed in Subsection 4.5.1 can be applied. The second option is to construct $\mathbf{\Psi}$ using right singular vectors of two selected user channel matrices. Assume users k_s and k_p where $k_s, k_p \in \{1, \ldots, K\}$ are the indexes of users that will be ultimately scheduled by the proposed algorithm. In the proposed scheme, which is based on a heuristic approach, the precoding matrix is assumed to be

$$\mathbf{\Psi} = [\ \mathbf{v}_3^{(k_s)} \quad \mathbf{v}_3^{(k_p)} \quad \mathbf{v}_2^{(k_p)}\ ]. \tag{4.33}$$

The reasoning behind this choice of precoding matrix will be clarified once the algorithm is presented. Here are the steps of the proposed algorithm:

1. Each user performs the SVD of its channel matrix and sends back $\sigma_1^{(k)}$ to the base station.

2. The base station selects the user with the largest $\sigma_1^{(k)}$, user k_s, and asks that user for $\mathbf{V}_{k_s}$ matrix. To detect its data, user k_s uses $\mathbf{U}_{k_s}^H$ as its receiver processing matrix,

$$\begin{aligned} \mathbf{z}_{k_s} &= \mathbf{U}_{k_s}^H \mathbf{y}_{k_s} \\ &= \mathbf{U}_{k_s}^H \mathbf{U}_{k_s} \mathbf{\Lambda}_{k_s} \mathbf{V}_{k_s}^H \mathbf{\Psi} \mathbf{x} + \mathbf{U}_{k_s}^H \mathbf{n}_{k_s} \\ &= \begin{bmatrix} 0 & \lambda_1^{(k_s)} \chi_1 & \lambda_1^{(k_s)} \chi_2 \\ 0 & \lambda_2^{(k_s)} \chi_3 & \lambda_2^{(k_s)} \chi_4 \end{bmatrix} \mathbf{x} + \hat{\mathbf{n}}_{k_s} \end{aligned} \tag{4.34}$$

where $\chi_1 = \mathbf{v}_1^{(k_s)}\mathbf{v}_3^{(k_p)}$, $\chi_2 = \mathbf{v}_1^{(k_s)}\mathbf{v}_2^{(k_p)}$, $\chi_3 = \mathbf{v}_2^{(k_s)}\mathbf{v}_3^{(k_p)}$ and $\chi_4 = \mathbf{v}_2^{(k_s)}\mathbf{v}_2^{(k_p)}$. As seen in (4.34), the interference caused by the first data stream to the second and third data streams after Rx-processing at user k_s has been canceled. Therefore, a ZF linear receiver can be used and for the second data stream we have [108]

$$\gamma_2^{(k_s)} = \frac{\rho\lambda_1^{(k_s)}}{[(\mathbf{\Omega}^H\mathbf{\Omega})^{-1}]_{11}} \tag{4.35}$$

where $\mathbf{\Omega} = \begin{bmatrix} \chi_1 & \chi_2 \\ \chi_3 & \chi_4 \end{bmatrix}$. Thus, the achievable rate for this user will be $\log_2(1+\gamma_2^{(k_s)})$.

3. The base station broadcasts $\mathbf{V}_{k_s}$ and $\sigma_1^{(k_s)}$ to all users.

4. For now, let us assume user k is the second selected user. Then the precoding matrix will be

$$\mathbf{\Psi} = [\ \mathbf{v}_3^{(k_s)} \quad \mathbf{v}_3^{(k)} \quad \mathbf{v}_2^{(k)}\ ]. \tag{4.36}$$

User k once selected, uses $\mathbf{U}_k^H$ as its receiver processing matrix which will result in

$$\begin{aligned} \mathbf{z}_k &= \mathbf{U}_k^H\mathbf{y}_k \\ &= \mathbf{U}_k^H\mathbf{U}_k\mathbf{\Sigma}_k\mathbf{V}_k^H\underbrace{\mathbf{\Psi}\mathbf{s}}_{\mathbf{x}}+\mathbf{U}_k^H\mathbf{n}_k \\ &= \begin{bmatrix} \sigma_1^{(k)}\alpha_k & 0 & 0 \\ \sigma_1^{(k)}\beta_k & 0 & \sigma_2^{(k)} \end{bmatrix}\begin{bmatrix} s_1 \\ s_2 \\ s_3 \end{bmatrix} + \hat{\mathbf{n}}_k \end{aligned} \tag{4.37}$$

where $\mathbf{z}_k = [\ z_1^{(k)} \quad z_2^{(k)}\ ]^T$, $\alpha_k = \mathbf{v}_1^{(k)^H}\mathbf{v}_3^{(k_s)}$ and $\beta_k = \mathbf{v}_2^{(k)^H}\mathbf{v}_3^{(k_s)}$. It is evident that the interfering effect of s_2 on the other data streams is canceled and the first data stream can be detected using a matched filter, which results in $\gamma_1^{(k)} = \rho\lambda_1^{(k)}|\alpha_k|^2$ as post-processing SNR for the first data stream ($\lambda_1^{(k)} = |\sigma_1^{(k)}|^2$).

To detect the third data stream, the effect of the first detected data stream is subtracted out, i.e., $\hat{z}_2^{(k)} = z_2^{(k)} - \sigma_1^{(k)}\beta_k\tilde{s_1}$ ($\tilde{s_1}$ denotes the first detected data symbol). Canceling the effect of the the first data stream is possible due to the knowledge of $\mathbf{v}_3^{(k_s)}$ at user k which enables it to evaluate β_k. The SNR for the third data stream, s_3, after interference cancelation and matched filtering, is obtained as $\gamma_3^{(k)} = \rho\lambda_2^{(k)}$ (ignoring error propagation).

Considering (4.35) and the third step of the algorithm, user k has all the required information to evaluate the rate of user k_s as well as its own rate.

Therefore, it will send back a sum rate value, $R_k = \log_2(1+\gamma_1^{(k)}) + \log_2(1+\gamma_3^{(k)}) + \log_2(1+\gamma_2^{(k_s)})$, that is achieved by scheduling data transmission to itself and user k_s.

5. The base station selects the second user, user k_p, which has the largest R_k and asks that user to send back $\mathbf{v}_2^{(k_p)}$ and $\mathbf{v}_3^{(k_p)}$ vectors.

   At this stage data transmission to the selected users begins. User k_p will receive its data from the first and third Tx antennas and user k_s will receive its data from the second Tx antenna.

4.6 Numerical Results

In this section, the expected throughputs of the proposed schemes are compared to MIMO-downlink techniques based on transmit beam-matching (TBM) [94], which is a modified version of PU^{2}RC for multiple antenna users, zero-forcing beamforming (ZF-BF) using channel vector quantization (CVQ)[116, 117, 95], spatial multiplexing with zero-forcing receiver processing and TDM with eigenmode transmission for different numbers of antennas, users and SNR values. The throughput of the DPC scheme is also given as an upper bound on the sum rate. The sum rate curves for DPC have been obtained using the iterative water-filling algorithm introduced in[118].

In Fig. 4.1 a MU-MIMO downlink is considered where the base station and each of the users are equipped with 2 antennas. According to Fig. 4.1, the proposed scheme with $M_s = 1$ achieves a considerably higher sum rate compared to ZF linear processing. For the TBM scheme, a codebook size of 4 has been considered, where each codebook consists a 2×2 unitary matrix and it is assumed each user sends back to the base station 8 SNR values, corresponding to all vectors of all unitary matrices in the codebook. As the figure shows, even for a very small user pool, e.g., $K = 5$ users, the proposed scheme has a great sum rate advantage over the sum rate of other schemes with partial CSIT, which are plotted. Sum rate curves obtained using the analytical expressions of Section 4.5.1 have also been plotted, and are in good agreement with the numerical results.

In Fig. 4.2, the sum rate of the proposed scheme is compared to the other schemes for a MU-MIMO downlink, where this time the base station and each user have 3 antennas. As seen in the figure, the proposed scheme with $M_s = 2$ achieves a higher

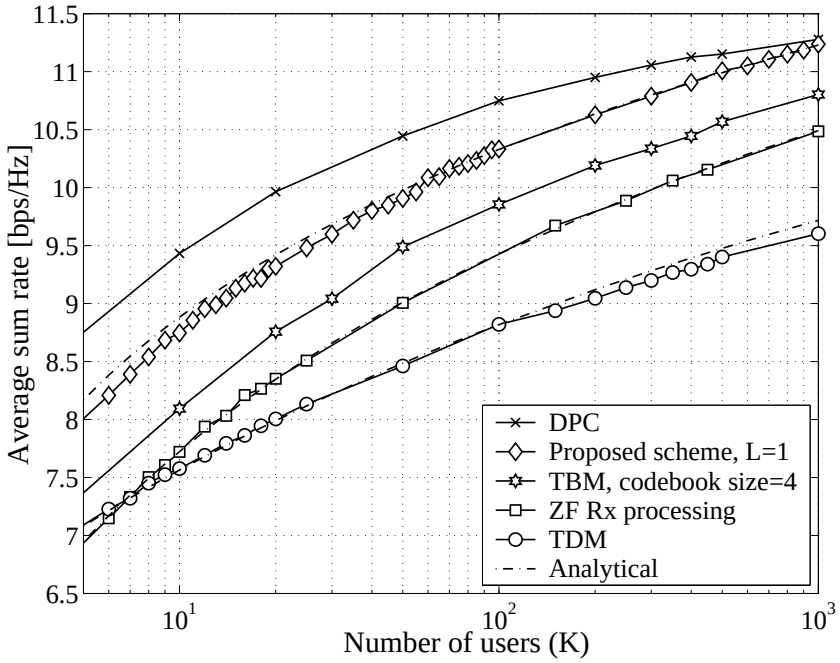

Figure 4.1: Sum rate of the proposed scheme compared to a number of multiuser MIMO techniques for $M = 2$ Tx and $N = 2$ Rx antennas at 10 dB SNR.

average sum rate compared to the case of $M_s = 1$ while there are up to $K = 12$ users in the system. When there are more users in the system, the proposed scheme with $M_s = 1$ achieves a higher sum rate. The intersection of the average sum rate curves for $M_s = 1$ and $M_s = 2$ can be explained by considering the fact that for a small pool of users it is less likely that a subset of users with high ZF post-processing SNR (good channel conditions) exist in the system and therefore transmitting on the first two non-interfering eigenmodes to one user leads to a higher sum rate. For larger user pools and in agreement with Theorem 2 due to multiuser diversity it is more likely that a user subset can be found such that it achieves higher sum rate than eigenmode transmission on the first two eigenmodes to one user. According to Fig. 4.2, the proposed scheme achieves a considerably higher sum rate compared to ZF receiver processing. For transmit beam-matching (TBM), a codebook size of 4 has been considered, where each codebook consists of a 3×3 unitary matrix and it is assumed that each user sends back 12 SNR values to the base station. Sum rate curves obtained using the analytical expressions of Section 4.5.1 have also been plotted, and are in good agreement with the simulation results.

Fig. 4.3 shows the sum rate advantage of the proposed scheme to two well known MU-MIMO schemes with partial CSIT. As seen on the figure, the proposed scheme

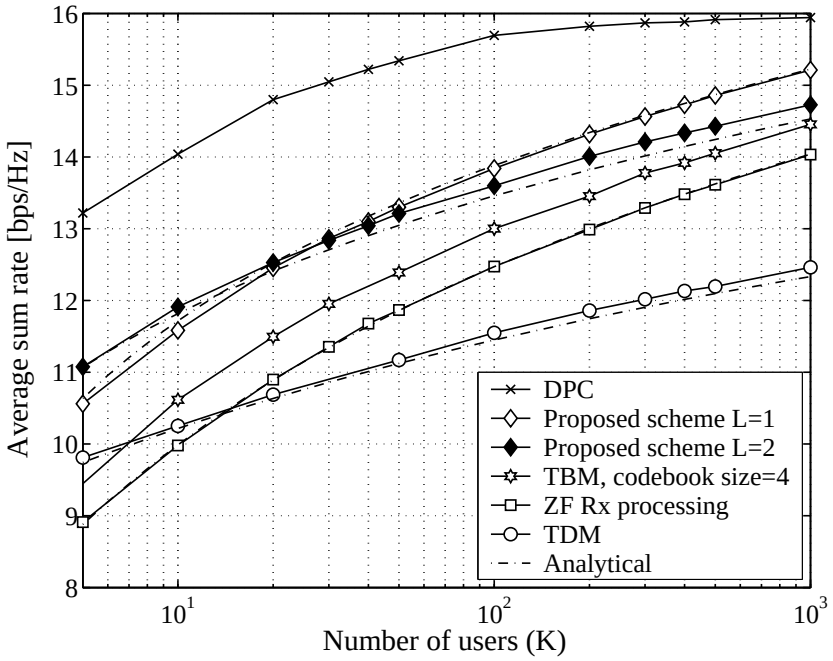

Figure 4.2: Sum rate of the proposed scheme for $M_s = 1$ and 2 compared to a number of multiuser MIMO techniques for $M = 3$ Tx and $N = 3$ Rx antennas at 10 dB SNR.

achieves a higher sum rate compered to TBM, and zero-forcing beamforming (ZF-BF) with channel vector quantization (CVQ). The proposed scheme has over 1 bit/s/Hz advantage over TBM and ZF-BF with CVQ for even small size user pools ($K < 10$).

4.6.1 Comparison of feedback requirements for different schemes

In MU-MIMO schemes with partial CSIT, there is usually a tradeoff between the sum rate and feedback load. An example of this tradeoff is seen in the PU^{2}RC scheme where there are two feedback modes, in one mode which achieves higher average sum rate, the SINR of all codewords are sent back to the base station, and in the other mode only the largest SINR and the index of its corresponding codeword are sent back to the base station. In ZF-BF with CVQ each user sends back the index of a selected quantization vector along with its corresponding SINR lower bound [95, 116]. In the transmission scheme based on spatial multiplexing at the base station with linear receiver processing at each user terminal, each user sends back M SNR values to the base station. In TDM with eigenmode transmission, each user sends back only one real value (a rate value), before the user with the highest

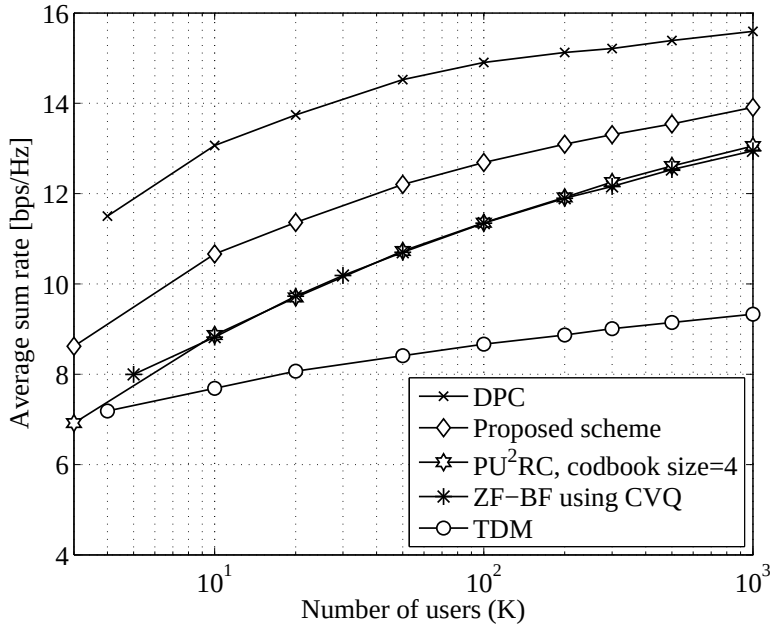

Figure 4.3: Sum rate of the proposed schemes compared to multiuser MIMO techniques based on TBM (modified PU^{2}RC), ZFBF with CVQ, and TDM with eigenmmode transmission for $M = 3$ Tx and $N = 2$ Rx antennas at 10 dB SNR.

reported rate is asked to send back its right singular matrix, which has $2M^2$ real terms.

In our proposed scheme and for the case of $N \geq M$, users send back information in three stages. At the first stage all users send back a single rate value, in the second stage one user sends back an $N \times N$ matrix of complex values, and in the the third stage all users except one send back $M - M_s$ SNR values. This amount of feedback is larger than the amount required in TDM with eigenmode transmission, yet it is comparable to PU^{2}RC and spatial multiplexing at the base station with ZF receiver processing schemes at user terminals described in Section 4.4.

For the proposed scheme in case of $M = 3$ and $N = 2$, each user needs to feedback only one real value to the base station at the first stage. In the second stage, one user needs to send back a 2×2 matrix, and in the third stage all users except one need to send back one rate value. Finally, the second select user sends back two vectors to the base station. This amount of feedback is larger than the amount required in TDM with eigenmode transmission, yet, less than ZF-BF with CVQ [116], since except for the two users, all other users send back only two real values in two stages.

4.7 Summary

We have proposed MIMO downlink transmission schemes with partial CSIT requirement for a system in which the base station and each user terminal are equipped with $M(>1)$ and $N(>1)$ antennas, respectively. For the case of $N \geq M$, one user receives data through eigenmode transmission on its M_s ($M_s < M$ is a predetermined value, which maximizes the average sum rate) strongest eigenmodes, while each of the remaining $M - M_s$ data streams is assigned to a user with the highest ZF receiver post-processing SNR. We have shown that in this case the average sum rate of the proposed scheme scales with $\ln[\ln(MK)]$ (K is the number of users in the system), which is asymptotically optimal. In case of $M > N$, the precoding matrix consists of right singular vectors of at least two, and at most M users such that the number of interfering streams at each selected user terminal is reduced to the number of its receive antennas and hence, the inter-stream interference can be effectively removed using ZF receiver processing. The results show that the proposed schemes lead to a higher average sum rate compared to a number of well-known limited feedback schemes, especially for a small pool of users.

Chapter 5

Net Throughput Maximization of Limited Feedback MIMO-OFDM Downlink with Per-Chunk User Scheduling

5.1 Introduction

Multiple-input multiple-output (MIMO) downlink transmission schemes based on limited feedback were briefly discussed in Chapter 4. Spatial multiplexing with opportunistic feedback and linear receivers [119], and opportunistic beamforming with signal-to-interference-plus-noise ratio (SINR) feedback [86] are some examples ([26, 27] and references therein contain an overview of the subject).

In general, any MIMO downlink scheme can be applied to individual subcarriers of MIMO-OFDM with additional complexity of finding the optimum subcarrier-antenna power allocation strategy compared to only antenna power allocation. Nevertheless, for MIMO downlink schemes which do not consider the problem of power allocation, their extension to MIMO-OFDM is very straightforward.

In the multiuser OFDM scheme described in [120], the base station (BS) modulates the data of each selected user onto a subcarrier designated exclusively to that user and due to the orthogonality of the subcarriers there is no inter-user interference. In a similar scheme involving MIMO spatial multiplexing [121] the data rate on each given subcarrier is increased by eigen-beamforming, which creates parallel spatial channels. In the aforementioned schemes, the user which achieves the highest rate on a given subcarrier is selected by the base station's scheduler to be served on that subcarrier. This type of resource allocation is a case of frequency division

multiplexing (FDM). In [122] a scheduling and beamforming scheme is proposed for MIMO-OFDM downlink, in which by using a new channel decomposition technique and also grouping adjacent subcarriers into clusters (chunks), the sum rate is slightly increased and required feedback is reduced compared to per subcarrier eigen-beamforming. Three low complexity, high throughput schemes are selected for comparison from existing limited feedback MIMO downlink techniques, each being a representative member of a class of limited feedback MIMO-downlink transmission methods. They are briefly described in the following.

In[32], a limited feedback MIMO-downlink scheme based on eigenvector precoding and zero forcing (ZF) receiver processing is proposed, in which system parameters determine the number of data streams to be assigned to one user to receive these streams through eigenmode transmission, while the remaining data streams are assigned to other users with ZF receiver (Rx) processors.

In [94], a multiuser MIMO downlink scheme called transmit beam matching (TBM) is introduced, which extends to multiple antenna users the per-user unitary rate control (PU^{2}RC)[102, 89] scheme, which is the Samsung's proposal to the 3rd Generation Partnership Project (3GPP). This scheme has the relatively low complexity structure of PU^{2}RC and it uses the channel matrix pseudo-inverse operation in order to minimize inter-stream interference at each user terminal.

In [107], a multiuser MIMO downlink scheme with spatial multiplexing at the BS is proposed, in which users use linear processors and send back the signal to noise ratio (SNR) of each spatial channel to the BS, and the BS selects the user with the highest SNR for each data stream.

In multiuser MIMO-OFDM systems, the control overhead and signal processing complexity can be quite large. Therefore, to reduce the overhead and complexity, the available time-frequency resources are divided into tiles or chunks [123]. The chunks are considered two-dimensional, and each chunk consists of a number of adjacent subcarriers in frequency domain and a number of consecutive OFDM symbols in time domain. For all subcarriers and all OFDM symbols within the chunk, the same spatial signal processing is applied, reducing the signal processing complexity and the feedback overhead considerably.

Most contributions available in the literature on multiuser MIMO downlink use average sum rate as a comparison benchmark. Usually the average sum rate increase of different schemes with respect to the increase in the number of users is compared.

However, the average sum rate does not account for the amount of feedback required for any given scheme. Furthermore, wireless channels are time-varying by nature, and only approximately a wireless channel stays almost unchanged over a time interval (coherence time) of limited duration, which here we refer to as a frame. When considering time division duplex (TDD) multiuser MIMO-downlink, it is required that CSIT from all users be available at the BS in a time much shorter than the frame duration, which itself implies that the user pool can not be arbitrarily large. This is due to the fact that uplink channel (when the channel is reciprocal only pilot symbols for channel estimation are required to be sent on the uplink channel) has a limited capacity and as the number of users increases, the number of pilot symbols required to be send back reliably to the BS increases, which itself results in a longer time necessary to deliver to the transmitter full CSI for all users. Since data transmission can not begin before having CSI for all users, transmission time is effectively reduced to only the portion of the frame duration that is left after pilot transmission is completed. This reduction of time for data transmission results in a lower average sum rate, also known as net throughput, which will be defined later in this chapter. In the remaining of this chapter, required pilots on the uplink channel will be considered as feedback information from mobile users.

In this chapter, we propose per chunk user scheduling for limited feedback multiuser MIMO-OFDM downlink with optimized chunk size and obtain a very close approximation for the sum rate of the system. We also show net throughput advantage of per-chunk user scheduling with optimized chunk size over a number of limited feedback multiuser MIMO-OFDM downlink schemes. Further reduction of the feedback requirement of the proposed scheme is also investigated when opportunistic feedback is applied.

5.2 Preliminaries

5.2.1 Channel and system model

We consider multiuser MIMO-OFDM downlink in a single cell, in which the base station is equipped with M antennas and there are K homogeneous users each equipped with N ($N = M$) antennas. The assumption of $N = M$ is reasonable for small values of M ($M \leq 4$) considered in this work. The system block diagram is shown in Fig. 5.2.1.

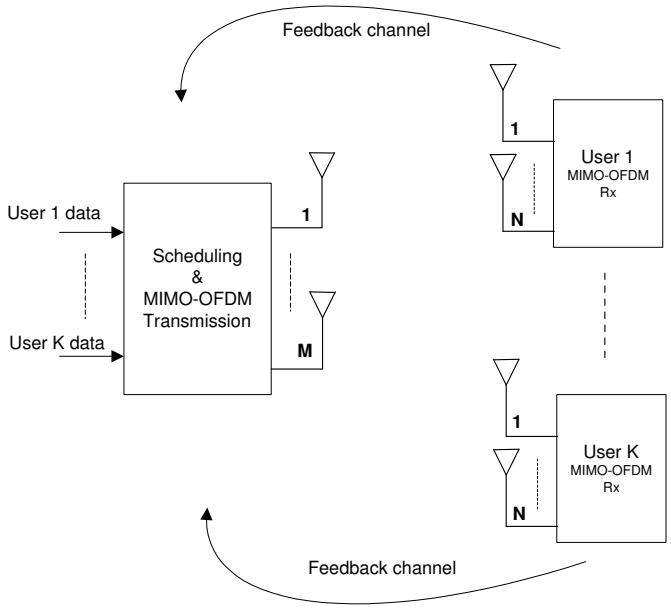

Figure 5.1: Multiuser MIMO-OFDM system model.

The channel is assumed to be frequency selective and is modeled as a length P finite impulse response (FIR) filter [124]. The space frequency channel at the l^{th} tone for the kth user can be described as

$$\mathbf{H}_l^{(k)} = \sum_{p=0}^{P-1} \sigma_p \mathbf{H}[k,p] \exp\left(-j2\pi \frac{l}{L} p\right), \quad 0 \leq l \leq L-1 \tag{5.1}$$

where $\exp(\cdot)$ denotes the exponential function, L is the total number of subcarriers in the system, and the size $M \times M$ $\mathbf{H}[k,p]$ matrices for $p = 0, \ldots, P-1$, represent the MIMO channel impulse responses of the kth user. The $\mathbf{H}[k,p]$ matrices are assumed to be mutually uncorrelated. It is also assumed that the channel gains within each matrix exhibit spatially uncorrelated Rayleigh fading; each $\mathbf{H}[k,p]$ contains independent $\mathcal{CN}(0,1)$ elements. Also, σ_p^2 for $p = 0, \ldots, P-1$, represents the channel power delay profile normalized by assuming $\sum_{p=0}^{P-1} \sigma_p^2 = 1$. The channel is assumed to be quasi-static, remaining constant for the duration of one frame containing a number of OFDM symbols, and changing independently between frames. The correlation coefficients between the channel elements on two arbitrary subcarriers l and

u are given by [125],

$$\begin{aligned}\beta_{l,u} &= \mathrm{E}[(\mathbf{H}_l^{(k)})_{m,n}(\mathbf{H}_u^{(k)})^*_{m',n'}] \\ &= \sum_{p=0}^{P-1} \sigma_p^2 \exp\left(-j2\pi(l-u)p/L\right)\delta[m-m']\delta[n-n']\end{aligned} \tag{5.2}$$

where $(\mathbf{A})_{i,j}$ denotes the element of matrix $\mathbf{A}$ at the ith row and jth column, $(\cdot)^*$ denotes complex conjugate and $\delta(\cdot)$ denotes the Dirac's delta function. The closer the subcarriers are, the larger the magnitude of the correlation coefficient, $|\beta_{l,u}|$, is.

The kth user receives the following signal vector on the lth subcarrier

$$\mathbf{y}_l^{(k)} = \mathbf{H}_l^{(k)}\mathbf{x}_l + \mathbf{n}_l^{(k)}, \tag{5.3}$$

where $\mathbf{H}_l^{(k)}$ is given by (5.1), and $\mathbf{x}_l$ is the transmitted signal vector on the lth subcarrier. The vector $\mathbf{n}_l^{(k)}$ is the normalized noise vector with $\mathcal{CN}(0,1)$ elements. Hence, the average SNR is equal to P_T where $P_T = \frac{1}{L}\sum_{l=0}^{L-1}(\mathbf{E}[\mathbf{x}_l\mathbf{x}_l^H])$ defines the power constraint of the base station. Let the total rate delivered by the base station to the users during one time slot be R. Then the expected throughput of the system is obtained by taking ensemble average of R over $\mathbf{H}_l^{(k)}$s, i.e., $\bar{R} = E_{\mathbf{H}_0^{(k)},\ldots,\mathbf{H}_{L-1}^{(k)},k=1,\ldots,K}[R]$. Throughout the chapter, the terms system throughput and sum rate are used interchangeably.

5.2.2 Net throughput

Consider MIMO-OFDM downlink with finite coherence time, denoted here as T. The feedback overhead reduces the average throughput, $\bar{R}$, to the average net (effective) throughput, $\bar{R}_{net}$, given by [123]

$$\bar{R}_{net} = \bar{R}\left(1 - N_f\frac{T_f}{T}\right) \tag{5.4}$$

where N_f is the average number of feedback values per subcarrier sent back by all users during time T. T_f is the time required to send back each quantized feedback value to the base station. The term N_fT_f is the portion of the coherence time used for sending the feedback information (i.e., pilot symbols in a time division duplex (TDD) system). Similar definitions for net throughput can be found in [126, 127]. By replacing $1 - N_f\frac{T_f}{T}$ with the ratio of the bandwidth used for feedback over the total available bandwidth, the net throughput definition can be applied to frequency division duplex (FDD) systems, which however are not considered in this work.

5.3 MIMO-OFDM Downlink with Per-Chunk User Scheduling and Optimized Chunk Size

As it was mentioned in Section 5.1 the chunks are two-dimensional tiles, each consisting of a number of adjacent subcarriers in frequency domain and a number of consecutive OFDM symbols in time domain. Assuming the number of subcarriers in each chunk is L_c (for simplicity we assume all chunks have the same number of subcarriers and L is an integer multiple of L_c), the highest instantaneous reliable rate on the qth chunk in bits per second per Hertz (b/s/Hz) for user k is given by

$$r_{chk,q}^{(k)} = \frac{1}{L_c} \sum_{l_c=(q-1)L_c}^{qL_c-1} r_{l_c}^{(k)} \quad 1 \leq q \leq Q \tag{5.5}$$

where $Q = \frac{L}{L_c}$ denotes the number of chunks in the system and $r_{l_c}^{(k)}$ is defined as [128]

$$r_{l_c}^{(k)} = \log_2 \det(\mathbf{I} + \rho \mathbf{H}_{l_c}^{(k)} \mathbf{H}_{l_c}^{(k)^H}), \quad 0 \leq l_c \leq L-1. \tag{5.6}$$

where $\rho = \frac{P_T}{M}$. This rate is the MIMO link's open loop capacity and is achieved by spatially multiplexed transmission and successive interference cancellation at each receiver [128]. In this proposed scheme, each user sends back the achievable rate of each chunk, Q in total, to the base station and the base station assigns each chunk to the user, which has reported the highest rate for that chunk. It is expected that by grouping subcarriers into chunks, especially chunks containing a small number of adjacent subcarriers, which have higher correlation compared to subcarriers further apart, the sum rate will not significantly decrease, while the amount of feedback will be reduced by a factor of L_c. In the following subsection we present an analytical framework for finding the optimum chunk size.

5.3.1 Sum rate analysis

The average sum rate for this scheme is given by

$$\bar{R} = \mathrm{E}\left[\frac{1}{Q}\sum_{q=1}^{Q} \max_{1\leq k\leq K} r_{chk,q}^{(k)}\right], \tag{5.7}$$

where the expectation is over all channel realizations. As $r_{l_c}^{(k)}$ is well approximated to be Gaussian [129], $r_{chk,q}^{(k)}$ can also be approximated by Gaussian distribution. In [32], it has been shown that a close approximation for the expected value of the

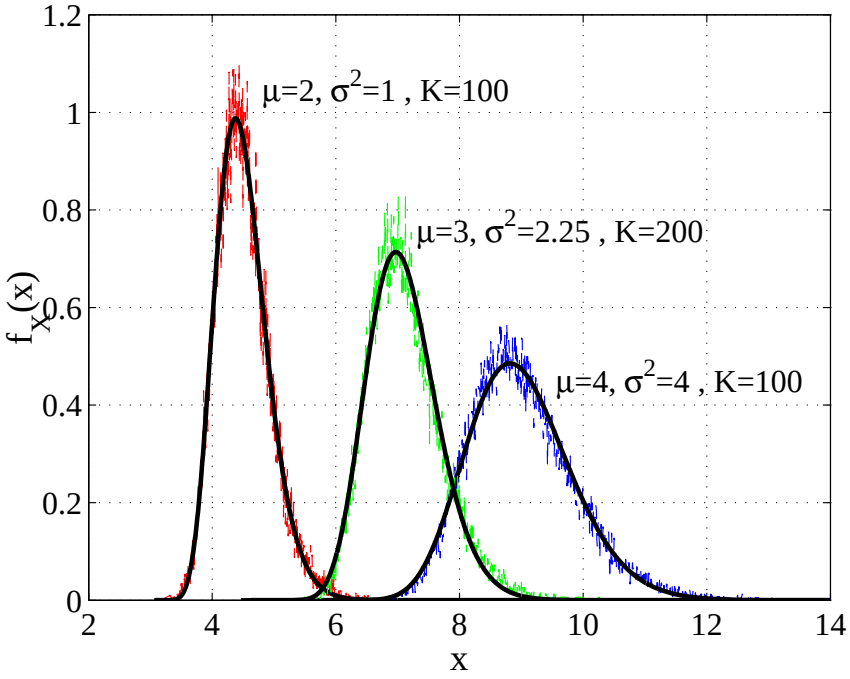

Figure 5.2: Comparison of the approximate PDF of maximum of K i.i.d. Gaussian random variables each with mean μ and variance σ^2 (solid lines) with the PDF obtained from simulations (dashed line).

maximum of a set of K independent and identically distributed (i.i.d.) Gaussian random variables each having mean μ and variance σ^2, is given by

$$\mathrm{E}\left[\max_{1\leq k\leq K}\mathcal{N}^{(k)}(\mu,\sigma^2)\right]\approx\sigma\,\mathrm{G}(K)+\mu. \tag{5.8}$$

where

$$G(K)=\frac{1}{0.1975}\left[0.5264^{\frac{0.135}{K}}-(1-0.5264^{\frac{1}{K}})^{0.135}\right]. \tag{5.9}$$

Fig. 5.2 shows the accuracy of the approximation. Therefore, in order to be able to use (5.8) to approximate $\bar{R}$, the mean and variance of $r_{chk,q}^{(k)}$ are required. In [125] it has been shown that the mean of the rate of each chunk, $\mathrm{E}[r_{chk,q}]$ (since homogenous users are considered, the user index, k, is discarded), is the same for all chunks, i.e., $\mathrm{E}[r_{chk,q}]=\mathrm{E}[r_{chk,u}],\ q\neq u$, even if the chunk sizes are not equal and is given by[130]

$$\mathrm{E}[r_{chk,q}]=\frac{1}{\ln(2)\prod_{m=1}^{M}[\Gamma(M-m+1)]^2}\sum_{k=1}^{M}\det(\mathbf{A}(k)) \tag{5.10}$$

where $\mathbf{A}(k)$, $k=1,\ldots,M$, are $M\times M$ matrices whose entries are defined by

$$\{\mathbf{A}(k)\}_{i,j}=\begin{cases}(x_{i,j}-1)!\exp(1/\rho)\sum_{s=1}^{x_{i,j}}\frac{\gamma(s-x_{i,j},\frac{1}{\rho})}{\rho^{(x_{i,j}-s)}}, & j=k\\ (x_{i,j}-1)!, & j\neq k.\end{cases} \tag{5.11}$$

where $x_{i,j} = 2M - i - j + 1$, $n!$ denotes factorial of n, and $\gamma(\cdot,\cdot)$ denotes the incomplete Gamma function defined as [110]

$$\gamma(x,a) = \int_a^{\infty} t^{x-1}\exp(-t)dt. \tag{5.12}$$

For a point-to-point MIMO-OFDM, the variance of the instantaneous reliable rate $r_{l_c}^{(k)}$ has been derived in [125]. For the variance of the rate of each chunk we prove the following theorem.

Theorem 4 *For a MIMO-OFDM link with channel gains exhibiting spatially uncorrelated Rayleigh fading, the variance of the instantaneous reliable rate on each chunk, variance of $r_{chk,q}$, for all chunks with equal number of subcarriers, L_c, is the same and is given by*

$$\begin{aligned}\mathrm{Var}(r_{chk,q}) = &\frac{2[\log_2(e)]^2\exp(2/\rho)}{(L_c)^2[\prod_{m=1}^{M}\Gamma(M-m+1)]^2}\sum_{d=1}^{L_c-1}\left[(L_c-d)\sum_{r=1}^{M}\sum_{s=1}^{M}\det\left(\mathbf{C}_{r,s}(\beta_{0,d})\right)\right]\\ &+\frac{1}{L_c\ln^2(2)[\prod_{m=1}^{M}\Gamma(M-m+1)]^2}\sum_{k=1}^{M}\sum_{l=1}^{M}\det\left(\mathbf{B}(k,l)\right)-\mathrm{E}^2\left[r_{chk,q}\right]\end{aligned} \tag{5.16}$$

where the matrices $\mathbf{C}_{r,s}(\beta_{0,d})$ and $\mathbf{B}(k,l)$ are given at the bottom of this page. $\beta_{0,d}$ is defined by (5.2). The functions g_1 and g_2 are defined as $g_1(z) = \sum_{n=1}^{z}\mathrm{E}_n(\rho)$ and

---

$$[\mathbf{C}_{r,s}(\beta_{0,d})]_{i,j} = \begin{cases}\eta_{i,j}(1,\beta_{0,d}), & \text{for } i\neq r, j\neq s\\ \eta_{i,j}(g_1(i+j-1),\beta_{0,d}), & \text{for } i=r, j\neq s\\ |\beta_{0,d}|^{2(i-j)}\eta_{j,i}(g_1(i+j-1),\beta_{0,d}), & \text{for } i\neq r, j=s\\ \frac{(1-|\beta_{0,d}|^2)^{i+j-1}}{|\beta_{0,d}|^{2(j-1)}}\exp\left(\frac{2|\beta_{0,d}|^2}{\rho(1-|\beta_{0,d}|^2)}\right)\times & \\ \sum_{t=0}^{\infty}\frac{|\beta_{0,d}|^{2t}\Gamma(i+t)\Gamma(j+t)g_2(i+t)g_2(j+t)}{(t!)^2} & \text{for } i=r, j=s\end{cases} \tag{5.13}$$

where $1\leq i,j\leq M$ and

$$\eta_{i,j}(f(z),\beta_{0,d}) = \Gamma(j)\sum_{t=0}^{j-1}\binom{j-1}{t}\left(\frac{1-|\beta_{0,d}|^2}{|\beta_{0,d}|^2}\right)^t\frac{\Gamma(i+j-t-1)}{\Gamma(j-t)}f(z-t) \tag{5.14}$$

for an arbitrary f function.

$$\{\mathbf{B}(k,l)\}_{i,j} = \begin{cases}\int_0^{\infty} y^{x_{i,j}-1}\ln^2(1+\rho y)\exp(-y)dy & \text{for } j=k=l\\ (x_{i,j}-1)!\exp(\frac{1}{\rho})\sum_{m=1}^{x_{i,j}}\frac{\gamma(m-x_{i,j},\frac{1}{\rho})}{\rho^{x_{i,j}-m}} & \text{for } j=k \text{ or } l; k\neq l\\ (x_{i,j}-1)! & \text{for } j\neq k; j\neq l\end{cases} \tag{5.15}$$

$g_2(z) = \sum_{n=1}^{z} \mathrm{E}_n\left(\frac{1}{\rho[1-|\beta_{0,d}|^2]}\right)$, *respectively.* $\mathrm{E}_n(\cdot)$ *is the exponential integral defined as [110]*

$$\mathrm{E}_n(x) = \begin{cases} \int_x^\infty \frac{\exp(-t)}{t} dt, & n = 1 \\ \int_{t=1}^\infty \frac{\exp(-xt)}{t^n} dt, & n > 1 \end{cases} \tag{5.17}$$

and for $n > 1$, $\mathrm{E}_n(\cdot)$ *can be evaluated using the following recursive equation [110]*

$$\mathrm{E}_n(x) = \frac{1}{n-1}\left[\exp(-x) - x\,\mathrm{E}_{n-1}(x)\right]. \tag{5.18}$$

Proof 4 *See Appendix D for the proof.*

Using (5.8), (5.10) and (5.16), the average sum rate of the proposed per-chunk user scheduling scheme is approximated by

$$\bar{R} \approx \sqrt{\mathrm{Var}(r_{chk,q})}\,\mathrm{G}(K) + \mathrm{E}[r_{chk,q}] \tag{5.19}$$

The unique feature of (5.19) is that the effect of the chunk size and the effect of the number of available users in the system on the sum rate are clearly separate through $\sqrt{\mathrm{Var}(r_{chk,q})}$ and $G(K)$. The maximum net throughput for this scheme is then approximated by

$$\bar{R}_{net}^{max} \approx \bar{R}(1 - \frac{N_f^{(max)} T_f}{T}). \tag{5.20}$$

where $N_f^{(max)} = \frac{K}{L_c^{(max)}}$ is the average number of feedback terms per subcarrier. $L_c^{(max)}$ is the chunk size which maximizes $\bar{R}_{net}$, the net throughput given by (5.20), for an arbitrary chunk size.

5.3.2 Further feedback reduction by opportunistic feedback

In this subsection, similarly to [98] we consider the case where users do not send back the rate of all chunks, but only chunk rates above a certain threshold are allowed to be sent back to the BS. We simply use the expected value of the sum rate, $\bar{R}$, as the threshold, as finding the optimum threshold [98] is beyond the scope of this thesis. The average net throughput then is obtained using the following theorem.

Theorem 5 *Consider limited feedback MIMO-OFDM downlink with per chunk user scheduling, in which users report back the achievable rates of only those chunks that have achievable rates greater than a predetermined threshold. When the system's average sum rate is used as the threshold, the average net throughput can then be approximated by*

$$\bar{R}_{net}^{opp} \approx \bar{R}(1 - \frac{2KT_f}{TL_c} F_R(\bar{R})) \tag{5.21}$$

where $F_R(\cdot)$ is the cumulative distribution function (CDF) of the instantaneous sum rate, R, and is given in Appendix E.

Proof 5 *See Appendix E for the proof.*

5.3.3 Number of feedback terms

In this subsection we evaluate the number of feedback terms per subcarrier for the limited feedback multiuser MIMO-OFDM downlink schemes considered in this work. For schemes which require full channel state information at the BS, assuming there are K users in the system, and each user sends back complex elements of P matrices (each of size $M \times M$), $N_f = \frac{2KPM^2}{L}$ terms per subcarrier that are sent back by all users. P is defined in Subsection 5.2.1.

For eigenvector precoding with ZF Rx processing, each user sends back L rate values, each corresponding to one subcarrier, at the first stage. At the next stage, one user which has been selected in the previous stage sends back its right eigenvector matrix consisting of $2M^2$ real values, and at the last stage all users except the one already selected send back $M - L_s$ values where $1 \leq L_s < M$ is a predetermined value which depends on the system parameters. Therefore, $N_f = K + 2M^2 + (K - 1)(M - L_s)$ is the total number of feedback terms per subcarrier send back by all users.

In transmit beam matching, we assume that each user sends back the post-processing SNR of all vectors of all codewords on each subcarrier which results in $N_f = KN_cM$ where N_c is the number of codewords and each codeword has M vectors.

In spatial multiplexing with linear receivers, each user sends back M SNR values per subcarrier which results in $N_f = KM$.

In per chunk user scheduling each user sends back Q rate values, each corresponding to a chunk. Therefore, $N_f = \frac{KQ}{L} = \frac{K}{L_c}$. This amount of feedback is reduced to $\bar{N}_f = \frac{2KF_R(\bar{R})}{L_c}$ (see Appendix E) by adopting the opportunistic feedback strategy described in the previous subsection.

The numbers of feedback terms (per subcarrier), N_f, for different schemes have been summarized in Table 5.1.

Table 5.1: Numbers of feedback terms for different schemes in terms of number of users, K, number of antennas at the BS and each user terminal, M, chunk size, L_c, and other parameters specified for each scheme above.

Scheme	N_f
All schemes requiring full CSIT	$2KPM^2/L$
Eigenvector precoding with ZF Rx processing	$K + 2M^2 + (K-1)(M - L_s)$
Transmit beam matching	KN_cM
Per chunk user scheduling	K/L_c
Per chunk user scheduling with opportunistic feedback	$2KF_R(\bar{R})/L_c$

5.4 Numerical Results

For the numerical results presented in this section, we model the channel using the exponential power delay profile [125]:

$$\sigma_p^2 = \frac{1 - \exp(-1/K_{exp})}{1 - \exp(-P/K_{exp})} \exp(-p/K_{exp}), \quad 0 \leq p \leq P-1. \tag{5.22}$$

where P is the total number of resolvable paths and K_{exp} characterizes the rate of decay of the power delay profile as a function of p, and is loosely related to the root mean square (RMS) delay spread[131]. Without loss of generality, throughout this section we have set $K_{exp} = 2$ and $P = 8$.

Fig. 5.3 examines the accuracy of the average sum rate approximation of (5.19) by comparing it to the average sum rate values obtained through a semi-analytical approach for $M = N = 2$, or 3 antennas at both the BS and each user terminal, and plotted versus the number of users at $P_T = 10$ dB. The system considered has $L = 64$ subcarriers with chunk size of $L_c = 16$. In the semi-analytical approach, for one system realization, a set of random channel matrices is generated and used to evaluate the sum rate of each scheme according to the scheme's scheduling and signal processing approach. The average sum rate is then obtained by averaging the sum rates over a large number of realizations. The analytical results are in good agreement with the semi-analytical results. As expected and due to multiuser diversity, the average sum rate increases with the number of users.

In Fig. 5.4, the average net throughput of the proposed scheme is plotted versus the chunk size, L_c. The system considered has $L = 64$ subcarriers with $M = N = 3$ as the number of antennas at the base station and each user terminal. It is also assumed that $\frac{T_f}{T} = 0.002$. Furthermore, the frame size is assumed to be equal to the channel's coherence time and long enough to allow transmission rates close to

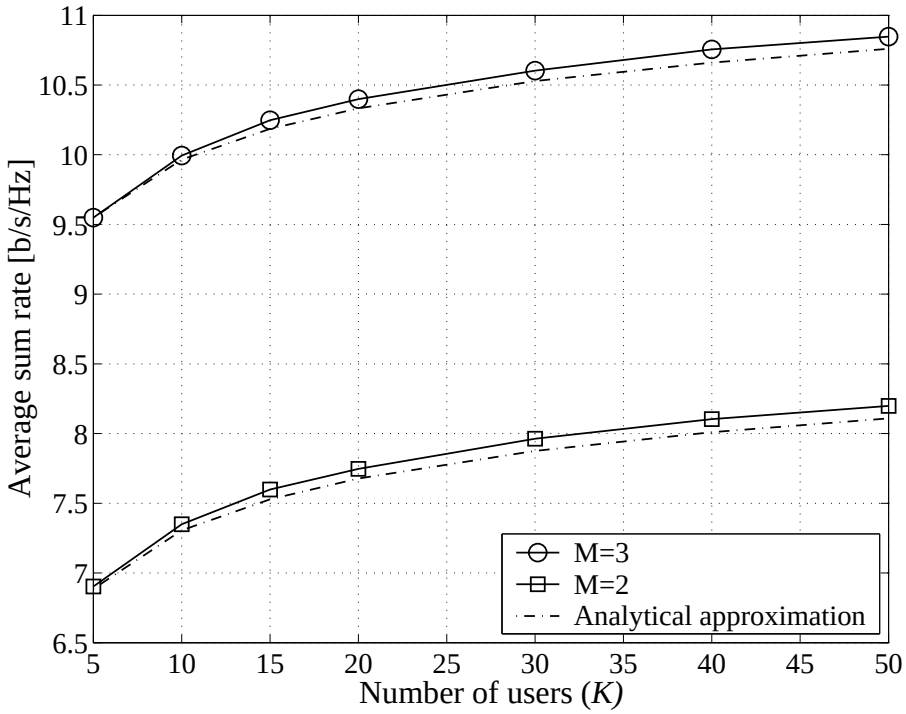

Figure 5.3: Average sum rate for a system with $L = 64$ subcarriers, $P_T = 10$ dB, $L_c = 8$ chunk size, and $K_{exp} = 2$, versus the number of users for MIMO-OFDM systems with $M = 2$ and 3 antennas at the BS and each user terminal.

each links capacity; since the average net throughput only depends on $\frac{T_f}{T}$ and not T itself, the actual value of T is irrelevant to the results presented here. In this figure the effect of varying the number of users in the system, K, and the chunk size, L_c, on the average net throughput is examined. As seen in the figure, for any K value, there exists a chunk size which maximizes the average net throughput. Also by decreasing K from 500 to 100, the optimum chunk size varies from $L_c^{(max)} = 4$ to 16. In other words, the decrease in the number of users results in a larger optimum chunk size. This can be explained by considering (5.20), in which the average net throughput is given as the product of $\bar{R}$ and $1 - \frac{\bar{N}_f T_f}{T}$ where by substituting $\bar{N}_f$ with $K\frac{1}{L_c}$ (see Subsection 5.3.1) in the latter term, the average net throughput is simplified to $\bar{R}\left[1 - (\frac{K}{L_c})(\frac{T_f}{T})\right]$. Numerical results show that as the chunk size increases, $\mathrm{Var}\,(r_{chk,q})$ decreases and therefore, according to (5.19) for a fixed K, $\bar{R}$ decreases. On the other hand, by increasing L_c, the factor $1 - (\frac{K}{L_c})(\frac{T_f}{T})$ increases. The rate of increase of this factor depends on K and for smaller K values, the chunk size which maximizes the net throughput will move to larger L_c values.

In Figs. 5.5 and 5.6, the average net throughput of the proposed scheme is plot-

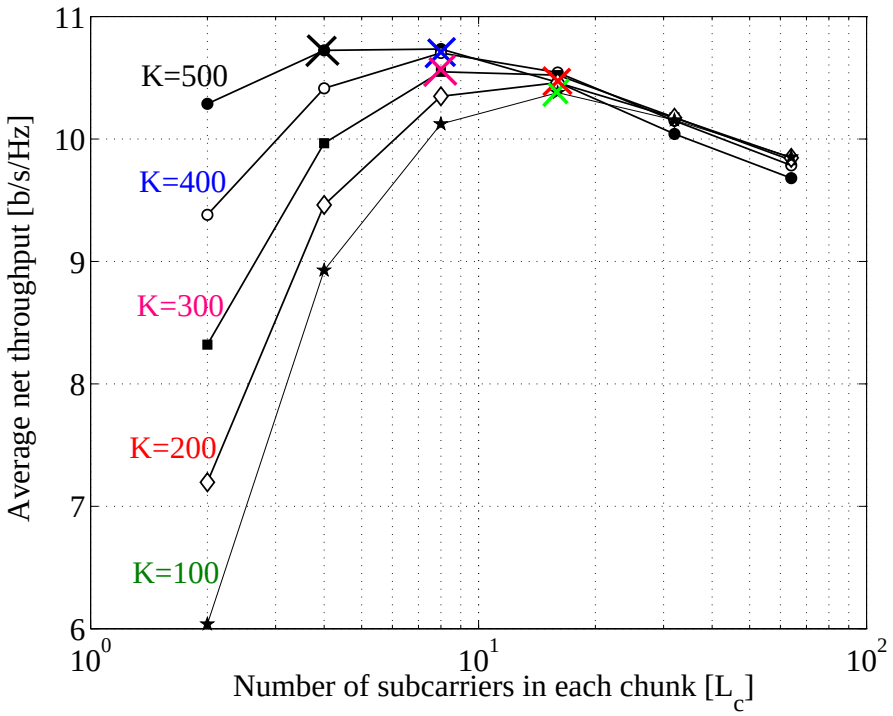

Figure 5.4: Average net throughput for a system with $L = 64$ subcarriers, $P_T = 10$ dB, $M = N = 3$ antennas, and $\frac{T_f}{T} = 0.002$ versus chunk size for different K values. The maximum net throughput coordinate of each curve has been labeled with a cross mark.

ted versus the number of users for a system with $L = 64$ subcarriers, for two $\frac{T_f}{T}$ values. The optimum chunk size, $L_c^{(max)}$ is used for each K value to obtain the net throughput of the proposed per chunk user scheduling scheme. For the proposed scheme with opportunistic feedback, $\bar{R}_{net}^{opp}$ is obtained through semi-analytical approach to find $\bar{R}$ and using $\bar{N}_f$ to evaluate the number of feedback terms. Fig. 5.5 shows that as the number of users increases, the net throughputs of DPC, eigenvector precoding with ZF Rx processing, spatial multiplexing with ZF Rx processing and PU^{2}RC, approach zero. This is due to the fact that the amount of feedback required for these schemes increases linearly with ζK where ζ is greater than one for these schemes (refer to III.C), while their sum rate in the best case increases with $M \ln(\ln(MK))$ [87]. However, the proposed scheme's net throughput stays almost constant (for some moderate K values it increases) with the increase in the number of users before starting to decrease at large values of $K(> 1000)$. This is due to the factor $\zeta = \frac{1}{L_c}$ being less than one. This decrease in net throughput for large user pools is shifted to even higher K values by adopting opportunistic feedback. Net throughput of TDM is also shown in Figs. 5.5 and 5.6 for comparison. In TDM all subcarriers are assigned to one user which results in $\zeta = \frac{1}{L} << 1$. While TDM

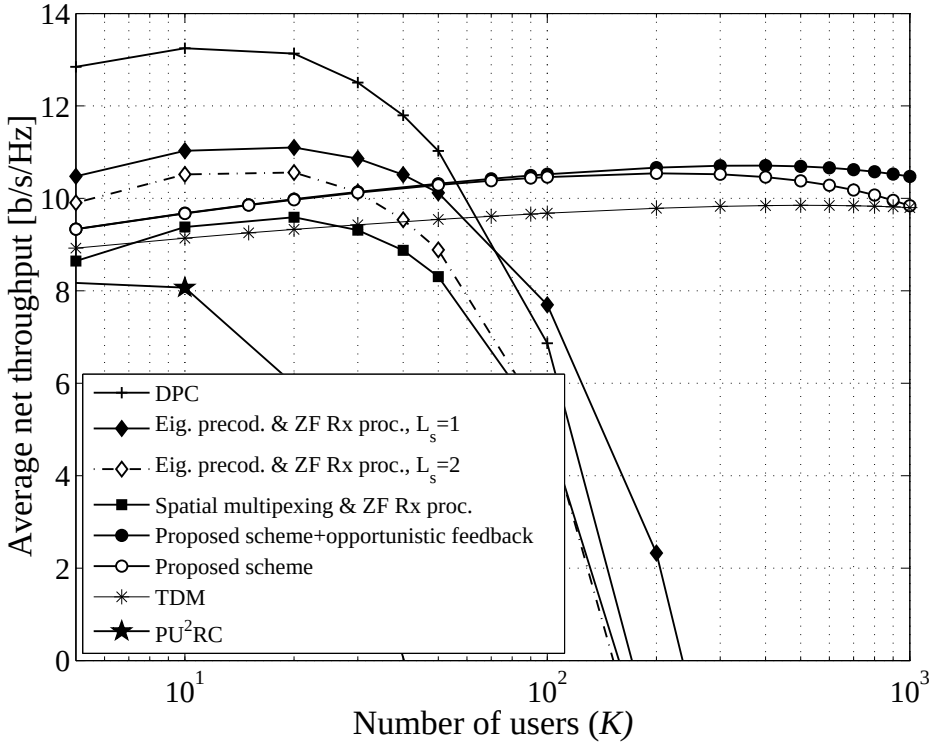

Figure 5.5: Average net throughput comparison of the proposed scheme ($L_c^{max} = 16$) with a number of existing schemes for a system with $L = 64$ subcarriers, $\frac{T_f}{T} = 0.002$, $P_T = 10$ dB, and $M = N = 3$ antennas, versus the number of users.

has a relatively poor sum rate compared to other schemes, its net throughput is comparable and even for large number of users, higher than other schemes (except the proposed scheme) shown is these figures. Note that for schemes requiring full CSIT, $\zeta = \frac{2PM^2}{L}$, and for large values of L the coefficient ζ is less than one which slightly improves the net throughput of these schemes.

The results shown in Fig. 5.6 are similar to those of Fig. 5.5. However, the increase in $\frac{T_f}{T}$ has resulted in greater net throughput advantage of the proposed scheme over other schemes. Assuming this increase is due to the decrease in channel coherence time, T (T_f, the time required to send back one feedback term is the same in both cases), and by comparing Figs. 5.5 and 5.6, it is concluded that over time varying channels the advantage of the proposed scheme over other MIMO-OFDM downlink schemes increases as channel varies faster in time. Faster channel variations mean that CSIT needs to be updated more often and that increases the feedback overhead. Therefore, the net throughput of the schemes which have a

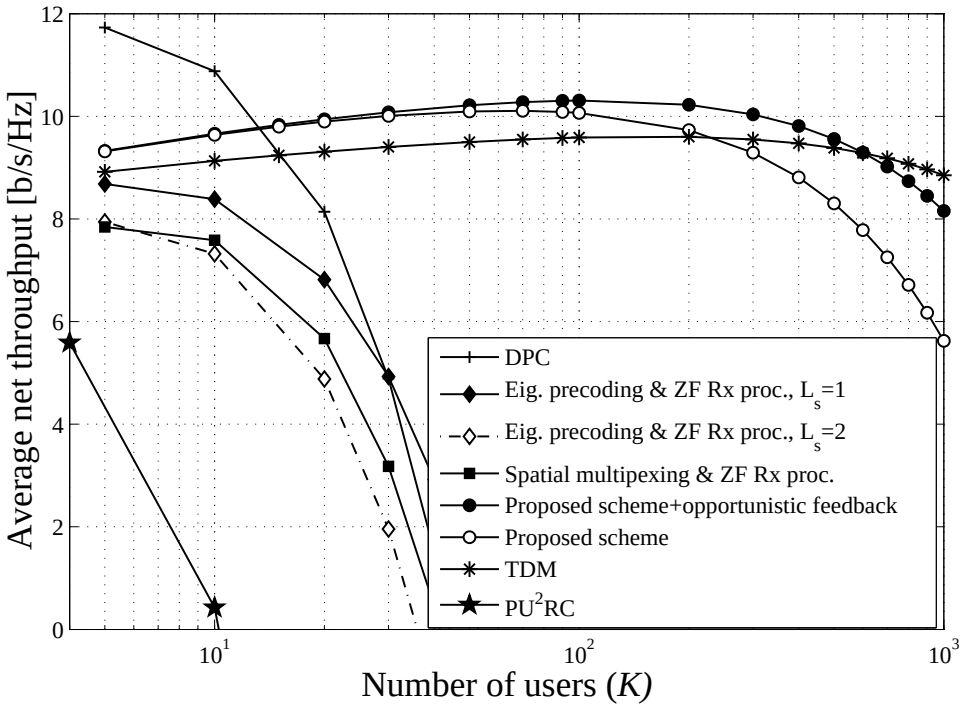

Figure 5.6: Average net throughput comparison of the proposed scheme ($L_c^{max} = 16$) with a number of existing schemes for a system with $L = 64$ subcarriers, $\frac{T_f}{T} = 0.008$, $P_T = 10$ dB, and $M = N = 3$ antennas, versus the number of users.

feedback requirement of ζK with $\zeta \geq 1$ decreases at a faster rate.

Furthermore, it is known that the sum rate of DPC, as well as spatial multiplexing with ZF Rx processing, have asymptotically optimum increase with the number of users, when the number of users approaches infinity [107], while this is not true for the proposed scheme. Therefore, as we can see with a more realistic throughput definition, the throughput superiority of these schemes, especially for large user pools, no longer exists.

5.5 Summary

We have proposed a net throughput maximizing limited feedback scheme for multiuser MIMO-OFDM downlink based on per-chunk user scheduling and compared its average net throughput with a number of limited feedback MIMO-OFDM downlink schemes. The results show that while other schemes' net throughput drops down to zero as the number of users increases, the proposed scheme's net throughput has a slight increase with the number of users, before decreasing to zero. This increase

is present even for large user pools (i.e., $K = 1000$). We have also shown that the net throughput maximizing chunk size depends on the number of users available in the system. Numerical results show that as the channel coherence time decreases (assuming fixed feedback rate), the proposed scheme's net throughput superiority over other schemes increases. The net throughput of the proposed scheme has been further increased by adopting an opportunistic feedback strategy.

Chapter 6

Conclusions and Future Work

Spread spectrum OFDM or MC-CDM over SISO links has been around for some time now and is well investigated. In this thesis we examine the frequency domain spreading of spatially multiplexed MIMO-OFDM signals. In Chapter 2 a low complexity detection algorithm is proposed for SM-MC-CDM which achieves a promising performance. The performance of the proposed detector improves with the number of subcarriers, yet, the amount of improvement itself decreases as the numbers of subcarriers are increased.

In Chapter 3, the performance of the unified SIC detector for SM-MC-CDM is analyzed. Analytical results obtained show that the ZF unified SIC achieves higher diversity order than ZF detectors on individual subcarriers of MIMO-OFDM, and the BER of this detector is reduced by increasing number of subcarriers. On the other hand, the ergodic capacity of SM-MC-CDM decreases with increasing the number of subcarriers. Therefore, based on the results from Chapters 2 and 3, it is recommended that for systems with large number of subcarriers, adjacent subcarriers be grouped (each group is called a chunk) before their data is spread.

This thesis gives a good insight into the effect of using frequency domain spreading in MIMO-OFDM systems while using low complexity detectors. However, there are still practical issues to be investigated. One important issue is the effect of imperfect CSI on the performance of different types of detectors for SM-MC-CDM, and designing low complexity detectors, which have a good performance and also are robust to imperfect CSI. Effect of using alternative spreading codes to Walsh-Hadamard codes used in this thesis on the system performance can also be examined. It is interesting to see if there exist codes, which simultaneously give better performance and lower peak to average power ratio (PAPR) compared to the Walsh-

Hadamard code.

Chapters 4 and 5 investigate the problem of finding efficient limited feedback MU-MIMO downlink transmission schemes. In Chapter 4 downlink of a multiuser system is considered, in which the base station (BS) and the user terminals are both equipped with multiple antennas. Efficient transmission schemes based on zero-forcing (ZF) linear receiver processing, eigenmode transmission and partial channel state information are proposed. The proposed schemes utilize a handshaking procedure between the BS and the users to select (schedule) a subset of users and determine the precoding matrix at the BS. The advantage of the proposed limited feedback schemes lies in their relatively low-complexity scheduling algorithms and high sum rate throughput, even for a small pool of users. For large user pools and when the number of antennas at each user terminal is at least equal to the number of antennas at the BS, we show that the proposed scheme is asymptotically optimum.

Limited feedback MIMO-OFDM downlink with per chunk user scheduling is considered in Chapter 5. By grouping adjacent subcarriers into chunks, the amount of required feedback is reduced. Using net throughput concept, which accounts for the reduction of sum rate due to feedback overhead, it is shown that there exists an optimum chunk size which maximizes the net throughput. To reduce the feedback requirement even further, an opportunistic feedback scheme is proposed and a close approximation for its net throughput is derived. The numerical results show that for a time division duplex (TDD) system with finite coherence time, increasing number of users in the system results in the net throughput of most existing MIMO-OFDM downlink schemes decreasing to zero for moderate size user pools, whereas the proposed scheme's net throughput slightly increases before approaching zero at a significantly lower rate with the number of users and when that number is relatively large (> 1000).

The use of net throughput, that as opposed to the sum rate accounts for the amount of feedback, as the benchmark for comparing MU-MIMO downlink schemes, enables a fairer comparison between different MU-MIMO downlink schemes. Net throughput maximization of MU-MIMO and multiuser MIMO-OFDM downlink seems to be an interesting area of research, currently in its early stages. It is known that DPC achieves the sum capacity for MU-MIMO downlink. However, the fundamental question of "in MU-MIMO downlink (single carrier or multicarrier) which scheme achieves the maximum average net throughput?" still remains to be

answered. Our preliminary work in this area suggests that the answer might be a hybrid of the existing schemes, in which depending on the number of users available in the system, one mode in the hybrid is activated.

Bibliography

[1] J. Winters, "Optimum combining in digital mobile radio with cochannel interference," *IEEE Journal on Selected Areas in Communications*, vol. 2, no. 4, pp. 528–539, July 1984.

[2] G. J. Foschini and J. Salz, "Digital communications over fading radio channels," *Bell Systems Technical Journal*, pp. 429–456, Feb. 1983.

[3] A. Paulraj, R. Nabar, and D. Gore, *Introduction to Space-Time Wireless Communications*. Cambridge University Press, 2003.

[4] V. Tarokh, N. Seshadri, and A. Calderbank, "Space-time codes for high data rate wireless communication: performance criterion and code construction," *IEEE Transactions on Information Theory*, vol. 44, no. 2, pp. 744–765, March 1998.

[5] G. Raleigh and J. Cioffi, "Spatio-temporal coding for wireless communication," *IEEE Transactions on Communications*, vol. 46, no. 3, pp. 357–366, March 1998.

[6] G. J. Foschini and M. J. Gans, "On limits of wireless communications in a fading environment when using multiple antennas," *Wireless Personal Communications*, vol. 6, no. 3, pp. 311–335, March 1998.

[7] G. J. Foschini, G. Golden, R. Valenzuela, and P. Wolniansky, "Simplified processing for high spectral efficiency wireless communication employing multi-element arrays," *IEEE Journal on Selected Areas in Communications*, vol. 17, no. 11, pp. 1841–1852, Nov. 1999.

[8] L. Brandenburg and A. Wyner, "Capacity of the Gaussian channel with memory: The multivariate case," *Bell System Technical Journal*, vol. 53, pp. 745–778, May/June 1974.

[9] I. E. Telatar, "Capacity of multi-antenna Gaussian channels," *European Transactions on Telecommunications (ETT)*, vol. 10, no. 6, pp. 585–596, Nov. 1999.

[10] R. W. Chang, "Synthesis of band-limited orthogonal signals for multichannel data transmission," *Bell Systems Technical Journal*, vol. 45, pp. 1775–1796, Dec. 1998.

[11] B. Saltzberg, "Performance of an efficient parallel data transmission system," *IEEE Transactions on Communication Technology*, vol. 15, no. 6, pp. 805–811, Dec. 1967.

[12] S. Weinstein and P. Ebert, "Data transmission by frequency-division multiplexing using the discrete Fourier transform," *IEEE Transactions on Communication Technology*, vol. 19, no. 5, pp. 628–634, Oct. 1971.

[13] R. V. Nee and R. Prasad, *OFDM for Wireless Multimedia Communications*. Boston: Artech House, 2000.

[14] Y. Li and G. L. Stuber, *Orthogonal Frequency Division Multiplexing for Wireless Communications*. USA: Springer, 2006.

[15] K. Fazel and L. Papke, "On the performance of convolutionally-coded CDMA/OFDM for mobile communication system," in *Proc. IEEE Personal Indoor and Mobile Radio Communications (PIMRC)*, Yokohama, Japan, Sept. 1993, pp. 468–472.

[16] A. Chouly, A. Barajal, and S. Jourdan, "Orthogonal multicarrier techniques applied to direct sequence spread spectrum CDMA systems," in *Proc. IEEE Global Communications Conf. (Globecom)*, Nov. 1993, pp. 1723–1728.

[17] S. Kaiser, "OFDM code-division multiplexing in fading channels," *IEEE Transactions on Communications*, vol. 50, no. 8, pp. 1266–1273, Aug. 2002.

[18] S. Hara and R. Prasad, "Overview of multicarrier CDMA," *IEEE Communications Magazine*, vol. 35, no. 12, pp. 126–133, Dec 1997.

[19] K. Fazel, "Performance of CDMA/OFDM for mobile communication system," in *Proc. IEEE International Conf. on Universal Personal Commun. (ICUPC'93)*, vol. 2, Oct. 93, pp. 975–979.

[20] N. Yee, J. P. Linnartz, and G. Fettweis, "Multi-carrier CDMA in indoor wireless radio networks," in *Proc. IEEE International Symposium on Personal, Indoor and Mobile Radio Commun. (PIMRC)*, Sept. 93, pp. 109–113.

[21] Z. Lei, X. Peng, and F. P. S. Chin, "V-BLAST receivers for downlink MC-CDMA systems," in *Proc. IEEE Vehicular Technology Conf. (VTC)*, vol. 2, Oct. 2003, pp. 866–870.

[22] S. Kondo and L. B. Milstein, "On the use of multicarrier direct sequence spread spectrum systems," in *Proc. IEEE Military Communications Conference (MILCOM)*, Boston, USA, Oct. 1993, pp. 52–56.

[23] K. Fazel and S. Kaiser, *Multi-Carrier and Spread Spectrum Systems: From OFDM and MC-CDMA to LTE and WiMAX*, 2nd ed. John Wiley & Sons, 2008.

[24] K. Zheng, G. Zeng, and W. Wang, "Performance analysis for OFDM-CDMA with joint frequency-time spreading," *IEEE Transactions on Broadcasting*, vol. 51, no. 1, pp. 144–148, March 2005.

[25] H. Weingarten, Y. Steinberg, and S. Shamai, "The capacity region of the Gaussian MIMO broadcast channel," in *Proc. IEEE Int. Symp. on Infor. Theory (ISIT)*, Chicago, IL USA, Jun./Jul. 2004, p. 174.

[26] Q. H. Spencer, C. B. Peel, A. L. Swindlehurst, and M. Haardt, "An introduction to the multi-user MIMO downlink," *IEEE Communications Magazine*, vol. 42, no. 10, pp. 60–67, Oct. 2004.

[27] D. Gesbert, M. Kountouris, R. W. Heath, C.-B. Chae, and T. Salzer, "Shifting the MIMO paradigm," *IEEE Signal Processing Magazine*, vol. 24, no. 5, pp. 36–46, Sept. 2007.

[28] M. Eslami and W. Krzymień, "An efficient low complexity detector for spatially multiplexed MC-CDM," *submited to IEEE Transactions on Sinal Processing*, Aug. 2009.

[29] M. Eslami and W. Krzymień, "An efficient detector for spatially multiplexing MC-CDM communications," in *Proc. IEEE Vehicular Technology Conf. (VTC)*, Montreal, Canada, Sept. 2006.

[30] M. Eslami and W. Krzymień, "Turbo coded MC-CDM communications with spatial multiplexing," in *Proc. IEEE Global Communications Conf. (Globecom)*, San Francisco, CA, USA, Nov.-Dec. 2006, pp. 1–5.

[31] M. Eslami and W. Krzymień, "On the performance of spatially multiplexed MC-CDM with zero-forcing unified successive interference cancellation detection," *IET/Proceedings Communications*, vol. 3, no. 8, pp. 1410–1419, Aug. 2009.

[32] M. Eslami and W. Krzymień, "Efficient transmission schemes for multiuser MIMO downlink with linear receivers and partial side information," *submitted to EURASIP Journal on Wireless Commun. and Networking*, Aug. 2009.

[33] M. Eslami and W. Krzymień, "Scheduling for MIMO broadcast channels with linear receivers and partial CSI," in *Proc. IEEE Vehicular Technology Conf. (VTC)*, Singapore, May 2008, pp. 2467–2471.

[34] M. Eslami and W. Krzymień, "Efficient transmission technique for MIMO-OFDM broadcast channels with limited feedback," in *Proc. IEEE International Symposium in Spread Spectrum Techniques and Applications (ISSSTA)*, Bologna, Italy, Aug. 2008.

[35] M. Eslami and W. Krzymień, "Downlink limited feedback transmission schemes for asymmetric MIMO channels," in *Proc. IEEE Vehicular Technology Conf. (VTC)*, Calgary, Canada, Sept. 2008, pp. 1–5.

[36] M. Eslami and W. Krzymień, "Net throughput maximization of limited feedback MIMO-OFDM downlink with per-chunk user scheduling," *submited to IEEE Transactions on Vehicular Technology*, May 2009.

[37] M. Eslami and W. Krzymień, "Limited-feedback multiuser MIMO-OFDM downlink with per-chunk / per-antenna user scheduling and linear receivers," in *Proc. IEEE 7th Workshop on Multi-Carrier Systems & Solutions (Springer Lecture Notes in Electrical Engineering)*, Herrsching, Germany, May 2009.

[38] V. L. Nir, M. Hélard, and R. L. Gouable, "Spatial multiplexing applied to turbo coded multi-carrier CDMA," in *Proc. IEEE International Symposium on Spread Spectrum Techniques and Applications (ISSSTA)*, Aug. 2004, pp. 565–569.

[39] J. Adeane, M. R. D. Rodrigues, I. Berenguer, and I. J. Wassell, "OFDM-CDM with V-BLAST detection and its extension to MIMO systems," in *Proc. IEEE Vehicular Technology Conf. (VTC)*, vol. 1, April 2003, pp. 764–768.

[40] J. Adeane, M. Rodrigues, and I. Wassell, "Lattice-reduction-aided detection for MIMO-OFDM-CDM communication systems," *IET Communications*, vol. 1, no. 3, pp. 526–531, June 2007.

[41] W. Yan, C. K. Ho, S. Sun, and Z. Lei, "Iterative receivers for pre-transformed MIMO-OFDM systems," in *Proc. IEEE International Symposium on Personal, Indoor and Mobile Radio Communications (PIMRC)*, vol. 1, Sept. 2005, pp. 221–225.

[42] C.-K. Ho, Z. Lei, S. Sun, and W. Yan, "Iterative detection for pretransformed OFDM by subcarrier reconstruction," *IEEE Transactions on Signal Processing*, vol. 53, no. 8, pp. 2842–2854, Aug. 2005.

[43] L. Zheng and D. Tse, "Diversity and multiplexing: a fundamental tradeoff in multiple-antenna channels," *IEEE Transactions on Information Theory*, vol. 49, no. 5, pp. 1073–1096, May 2003.

[44] K. Fazel and S. Kaiser, *Multicarrier and Spread Spectrum Systems.* John Wiley & Sons, 2003.

[45] E. Yoon, J. Hansen, and A. Paulraj, "Space-frequency precoding for an OFDM based system exploiting spatial and path correlation," in *Proc. IEEE Global Communications Conf. (Globecom)*, vol. 1, Nov. 2004, pp. 436–440.

[46] A. Intarapanich, P. Kafle, R. Davies, and A. Sesay, "Effect of tap gain correlation on capacity of OFDM MIMO systems," *IEE Electronics Letters*, vol. 40, no. 1, pp. 86–88, Jan. 2004.

[47] J. Kermoal, L. Schumacher, K. Pedersen, P. Mogensen, and F. Frederiksen, "A stochastic MIMO radio channel model with experimental validation," *IEEE Journal on Selected Areas in Communications*, vol. 20, no. 6, pp. 1211–1226, Aug 2002.

[48] C. Oestges, B. Clerckx, D. Vanhoenacker-Janvier, and A. Paulraj, "Impact of fading correlations on MIMO communication systems in geometry-based statistical channel models," *IEEE Transactions on Wireless Communications*, vol. 4, no. 3, pp. 1112–1120, May 2005.

[49] C. Oestges, "Validity of the Kronecker model for MIMO correlated channels," in *IEEE Vehicular Technology Conference (VTC'06-Spring)*, vol. 6, May 2006, pp. 2818–2822.

[50] H. Tong and S. Zekavat, "On the suitable environments of the Kronecker product form in MIMO channel modeling," in *IEEE Wireless Communications and Networking Conference (WCNC'08)*, April 2008, pp. 780–784.

[51] B. Hassibi and H. Vikalo, "On the sphere-decoding algorithm I. Expected complexity," *IEEE Transactions on Signal Processing*, vol. 53, no. 8, pp. 2806–2818, Aug. 2005.

[52] J. Jalden and B. Ottersten, "On the complexity of sphere decoding in digital communications," *IEEE Transactions on Signal Processing*, vol. 53, no. 4, pp. 1474–1484, April 2005.

[53] E. Larsson, "MIMO detection methods: How they work," *IEEE Signal Processing Magazine*, vol. 26, no. 3, pp. 91–95, May 2009.

[54] W. Zhang, X. Ma, B. Gestner, and D. Anderson, "Designing low-complexity equalizers for wireless systems," *IEEE Communications Magazine*, vol. 47, no. 1, pp. 56–62, January 2009.

[55] H. Yao and G. W. Wornell, "Lattice-reduction-aided detectors for MIMO communication systems," in *Proc. IEEE Global Communications Conf. (Globecom)*, vol. 1, Nov. 2002, pp. 424–428.

[56] M. Taherzadeh, A. Mobasher, and A. Khandani, "LLL reduction achieves the receive diversity in MIMO decoding," *IEEE Transactions on Information Theory*, vol. 53, no. 12, pp. 4801–4805, Dec. 2007.

[57] J. Adeane, M. R. D. Rodrigues, I. Berenguer, and I. J. Wassell, "Improved detection methods for MIMO-OFDM-CDM communication systems," in *Proc. IEEE Vehicular Technology Conf. (VTC)*, vol. 3, Sept. 2004, pp. 1604–1608.

[58] J. Jalden, D. Seethaler, and G. Matz, "Worst- and average-case complexity of LLL lattice reduction in MIMO wireless systems," in *Proc. IEEE International Conference on Acoustics, Speech and Signal Processing (ICASSP)*, April 2008, pp. 2685–2688.

[59] X. Ma and W. Zhang, "Performance analysis for MIMO systems with lattice-reduction aided linear equalization," *IEEE Transactions on Communications*, vol. 56, no. 2, pp. 309–318, February 2008.

[60] C. Ling, W. H. Mow, K. H. Li, and A. C. Kot, "Multiple-antenna differential lattice decoding," *IEEE Journal on Selected Areas in Communications*, vol. 23, no. 9, pp. 1821–1829, Sept. 2005.

[61] A. K. Lenstra, H. W. Lenstra, and L. Lovasz, "Factoring polynomials with rational coefficients," *Math. Ann.*, vol. 261, pp. 515–534, 1982.

[62] A. Papoulis and S. U. Pillai, *Probability, Random Variables, and Stochastic Processes*, 4th ed. McGrawHill, 2002.

[63] P. W. Wolniansky, G. J. Foschini, G. D. Golden, and R. A. Valenzuela, "V-BLAST: An architecture for realizing very high data rates over the rich-scattering wireless channel," in *Proc. International Symposium on Signals, Systems, and Electronics (ISSSE)*, Sept.-Oct 1998, pp. 295–300.

[64] W. K. Wai and C. Y. Tsui, "A low complexity architecture of the V-BLAST system," in *Proc. IEEE Wireless Communications and Networking Conf. (WCNC)*, vol. 1, Sept. 2000, pp. 310–314.

[65] W. Yan, S. Sun, and Z. Lei, "A low complexity VBLAST OFDM detection algorithm for wireless LAN systems," *IEEE Communications Letters*, vol. 8, no. 6, pp. 374–376, June 2004.

[66] J. Hagenauer, E. Offer, and L. Papke, "Iterative decoding of binary block and convolutional codes," *IEEE Transactions on Information Theory*, vol. 42, no. 2, pp. 429–445, Mar 1996.

[67] J. Woodard and L. Hanzo, "Comparative study of turbo decoding techniques: an overview," *IEEE Transactions on Vehicular Technology*, vol. 49, no. 6, pp. 2208–2233, Nov 2000.

[68] C. Shen, Y. Zhu, S. Zhou, and J. Jiang, "On the performance of V-BLAST with zero-forcing successive interference cancellation receiver," in *Proc. IEEE Global Communications Conf. (Globecom)*, vol. 5, Nov.-Dec. 2004, pp. 2818–2822.

[69] Y. Jiang, X. Zheng, and J. Li, "Asymptotic performance analysis of V-BLAST," in *Proc. IEEE Global Communications Conf. (Globecom)*, vol. 6, Nov.-Dec. 2005, pp. 3882–3886.

[70] R. Xu and F. Au, "Analytical approach of V-BLAST performance with two transmit antennas," in *Wireless Communications and Networking Conference, 2005 IEEE*, vol. 1, March 2005, pp. 396–401.

[71] S. Loyka and F. Gagnon, "Performance analysis of the V-BLAST algorithm: an analytical approach," *IEEE Transactions on Wireless Communications*, vol. 3, no. 4, pp. 1326–1337, July 2004.

[72] R. Böhnke and K. D. Kammeyer, "SINR analysis for V-BLAST with ordered MMSE-SIC detection," in *Proc. The International Wireless Commun. and Mobile Computing Conference (IWCMC'06)*, July 2006.

[73] M. A. Milevsky and S. E. Posner, "Asian options, the sum of lognormals, and the reciprocal gamma distribution," *Journal of Financial and Quantitative Analysis*, vol. 409-423, no. 3, pp. 409–423, Sept. 1998.

[74] E. Kreyszig, *Advanced Engineering Mathematics*, 9th ed. New York: Wiley, 2005.

[75] A. M. Tulino and S. Verdu, *Random Matrix Theory and Wireless Communications*. Hanover, MA, USA: Now Publishers Inc., 2004.

[76] V. V. Gnedenko and A. Kolmogorov, *Limit Distributions of Sums of Independent Random Variables*, 1st ed. Wiley-Interscience, 1968.

[77] S. C. Choi and R. Wette, "Maximum likelihood estimation of the parameters of the gamma distribution and their bias," *Technometrics*, vol. 11, no. 4, pp. 683–690, Nov. 1969.

[78] J. Craig, "A new, simple and exact result for calculating the probability of error for two-dimensional signal constellations," in *Proc. IEEE Military Communications Conference (MILCOM)*, Nov. 1991, pp. 571–575.

[79] I. S. Gradshteyn and I. M. Ryzhik, *Table of Integrals, Series, and Products*, 6th ed. Academic Press, 2000.

[80] M. K. Simon and M. Alouini, *Digital Communication over Fading Channels*, 2nd ed. John Wiley & Sons, 2005.

[81] C. F. Papadias and G. J. Foschini, "On the capacity of certain space-time coding schemes," *EURASIP Journal on Applied Signal Process.*, vol. 5, pp. 447–458, May 2002.

[82] N. Sagias, G. Tombras, and G. Karagiannidis, "New results for the shannon channel capacity in generalized fading channels," *IEEE Communications Letters*, vol. 9, no. 2, pp. 97–99, Feb. 2005.

[83] G. Caire and S. Shamai, "On the achievable throughput of a multiantenna Gaussian broadcast channel," *IEEE Tranaction on Information Theory*, vol. 49, no. 7, pp. 1691–1706, Jul. 2003.

[84] S. Vishwanath, N. Jindal, and A. Goldsmith, "Duality, achievable rates, and sum-rate capacity of Gaussian MIMO broadcast channels," *IEEE Tranactions on Information Theory*, vol. 49, no. 10, pp. 2658–2668, Oct. 2003.

[85] W. Yu and J. Cioffi, "Sum capacity of Gaussian vector broadcast channels," *IEEE Transactions on Information Theory*, vol. 50, no. 9, pp. 1875–1892, Sept. 2004.

[86] P. Viswanath, D. N. C. Tse, and R. Laroia, "Opportunistic beamforming using dumb antennas," *IEEE Transactions on Information Theory*, vol. 48, no. 6, pp. 1277–1294, June 2002.

[87] M. Sharif and B. Hassibi, "A comparison of time-sharing, DPC, and beamforming for MIMO broadcast channels with many users," *IEEE Transactions on Communications*, vol. 55, no. 1, pp. 11–15, Jan. 2007.

[88] T. Yoo, N. Jindal, and A. Goldsmith, "Multi-antenna downlink channels with limited feedback and user selection," *IEEE Journal on Selected Areas in Communications*, vol. 25, no. 7, pp. 1478–1491, Sept. 2007.

[89] K. Huang, J. G. Andrews, and R. W. Heath, "Performance of orthogonal beamforming for SDMA with limited feedback," *IEEE Transactions on Vehicular Technology*, vol. 58, no. 1, pp. 152–164, Jan. 2009.

[90] W. Zhang and K. B. Letaief, "MIMO broadcast scheduling with limited feedback," *IEEE Journal on Selected Areas in Commununications*, vol. 25, no. 7, pp. 1457–1467, Sept. 2007.

[91] W. Choi, A. Forenza, J. G. Andrews, and R. W. Heath, "Opportunistic space-division multiple access with beam selection," *IEEE Transactions on Communnications*, vol. 55, no. 12, pp. 2371–2380, Dec. 2007.

[92] M. Trivellato, F. Boccardi, and F. Tosato, "User selection schemes for MIMO broadcast channels with limited feedback," in *Proc. IEEE Vehicular Technology Conf. (VTC)*, Dublin, April 2007, pp. 2089–2093.

[93] M. Kountouris, R. de Francisco, D. Gesbert, D. Slock, and T. Salzer, "A random precoding technique for the downlink of multiuser MIMO systems," in *Proc. IEEE Int. Conf. Acoustics, Speech, and Signal Process. (ICASSP)*, Honolulu, HI, April 2007, pp. 109–112.

[94] T. H. Kim, R. W. Heath, and S. Choi, "Multiuser MIMO downlink with limited feedback using transmit-beam matching," in *Proc. IEEE Int. Conf. Commun. (ICC)*, Beijing, China, May 2008, pp. 3506–3510.

[95] G. Dietl and G. Bauch, "Linear precoding in the downlink of limited feedback multiuser MIMO systems," in *Proc. IEEE Global Communications Conf. (Globecom)*, Washington, DC, USA, Nov. 2007, pp. 4359–4364.

[96] E. Bala and L. J. Cimini, "A random precoding technique for the downlink of multiuser MIMO systems," in *Proc. 40th Annual Conf. on Infor. Sciences and Systems*, Princeton, NJ, March 2006, pp. 750–754.

[97] F. Boccardi, H. Huang, and M. Trivellato, "Multiuser eigenmode transmission for MIMO broadcast channels with limited feedback," in *Proc. IEEE 8th Workshop on Signal Process. Advances in Wireless Commun. (SPAWC)*, Helsinki, Finland, June 2007, pp. 1–5.

[98] T. Tang, R. W. Heath, S. Cho, and S. Yun, "Opportunistic feedback for multiuser MIMO systems with linear receivers," *IEEE Transactions on Commununications*, vol. 55, no. 5, pp. 1020–1032, May 2007.

[99] C. Wang and R. D. Murch, "MU-MIMO decomposition transmission with limited feedback," in *Proc. IEEE Wireless Commun. and Networking Conf. (WCNC)*, Kowloon, Hong Kong, March 2007, pp. 1108–1113.

[100] M. A. Maddah-Ali, M. A. Sadrabadi, and A. K. Khandani, "Broadcast in MIMO systems based on a generalized QR decomposition: Signaling and performance analysis," *IEEE Transactions on Information Theory*, vol. 54, no. 3, pp. 1124–1138, March 2008.

[101] K. Huang, R. Heath, and J. Andrews, "Limited feedback beamforming over temporally-correlated channels," *IEEE Trans. Signal Proc.*, vol. 57, no. 5, pp. 1959–1975, May 2009.

[102] "Downlink MIMO for EUTRA," Samsung Electronics, 3GPP TSG RAN WG1 R1-060335, Feb. 2006.

[103] K. Huang, R. W. Heath, and J. G. Andrews, "Joint beamforming and scheduling for SDMA systems with limited feedback," *IEEE Transactions on Vehicular Technology*, to appear 2009.

[104] A. Bayesteh and A. Khandani, "On the user selection for MIMO broadcast channels," *IEEE Trans. Infor. Theory*, vol. 54, no. 3, pp. 1086–1107, March 2008.

[105] D. Tse and P. Viswanath, *Fundamentals of Wireless Communications*. New York, NY, USA: Cambridge University Press, 2005.

[106] N. Jindal and A. Goldsmith, "Dirty-paper coding versus TDMA for MIMO broadcast channels," *IEEE Transactions on Information Theory*, vol. 51, no. 5, pp. 1783–1794, May 2005.

[107] M. Airy, R. W. Heath, and S. Shakkottai, "Multi-user diversity for multiple antenna broadcast channel with linear receivers: asymptotic analysis," in *Proc. IEEE Conf. on Signals, Systems and Computers*, Pacific Grove, CA, USA, Nov. 2004, pp. 886–890.

[108] C. J. Chen and L. C. Wang, "Performance analysis of scheduling in multiuser MIMO systems with zero-forcing receivers," *IEEE J. Select. Areas Commun.*, vol. 25, no. 7, pp. 1435–1445, Sept. 2007.

[109] A. M. Tulino and S. Verdu, *Random Matrix Theory and Wireless Communications*. Hanover, MA, USA: Now Publishers Inc., 2004.

[110] M. Abramowitz and I. A. Stegun, *Handbook of Mathematical Functions with Formulas, Graphs, and Mathematical Tables*. New York: Dover, 1972.

[111] A. Edelman, "Eigenvalues and condition numbers of random matrices," Ph.D. dissertation, MIT, 1989.

[112] P. Smith and M. Shafi, "On a Gaussian approximation to the capacity of wireless MIMO systems," in *Proc. IEEE Int. Conf. Commun. (ICC)*, New York, NY, USA, May 2002, pp. 406–410.

[113] M. Sharif and B. Hassibi, "On the capacity of MIMO broadcast channels with partial side information," *IEEE Transactions on Information Theory*, vol. 51, no. 2, pp. 506–522, Feb. 2005.

[114] M. Sharif and B. Hassibi, "A comparison of time-sharing, DPC, and beamforming for MIMO broadcast channels with many users," *IEEE Transactions on Commununications*, vol. 55, no. 1, pp. 11–15, Jan. 2007.

[115] N. Jindal and A. Goldsmith, "Dirty paper coding versus TDMA for MIMO braodcast channels," *IEEE Transactions on Information Theory*, vol. 51, no. 5, pp. 1783–1794, May 2005.

[116] N. Jindal, "MIMO broadcast channels with finite-rate feedback," *IEEE Transactions on Information Theory*, vol. 52, no. 11, pp. 5045–5060, Nov. 2006.

[117] "Comparison between MU-MIMO codebook-based channel reporting techniques for LTE downlink," Philips, 3GPP TSG RAN WG1, Oct. 2006.

[118] N. Jindal, W. Rhee, S. Vishwanath, S. Jafar, and A. Goldsmith, "Sum power iterative water-filling for multi-antenna Gaussian broadcast channels," *IEEE Transactions on Information Theory*, vol. 51, no. 4, pp. 1570–1580, April 2005.

[119] T. Tang, R. W. Heath, S. Cho, and S. Yun, "Opportunistic feedback for multiuser MIMO systems with linear receivers," *IEEE Transactions on Communications*, vol. 55, no. 5, pp. 1020–1032, May 2007.

[120] P. Svedman, S. K. Wilson, L. J. Cimini, and B. Ottersten, "Opportunistic beamforming and scheduling for OFDMA systems," *IEEE Transactions on Communications*, vol. 55, no. 5, pp. 941–952, May 2007.

[121] Y. Peng, S. M. D. Armour, and J. P. McGeehan, "An investigation of dynamic subcarrier allocation in MIMO-OFDMA systems," *IEEE Transactions on Vehicular Technology*, vol. 56, no. 5, pp. 2990–3005, Sept. 2007.

[122] M. O. Pun, K. J. Kim, and H. V. Poor, "Opportunistic scheduling and beamforming for MIMO-OFDMA downlink systems with reduced feedback," in *Proc. IEEE Int. Conf. Commun. (ICC)*, May 2008, pp. 688–692.

[123] E. Jorswieck, A. Sezgin, B. Ottersten, and A. Paulraj, "Feedback reduction in uplink MIMO OFDM systems by chunk optimization," *EURASIP Journal on Advanced Signal Proc.*, vol. 2008, no. Article ID 597072, p. 14 pages, 2008.

[124] H. Bolcskei, D. Gesbert, and A. J. Paulraj, "On the capacity of OFDM-based spatial multiplexing systems," *IEEE Transactions on Communications*, vol. 50, no. 2, pp. 225–234, Feb. 2002.

[125] M. R. McKay, P. J. Smith, H. A. Suraweera, and I. B. Collings, "On the mutual information distribution of OFDM-based spatial multiplexing: Exact variance and outage approximation," *IEEE Transactions on Information Theory*, vol. 54, no. 7, pp. 3260–3278, Jul. 2008.

[126] J. Jose, A. Ashikhmin, P. Whiting, and S. Vishwanath, "Scheduling and preconditioning in multi-user MIMO TDD systems," in *Proc. IEEE Int. Conf. Commun. (ICC)*, Beijing, China, May 2008.

[127] C.-J. Chen and L.-C. Wang, "Performance analysis of scheduling in multiuser MIMO systems with zero-forcing receivers," *IEEE Journal on Selected Areas in Communications*, vol. 25, no. 7, pp. 1435–1445, September 2007.

[128] D. Tse and P. Viswanath, *Fundamentals of Wireless Communication*. Cambridge University Press, 2005.

[129] P. J. Smith and M. Shafi, "On a Gaussian approximation to the capacity of wireless MIMO systems," in *Proc. IEEE Int. Conf. Commun. (ICC)*, vol. 1, 2002, pp. 406–410.

[130] M. Kang and M. Alouini, "Capacity of MIMO Rician channels," *IEEE Transactions on Wireless Communications*, vol. 5, no. 1, pp. 112–122, Jan. 2006.

[131] S. H. Muller-Weinfurtner, "Coding approaches for multiple antenna transmission in fast fading and OFDM," *IEEE Transactions on Signal Processing*, vol. 50, no. 10, pp. 2442–2450, Oct. 2002.

[132] R. A. Horn and C. R. Johnson, *Matrix Analysis*. Cambridge University Press, 1985.

[133] C. C. Chen and C. W. Tyler, "Accurate approximation to the extreme order statistics of Gaussian samples," *Communications in Statistics: Simulation and Computation*, vol. 28, no. 1, pp. 177–188, 1999.

[134] H. Shore, "Enhancement for two commonly-used approximations for the inverse cumulative function of the normal distribution," *Communications in Statistics: Simulation and Computation*, vol. 26, no. 3, pp. 1041–1047, 1997.

Appendix A

It is assumed that perfect channel state information is available at the Rx. Hence, the only randomness in $\hat{w}_1^{(m)}$ and $\hat{w}_2^{(m)}$ is due to the data symbols, $d_l^{(m)}$s. To evaluate the variance of $\hat{w}_1^{(m)}$ in 2.16,

$$\hat{w}_1^{(m)} = \sum_{\substack{j=1 \\ j\neq l}}^{L} \sum_{i=1}^{L} \mathbf{C}_{l,i}\mathbf{C}_{i,j}\boldsymbol{\psi}_i(m,m)d_j^{(m)}, \tag{A-1}$$

we have

$$\begin{aligned}
\sigma^2_{\hat{w}_1^{(m)}} &= E\{|\hat{w}_1^{(m)}|^2\} \\
&= \sum_{\substack{j=1 \\ j\neq l}}^{L} \sum_{i=1}^{L} \sum_{i'=1}^{L} \mathbf{C}_{l,i}\mathbf{C}_{i,j}\mathbf{C}_{l,i'}\mathbf{C}_{i',j}\boldsymbol{\psi}_i(m,m)\boldsymbol{\psi}_{i'}^H(m,m) \\
&= \frac{1}{L^2}\sum_{\substack{j=1 \\ j\neq l}}^{L} \sum_{i=1}^{L} |\boldsymbol{\psi}_i(m,m)|^2 \\
&+ \sum_{i=1}^{L} \sum_{\substack{i'=1 \\ i'\neq i}}^{L} \mathbf{C}_{l,i}\mathbf{C}_{l,i'}\boldsymbol{\psi}_i(m,m)\boldsymbol{\psi}_{i'}^H(m,m) \sum_{\substack{j=1 \\ j\neq l}}^{L} \mathbf{C}_{i,j}\mathbf{C}_{i',j} \\
&= \frac{L-1}{L^2}\sum_{i=1}^{L} |\boldsymbol{\psi}_i(m,m)|^2 \\
&+ \sum_{i=1}^{L} \sum_{\substack{i'=1 \\ i'\neq i}}^{L} \mathbf{C}_{l,i}\mathbf{C}_{l,i'}\boldsymbol{\psi}_i(m,m)\boldsymbol{\psi}_{i'}^H(m,m)\left(-\mathbf{C}_{l,i}\mathbf{C}_{l,i'}\right) \\
&= \frac{L-1}{L^2}\sum_{i=1}^{L} |\boldsymbol{\psi}_i(m,m)|^2 - \frac{1}{L^2}\left(\left|\sum_{i=1}^{L}\boldsymbol{\psi}_i(m,m)\right|^2 - \sum_{i=1}^{L}|\boldsymbol{\psi}_i(m,m)|^2\right) \\
&= \frac{1}{L^2}\left(\sum_{i=1}^{L}|\boldsymbol{\psi}_i(m,m)|^2 - \left|\sum_{i=1}^{L}\boldsymbol{\psi}_i(m,m)\right|^2\right)
\end{aligned} \tag{A-2}$$

For $\hat{w}_2^{(m)}$ we have,

$$\begin{aligned}\sigma^2_{\hat{w}_2^{(m)}} &= E\left|\sum_{i=1}^{L}\sum_{n=1}^{L}\sum_{\substack{k=1\\k\neq m}}^{M}\boldsymbol{\psi}_i(m,k)\mathbf{C}_{j,i}\mathbf{C}_{i,n}d_n^{(k)}\right|^2 \\ &= \frac{1}{L^2}\sum_{i=1}^{L}\sum_{n=1}^{L}\sum_{\substack{k=1\\k\neq m}}^{M}|\boldsymbol{\psi}_i(m,k)|^2 \\ &+ \sum_{i=1}^{L}\sum_{\substack{i'=1\\i'\neq i}}^{L}\sum_{\substack{k=1\\k\neq m}}^{M}\boldsymbol{\psi}_i(m,k)\boldsymbol{\psi}_{i'}^H(m,k)\mathbf{C}_{j,i}\mathbf{C}_{j,i'}\underbrace{\sum_{n=1}^{L}\mathbf{C}_{i,n}\mathbf{C}_{i',n}}_{=0} \\ &= \frac{1}{L}\sum_{i=1}^{L}\sum_{\substack{k=1\\k\neq m}}^{M}|\boldsymbol{\psi}_i(m,k)|^2\end{aligned} \tag{A-3}$$

The variance for the the third term,

$$\begin{aligned}\hat{w}_3^{(m)} &= \mathbf{C}(l,:)\acute{\mathbf{w}}_3 \\ &= \mathbf{C}(l,:)\left[\ \mathbf{G}_1(m,:)\mathbf{w}_1\ldots\mathbf{G}_L(m,:)\mathbf{w}_L\ \right]^T \\ &= \sum_{i=1}^{L}\mathbf{C}_{l,i}\mathbf{G}_i(m,:)\mathbf{w}_i,\end{aligned} \tag{A-4}$$

is obtained as

$$\begin{aligned}&\sigma^2_{\hat{w}_3^{(m)}} = E|\hat{w}_3^{(m)}|^2 = \\ &E\left\{\sum_{i=1}^{L}\sum_{i'=1}^{L}\sum_{r=1}^{M}\sum_{r'=1}^{M}\mathbf{C}_{l,i}\mathbf{C}_{l,i'}\mathbf{G}_i(m,r)\mathbf{w}_i(r)\mathbf{G}_{i'}^H(m,r)\mathbf{w}_{i'}^H(r')\right\}.\end{aligned} \tag{A-5}$$

The whiteness of the noise samples, $E\{\mathbf{w}_i(r)\mathbf{w}_{i'}^H(r')\} = \sigma_w^2\delta(r-r')\delta(i-i')$ results in

$$\sigma^2_{\hat{w}_3^{(m)}} = \frac{\sigma_w^2}{L}\sum_{i=1}^{L}\mathbf{G}_i(m,:)\mathbf{G}_i^H(m,:). \tag{A-6}$$

Appendix B

To prove Lemma 1 consider the following equality,

$$\left[(\mathbf{H}_l^{(\pi_m)H}\mathbf{H}_l^{(\pi_m)})^{-1}\right]_{MM} = \left[(\mathbf{H}_l^H\mathbf{H}_l)^{-1}\right]_{mm}, \tag{B-1}$$

where π_m denotes the permutation realized by exchanging the mth and Mth columns of $\mathbf{H}_l$. Equality (B-1) itself is proved using the standard matrix inversion formula and the properties of the determinant [132]:

$$\begin{aligned}\left[(\mathbf{H}^{(\pi_m)H}\mathbf{H}^{(\pi_m)})^{-1}\right]_{MM} &= \frac{1}{\det(\mathbf{H}^{(\pi_m)H}\mathbf{H}^{(\pi_m)})}\det\left(\mathbf{H}_{-M}^{(\pi_m)H}\mathbf{H}_{-M}^{(\pi_m)}\right)\\ &= \frac{1}{\det(\mathbf{H}^H\mathbf{H})}\det\left(\mathbf{H}_{-m}^H\mathbf{H}_{-m}\right)\\ &= \left[(\mathbf{H}^H\mathbf{H})^{-1}\right]_{mm}\end{aligned} \tag{B-2}$$

where $\mathbf{A}_{-k}$ denotes the matrix obtained by eliminating the kth column of $\mathbf{A}$ and $\det(\cdot)$ denotes the determinant of the matrix argument.

Also, in [69] it has been shown that

$$(r_{MM}^{(l)})^{-2} = \left[(\mathbf{H}_l^H\mathbf{H}_l)^{-1}\right]_{MM}. \tag{B-3}$$

That completes the proof of Lemma 1.

Appendix C

Let $r_{k,M_s} = \sum_{l=1}^{M_s} R_l^{(k)}$ where $R_l^{(k)} = \log_2(1 + \rho\lambda_l^{(k)})$. Then similarly to [112] the pdf of r_{k,M_s} can be approximated by a Gaussian distribution. However, the parameters of the distribution are different from those given in [112] as in this case only the first M_s largest eigenvalues are considered. To obtain the mean value for this Gaussian approximation, the marginal pdfs of the first M_s eigenvalues are required which can be obtained from (4.13). The mean value is then obtained as:

$$\mu_{r_{k,M_s}} = \sum_{l=1}^{M_s} \int_0^\infty \log_2(1+\rho x) p_\lambda(\lambda_l^{(k)})(x) dx \tag{C-1}$$

The variance of r_{k,M_s} is obtained by evaluating

$$\sigma^2_{r_{k,M_s}} = \sum_{i=1}^{M_s}\sum_{j=1}^{M_s} \mathrm{Cov}\left(R_i^{(k)} R_j^{(k)}\right) \tag{C-2}$$

where $\mathrm{Cov}(x)$ denotes the covariance of x. (C-2) is further simplified to

$$\sigma^2_{r_{k,M_s}} = \sum_{i=1}^{M_s}\sum_{j=1}^{M_s} \left(\mathrm{E}\{R_{\lambda_i}^{(k)} R_{\lambda_j}^{(k)}\} - \mathrm{E}\{R_{\lambda_i}^{(k)}\}\,\mathrm{E}\{R_{\lambda_j}^{(k)}\}\right) \tag{C-3}$$

The cross correlation terms in (C-3) require evaluating the joint distribution of pairs of the eigenvalues, $p_\lambda(\lambda_i, \lambda_j)$, which is done by integrating (4.13) over all M_s eigenvalues, except the ith and the jth ones. In case of $M_s = M$, a further simplified expression for $\sigma^2_{r_{k,M}}$ is given in [112]. By approximating the pdf of r_{k,M_s} as Gaussian, $\mathcal{N}(\mu_{r_{k,M_s}}, \sigma^2_{r_{k,M_s}})$, $\mathrm{E}\{R_{eig}\} = \mathrm{E}\{\max_k r_{k,M_s}\}$ will be the mean value of maximum of K Gaussian distributed terms, which itself is approximated by [133]

$$\mathrm{E}\{R_{eig}\} \approx \sigma_{r_{k,M_s}} \Phi^{-1}(0.5264^{\frac{1}{K}}) + \mu_{r_{k,M_s}}. \tag{C-4}$$

The function $\Phi(\cdot)$ is the standard normal CDF. Φ^{-1} is well approximated by [134]

$$\Phi^{-1}(x) \approx \frac{1}{c_1}\left[x^{c_2} - (1-x)^{c_2}\right] \tag{C-5}$$

where $c_1 = 0.1975$ and $c_2 = 0.135$. Substituting (C-5) into (C-4) completes the proof.

Appendix D

Proof for Theorem 1:

Following the same lines as the [125] in deriving the variance of mutual information for a MIMO-OFDM system, we drive the variance of mutual information for each chunk of MIMO-OFDM by showing that the variances of mutual information for two arbitrary chunks of equal size are equal, then we conclude that the variances of all chunks are equal. Denote the achievable rate of each chunk, $r_{chk,q}$, by I_q, then we have

$$\begin{aligned}
\mathrm{Var}(I_q) &= \mathrm{E}[I_q^2] - \mathrm{E}^2[I_q] \\
&= \mathrm{E}\left[\frac{1}{L_c^2}\sum_{k=(q-1)L_c}^{qL_c-1}\sum_{l=(q-1)L_c}^{qL_c-1} I_k I_l\right] - \mathrm{E}^2\left[I_q\right] \\
&= \frac{1}{L_c^2}\left(\sum_{k=(q-1)L_c}^{qL_c-1}\sum_{l=(q-1)L_c, l\neq k}^{qL_c-1} \mathrm{E}[I_k I_l] + \sum_{k=(q-1)L_c}^{qL_c-1} \mathrm{E}[I_k^2]\right) - \mathrm{E}^2\left[I_q\right] \qquad \text{(D-1)} \\
&= \frac{1}{L_c^2}\left(\sum_{k=0}^{L_c-1}\sum_{l=0, l\neq k}^{L_c-1} \mathrm{E}[I_k I_l]\right) + \frac{1}{L_c}\mathrm{E}[I_q^2] - \mathrm{E}^2\left[I_q\right] \\
&= \mathrm{Var}(I_0)
\end{aligned}$$

where the second last line is obtained considering the fact that $\mathrm{E}[I_k I_l]$ only depends on $|k-l|$ and not k and l ($\beta_{k,l} = \beta_{0,|k-l|}$) and is given by[125]

$$\mathrm{E}[I_k I_l] = \frac{(\log_2(e))^2 \exp\left(2/\gamma\right)}{[\prod_{m=1}^{M}\Gamma(M-m+1)]^2}\sum_{r=1}^{M}\sum_{s=1}^{M}\det(\mathbf{C}_{r,s}(\beta_{k,l})) \qquad \text{(D-2)}$$

where the matrices $\mathbf{C}_{r,s}(\beta_{k,l})$ are taken from[125, eq. (14)]. For $\mathrm{E}^2\left[I_q\right]$ and $\mathrm{E}\left[I_q\right]$ closed form expressions have been given in [125], however, more simplified expressions can be found in[130, eqs. (29), (31)], which we have been used in Section III.

Appendix E

In Section 5.3, the achievable rate of each chunk was approximated to be Gaussian. Furthermore, the average sum rate, which is the average of the maximum of achievable rates of each chunk was approximated in (5.19). The average sum rate of the proposed scheme with opportunistic feedback, in which users send back only the rate of chunks that are above the average sum rate, $\bar{R}$, is given by

$$\bar{R}_{net}^{opp} = \bar{R}(1 - \frac{\bar{N}_f T_f}{T}) \tag{E-1}$$

where $\bar{N}_f$ is the average number of feedback terms per subcarrier. To obtain $\bar{N}_f$, the probability density function (PDF) of the sum rate, $f_R(x)$ where $R = \frac{1}{Q}\sum_{q=1}^{Q} \max_{1\leq k\leq K} r_{chk,q}^{(k)}$, is required. This PDF is well approximated by gamma distribution [133]

$$f_R(x) \approx \begin{cases} \frac{1}{\alpha\Gamma(\phi)} \left(\frac{x-c}{\alpha}\right)^{\phi-1} \exp\left(\frac{x-c}{\alpha}\right) & x \geq c \\ 0 & x < c \end{cases} \tag{E-2}$$

where the parameters of the above distribution are given as

$$\begin{aligned} \alpha &= \frac{\sigma'^2}{\mu' - c} \\ \phi &= \frac{(\mu' - c)^2}{\sigma'^2} \\ c &= 2.8989 \ln(\log_2[K]) + \mathrm{E}[r_{chk,q}] - 4.4291. \end{aligned} \tag{E-3}$$

In (E-3), σ' and μ' are given by

$$\begin{aligned} \mu' &= \sqrt{\mathrm{Var}(r_{chk,q})}\Phi^{-1}(0.5264^{\frac{1}{K}}) + \mathrm{E}[r_{chk,q}] \\ &= \sqrt{\mathrm{Var}(r_{chk,q})}\frac{1}{0.1975}\left[0.5264^{\frac{0.135}{K}} - (1 - 0.5264^{\frac{1}{K}})^{0.135}\right] + \mathrm{E}[r_{chk,q}] \end{aligned} \tag{E-4}$$

and,

$$\begin{aligned} \sigma' &= 0.5\sqrt{\mathrm{Var}(r_{chk,q})}\left[\Phi^{-1}(0.8832^{\frac{1}{K}}) - \Phi^{-1}(0.2142^{\frac{1}{K}})\right] \\ &= \frac{0.5\sqrt{\mathrm{Var}(r_{chk,q})}}{0.1975}\Bigg(\left[0.8832^{\frac{0.135}{K}} - (1 - 0.8832^{\frac{1}{K}})^{0.135}\right] \\ &\quad - \left[0.2142^{\frac{0.135}{K}} - (1 - 0.2142^{\frac{1}{K}})^{0.135}\right]\Bigg) \end{aligned} \tag{E-5}$$

In the above equations the function $\Phi(\cdot)$ is the standard normal CDF. Φ^{-1} is well approximated by [134]

$$\Phi^{-1}(x) \approx \frac{1}{0.1975}\left[x^{0.135} - (1-x)^{0.135}\right]. \tag{E-6}$$

The accuracy of approximation in (E-2) is shown in Fig. 6 in which the numerical and the approximate PDF have been plotted for different set of parameters.

Using (E-2), the cumulative distribution function (CDF) of R, $F_R(\cdot)$, given by

$$F_R(\bar{R}) = Pr(R > \bar{R}) \tag{E-7}$$

can be approximated by the CDF of gamma distribution [62] as

$$F_R(x) \approx \frac{\gamma(\phi, \frac{x-c}{\alpha})}{\Gamma(\phi)} \tag{E-8}$$

where $\gamma(\cdot,\cdot)$ is the incomplete gamma function defined in (5.12). Using the CDF of R, the approximate average number of feedback terms by all users is given by

$$\begin{aligned} \bar{N}_f &\approx \frac{2}{L} F_R(\bar{R}) KQ \\ &= \frac{2K}{L_c} F_R(\bar{R}), \end{aligned} \tag{E-9}$$

in which the coefficient 2 is inserted due to the fact that the index of chunk sizes with rates above threshold also need to be sent back along with their achievable rate. That completes the proof.